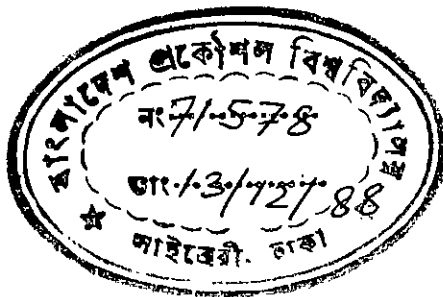


AN EXPERIMENTAL INVESTIGATION OF WIND EFFECT
ON RECTANGULAR CYLINDERS

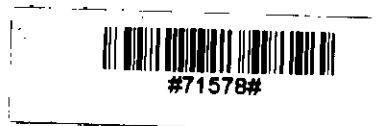
By

Alamgir Muhammed Tito Islam



Call no.
621.45
1988
ALA

A Thesis
Submitted to the Department of Mechanical Engineering
in partial fulfilment of the requirements for the degree
of
MASTER OF SCIENCE IN MECHANICAL ENGINEERING



BANGLADESH UNIVERSITY OF ENGINEERING AND TECHNOLOGY, DHAKA

October, 1988

621.45
1988
ALA

RECOMMENDATION OF THE BOARD OF EXAMINERS

The Board of Examiners hereby recommends to the Department of Mechanical Engineering, Bangladesh University of Engineering and Technology, Dhaka, the acceptance of the thesis, "AN EXPERIMENTAL INVESTIGATION OF WIND EFFECT ON RECTANGULAR CYLINDERS", submitted by Alamgir Muhammed Tito Islam, in partial fulfilment of the requirements for the degree of Master of Science in Mechanical Engineering.

Chairman

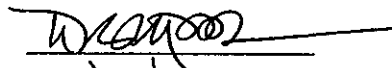
:



Dr. A.C. Mandal
Associate Professor
Deptt. of Mechanical Engineering
BUET, Dhaka

Member

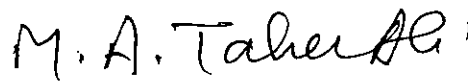
:



Dr. Dipak Kanti Das
Professor & Head
Deptt. of Mechanical Engineering
BUET, Dhaka

Member

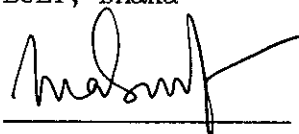
:



Dr. M.A. Taher Ali
Professor
Deptt. of Mechanical Engineering
BUET, Dhaka

Member (External)

:



Dr. M. Abdur Rouf
Associate Professor
Deptt. of Civil Engineering
BUET, Dhaka

October, 1988

CERTIFICATE OF RESEARCH

This is to certify that the work presented in this thesis is an outcome of the investigation carried out by the author under the supervision of Dr. Amalesh Chandra Mandal, Associate Professor, Department of Mechanical Engineering, Bangladesh University of Engineering and Technology, (BUET), Dhaka.

DR. AMALESH CHANDRA MANDAL

Supervisor

ALAMGIR MD. TITO ISLAM

Author

ACKNOWLEDGMENT

I wish to express my sincerest gratitude and indebtedness to Dr. Amalesh Chandra Mandal for his guidance and supervision throughout the entire period of the experimental investigation. His initiatives, encouragement, patience and invaluable suggestions are gratefully acknowledged without which this work would not have been possible.

I am truly grateful to Professor M.A. Taher Ali for his constructive suggestions and advice during several phases of this investigation. Without his kind co-operation and guidance this work could not have been carried out properly.

The co-operation and inspiration extended by Professor D.K. Das and Dr. M.Q. Islam are acknowledged with gratitude.

I would like to thank my colleagues M.A. Selim and Md. Durul Huda for providing me with constructive suggestions and helping me solve many problems during the investigation. I am also grateful to my friends and other colleagues for their profuse inspiration.

Sincere thanks are offered to Mr. Ahmed Ali Mollah, Chief foreman instructor, Machine shop, Md. Rafiqul Islam, Foreman instructor, Carpentry shop, Md. Nazimuddin, Foreman instructor, Welding and Sheet Metal Shop, BUET, for their co-operation in fabricating and assembling different parts and components of the experimental set-up. Thanks are also due to Messrs Shahabuddin, Bachchu and late Razzaque, technicians at the Fluid Mechanics Laboratory of Mechanical Engineering Department for their co-operation at different stages of the work. I would also like to acknowledge the help of Mr. A. Salam for drafting the figures.

Lastly, I would like to thank my wife who persistently kept me at my work and partly relieved me of family duties until this work was finished.

ABSTRACT

An experimental investigation of the mean pressure distributions around an isolated and a group of rectangular cylinders placed in a uniform cross flow is presented. The rectangular cylinders had side ratios of $H/D = 1.25$, 1.5 , 1.75 and 2.0 where D is section width normal to flow direction and H is section depth along the flow direction. The flow had a turbulence intensity of 0.33% and a constant free stream velocity of 18.3m/sec (60 fps) was used for the purpose.

Mean pressure distributions around each of the cylinders were measured for angles of attack varying from 0° to 45° in steps of 5° in an open circuit wind tunnel. Experiment on a group of cylinders of identical side ratio in the tunnel test section with one cylinder placed centrally in the upstream side and the other two placed symmetrically in the downstream side with respect to the tunnel axis. Pressure distribution around the upstream and downstream cylinders were measured for various combinations of transverse and longitudinal spacings of the cylinders. Four sets of measurements were taken for side ratios of $H/D = 1.25$, 1.5 , 1.75 and 2.0 . Finally, drag co-efficients, lift co-efficients and total force co-efficients were calculated by numerical integration.

The form drag on the rectangular cylinder with its axis normal to the approaching flow increased with rise of the value of side ratio upto about 0.6 , then decreased with the further increase in the side ratio. It was also observed that the drag on an isolated cylinder was higher in general than that on the same cylinder while it becomes part of a group. The rectangular cylinder with the highest side ratio ($H/D=2$) experienced minimum drag for all conditions of spacings.

CONTENTS

	Page
RECOMMENDATION OF THE BOARD OF EXAMINERS	ii
CERTIFICATE OF RESEARCH	iii
ACKNOWLEDGMENT	iv
ABSTRACT	v
CONTENTS	vi
LIST OF FIGURES	viii
LIST OF SYMBOLS	xii
CHAPTER 1 : INTRODUCTION	1
1.1 Nature of Wind Loading	1
1.2 Motivation for the study	2
1.3 Aim of the Study	3
1.4 Scope of the Thesis	4
CHAPTER 2 : REVIEW OF LITERATURES	6
2.1 Literatures Concerning Single Body	6
2.2 Literatures Concerning Multiple Bodies	13
CHAPTER 3 : EXPERIMENTAL SET UP	15
3.1 The Wind Tunnel	15
3.2 The Test Section	16
3.3 The Cylinders	17
3.4 Experimental Procedure	18
3.4.1 Single Cylinder	19
3.4.2 Cylinders in Group	20

CHAPTER 4 : RESULTS AND DISCUSSIONS	21
4.1 Single Rectangular Cylinder	21
4.1.1 Pressure Distribution	22
4.1.2 Aerodynamic Forces	25
4.1.3 Effect of Side Ratio of Drag	27
4.2 Staggered Rectangular Cylinders	28
4.2.1 Pressure Distribution on Upstream Cylinder	28
4.2.2 Variation of drag for Upstream Cylinder	30
4.2.3 Pressure Distribution on Downstream Cylinder	31
4.2.4 Drag on Downstream Cylinder	36
4.2.5 Lift on Downstream Cylinder	37
4.3 Observation of Pressure Fluctuations	39
4.4 Effect of Reynolds Number	39
4.5 Blockage Corrections	40
CHAPTER 5 : CONCLUSIONS AND RECOMMENDATIONS	42
5.1 Conclusions	42
5.2 Recommendations	43
REFERENCES	46
APPENDICES	50
Appendix-A: Determination of Coefficients	51
Appendix-B: Uncertainty Analysis	55
FIGURES	60

LIST OF FIGURES

<u>Figures</u>	<u>Page</u>
3.1 Schematic diagram of wind tunnel	61
3.2 Wooden vertical wall side of the test section	62
3.3 Perspex vertical wall side of the test section	63
3.4 Sectional view of a specimen rectangular cylinder	64
3.5 The arrangement of tapping points on adjacent sides	64
3.6 Cross section of rectangular cylinders from each set showing position of tapping points	65
3.7 Tunnel test section showing the position of the cylinders in staggered form	65
3.8 Velocity distribution in upstream side of test section	66
4.1 The nature of the flow pattern around rectangular prisms	67
4.2 Effect of angle of attack on C_p -distributions at side ratio(H/D) of 1.25	68
4.3 Effect of angle of attack on C_p -distributions at side ratio(H/D) of 1.5	69
4.4 Effect of angle of attack on C_p -distributions at side ratio(H/D) of 1.75	70
4.5 Effect of angle of attack on C_p -distributions at side ratio(H/D) of 2.0	71
4.6 Effect of side ratios(H/D) on C_p -distributions on the bottom surface at varying angles of attack	72
4.7 Effect of side ratios(H/D) on C_p -distributions on the back surface at varying angles of attack	73
4.8 Comparison of C_p -distributions at variable angle of attack on windward side	74
4.9 Variation of drag co-efficients(C_D) with angle of attack for different side ratios(H/D)	75

4.10	Variation of lift co-efficients(C_l) with angle of attack for different side ratios(H/D)	76
4.11	Variation of drag co-efficient(C_D) with side ratio(H/D)	77
4.12	Variation of total force co-efficient(C_F) with angle of attack for different side ratios(H/D)	78
4.13	Effect of longitudinal spacing(L_1) on C_p -values for upstream cylinder with side ratio of 1.25 keeping the transverse spacing(L_t) constant at 1D	79
4.14	Effect of longitudinal spacing(L_1) on C_p -values for upstream cylinder with side ratio of 1.25 keeping the transverse spacing(L_t) constant at 2D	80
4.15	Effect of longitudinal spacing(L_1) on C_p -values for upstream cylinder with side ratio of 1.25 keeping the transverse spacing(L_t) constant at 4D	81
4.16	Effect of longitudinal spacing(L_1) on C_p -values for upstream cylinder with side ratio of 1.5 keeping the transverse spacing(L_t) constant at 1D	82
4.17	Effect of longitudinal spacing(L_1) on C_p -values for upstream cylinder with side ratio of 1.5 keeping the transverse spacing(L_t) constant at 2D	83
4.18	Effect of longitudinal spacing(L_1) on C_p -values for upstream cylinder with side ratio of 1.5 keeping the transverse spacing(L_t) constant at 4D	84
4.19	Effect of longitudinal spacing(L_1) on C_p -values for upstream cylinder with side ratio of 1.75 keeping the transverse spacing(L_t) constant at 1D	85
4.20	Effect of longitudinal spacing(L_1) on C_p -values for upstream cylinder with side ratio of 1.75 keeping the transverse spacing(L_t) constant at 2D	86
4.21	Effect of longitudinal spacing(L_1) on C_p -values for upstream cylinder with side ratio of 1.75 keeping the transverse spacing(L_t) constant at 4D	87
4.22	Effect of longitudinal spacing(L_1) on C_p -values for upstream cylinder with side ratio of 2.0 keeping the transverse spacing(L_t) constant at 1D	88
4.23	Effect of longitudinal spacing(L_1) on C_p -values for upstream cylinder with side ratio of 2.0 keeping the transverse spacing(L_t) constant at 2D	89

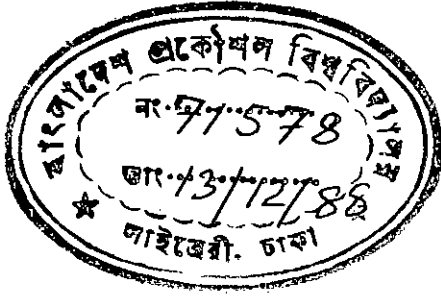
4.24	Effect of longitudinal spacing(L_1) on C_p -values for upstream cylinder with side ratio of 2.0 keeping the transverse spacing(L_t) constant at 4D	90
4.25	Variation of drag co-efficient(C_D) with longitudinal spacing(L_1) on upstream cylinder with different side ratios at constant transverse spacing(L_t) of 1D	91
4.26	Variation of drag co-efficient(C_D) with longitudinal spacing(L_1) on upstream cylinder with different side ratios at constant transverse spacing(L_t) of 2D	92
4.27	Variation of drag co-efficient(C_D) with longitudinal spacing(L_1) on upstream cylinder with different side ratios at constant transverse spacing(L_t) of 4D	93
4.28	Effect of longitudinal spacing(L_1) on C_p -distributions for downstream cylinder with side ratio of 1.25 keeping the transverse spacing(L_t) constant at 1D	94
4.29	Effect of longitudinal spacing(L_1) on C_p -distributions for downstream cylinder with side ratio of 1.5 keeping the transverse spacing(L_t) constant at 1D	95
4.30	Effect of longitudinal spacing(L_1) on C_p -distributions for downstream cylinder with side ratio of 1.75 keeping the transverse spacing(L_t) constant at 1D	96
4.31	Effect of longitudinal spacing(L_1) on C_p -distributions for downstream cylinder with side ratio of 2.0 keeping the transverse spacing(L_t) constant at 1D	97
4.32	Effect of longitudinal spacing(L_1) on C_p -distributions for downstream cylinder with side ratio of 1.25 keeping the transverse spacing(L_t) constant at 2D	98
4.33	Effect of longitudinal spacing(L_1) on C_p -distributions for downstream cylinder with side ratio of 1.5 keeping the transverse spacing(L_t) constant at 2D	99
4.34	Effect of longitudinal spacing(L_1) on C_p -distributions for downstream cylinder with side ratio of 1.75 keeping the transverse spacing(L_t) constant at 2D	100
4.35	Effect of longitudinal spacing(L_1) on C_p -distributions for downstream cylinder with side ratio of 2.0 keeping the transverse spacing(L_t) constant at 2D	101
4.36	Effect of longitudinal spacing(L_1) on C_p -distributions for downstream cylinder with side ratio of 1.25 keeping the transverse spacing(L_t) constant at 4D	102

4.37	Effect of longitudinal spacing(L_1) on C_p -distributions for downstream cylinder with side ratio of 1.5 keeping the transverse spacing(L_t) constant at $4D$	103
4.38	Effect of longitudinal spacing(L_1) on C_p -distributions for downstream cylinder with side ratio of 1.75 keeping the transverse spacing(L_t) constant at $4D$	104
4.39	Effect of longitudinal spacing(L_1) on C_p -distributions for downstream cylinder with side ratio of 2.0 keeping the transverse spacing(L_t) constant at $4D$	105
4.40	Variation of drag co-efficient(C_D) with longitudinal spacing(L_1) on downstream cylinder with different side ratios at constant transverse spacing(L_t) of $1D$	106
4.41	Variation of drag co-efficient(C_D) with longitudinal spacing(L_1) on downstream cylinder with different side ratios at constant transverse spacing(L_t) of $2D$	107
4.42	Variation of drag co-efficient(C_D) with longitudinal spacing(L_1) on downstream cylinder with different side ratios at constant transverse spacing(L_t) of $4D$	108
4.43	Variation of lift co-efficient(C_L) with longitudinal spacing(L_1) on downstream cylinder with different side ratios at constant transverse spacing(L_t) of $1D$	109
4.44	Variation of lift co-efficient(C_L) with longitudinal spacing(L_1) on downstream cylinder with different side ratios at constant transverse spacing(L_t) of $2D$	110
4.45	Variation of lift co-efficient(C_L) with longitudinal spacing(L_1) on downstream cylinder with different side ratios at constant transverse spacing(L_t) of $4D$	111

LIST OF SYMBOLS

A	Frontal area of cylinder
B	Denotes bottom downstream cylinder
C_D	Drag co-efficient
C_F	Total force co-efficient
C_L	Lift co-efficient
C_P	Mean pressure co-efficient
D	Width of cylinder normal to the approach flow
F	Denotes upstream cylinder
F_D	Drag force per unit length of the cylinder
F_L	Lift force per unit length of the cylinder
H	Depth of cylinder in the flow direction
L	Length of a side of the cylinder
L_l	Longitudinal spacing
L_t	Transverse spacing
P	Local static pressure
P_o	Free stream static pressure
P	Difference of ambient and local static pressure

- T Denotes top downstream cylinder
- u Mean axial velocity
- U_o Free Stream velocity
- x Distance from the front corner of cylinder
- y Distance from the bottom surface of test section
- α Angle of attack
- γ_w Specific weight of manometer water
- ν Kinematic viscosity of air
- ρ Density of air
- σ Turbulence intensity



CHAPTER 1 INTRODUCTION

Recent engineering problems regarding wind loads around a group of skyscrapers, chimneys, towers and the flow induced vibration of tubes in heat exchangers, bridges, oil rigs or marine structures need detailed investigation of flow patterns and aerodynamic characteristics on bluff bodies. However, the problem of wind load on buildings and structures is not a new one. The subject was considered for study as far back as the 17th century by Galileo and Newton[41]. But only in the last few decades much attention has been paid to the study of wind loading in different parts of the world. The occurrences of certain disastrous collapse of suspension bridges and damage to buildings due to wind effects at different places prove that wind loading on buildings and structures should not be encountered as a minor criteria for design purposes. Till now extensive research work has been carried out on isolated bluff bodies which interfere with each other is a very recent endeavour. Even then, very little information is available concerning the flow over staggered rectangular cylinders although this is a problem of considerable practical significance.

1.1 Nature of Wind Loading

Wind loadings on buildings and structures as a whole may be treated as the static and dynamic effects of wind action. The static effects refer to the steady(time-average) forces and pressures tending to give the structure a steady displacement. On the other hand dynamic effect has the tendency to set the structure oscillating. A steady wind load on a building is very difficult to achieve. In fact always wind loads are of a fluctuating nature because of

varying speeds and directions of winds. The type of wind and the stiffness of the structure determine the nature of loading on a building. When a building is very stiff the dynamic response of the structure may be neglected and only the static loads may be considered. This is because the natural frequency of an extremely stiff building is too high to be excited by wind. In the present study the effect of static loading is taken into account due to steady wind. Since natural winds are continually fluctuating it is generally assumed that these fluctuations are so irregular and random that the response of a structure will not differ from that due to a steady wind of the same average speed.

Recently the dynamic response of buildings has been emphasized for study because of the present tendency to build more slender and lighter structures.

1.2 Motivation for the Study

Designing buildings with the consideration of wind effects is a recent innovation. Now-a-days the effects of wind regarding both wind loading and environmental problem is considered as one of the important design criterion in order to design a tall building both in a free standing condition and as a part of a group of buildings. In Bangladesh urban environmental problems due to buildings is not yet recorded. However, the cities are rapidly growing with emphasis given to the construction of multistoried buildings to cope with the urban population pressure. The need to build in more windy sites or the need to locate a number of tall buildings close together will undoubtedly pose problems not yet encountered by the architects and townplanners of Bangladesh. The knowledge of wind loading on a single tall building or on a group of tall buildings is essential for sound planning and design. For designing groups of tall buildings, knowledge of the effect of wind loading on a single tall

building is insufficient because the interference of the neighbouring buildings in a group makes the nature of wind loadings different from that on a free standing building.

One approach to the problem of predicting the flow around buildings in close proximity is to develop an understanding of the nature of flows on relatively simple arrangement of bluff bodies by wind tunnel experiments. With this end in view, the present investigation of pressure distributions about rectangular cylinders with varying side ratios was carried out. Rectangular cylinders ideally represent the general shape of tall buildings. So a study on groups of rectangular cylinders arranged simply in the staggered form would be helpful in the analysis of wind effects on groups of buildings.

Apart from wind loading problems, concentration of high rise buildings in a locality can produce environmental problems like unpleasant wind conditions near ground level (e.g. blowing dust off the ground), too high wind load on people, too high wind speed in streets and passages or stagnation of air in certain areas causing air pollution. To find acceptable solutions of the above mentioned problems a more detailed study in this regard is essential.

1.3 Aim of the Study

It is expected that when more than one bluff body is placed in a uniform flow, the surrounding flow and vortex shedding patterns would be different from the case of a single body, because there would be interference in the flow by one body on the other depending on the arrangement or spacings of the bodies. The present study does not take into account the complexities of such flows. Rather the study is of a fundamental nature confined to the investigation of aerodynamic forces and pressure distribution on the body. The present study is an attempt to give an understanding about the variation of

wind load pattern imposed on a building due to the change in side dimension as well as the influence of nearby buildings. With a view to meet the above mentioned requirements, the study was performed. The prime objectives of the study were:

(1) To measure the pressure distribution around single rectangular cylinder, and to observe the effects of varying angle of attack and side dimensions of the rectangular bodies.

(2) To measure the pressure distribution around staggered rectangular cylinders and observe the effects of changing the longitudinal and transverse spacing of the cylinders.

(3) To compare the difference in wind effects for various spacings and side dimensions of the rectangular cylinders.

The results were expressed in the form of non-dimensional co-efficients, i.e. pressure, drag, lift and total force co-efficients.

1.4 Scope of the Thesis

The present research programme covers only the experimental investigation of pressure distributions around bluff bodies of different side ratios. The several phases of the entire investigation are described in this thesis. Chapter 2 provides with the brief description of the findings of several researchers in the field of flow over single and multiple bodies. Notable contributions were mainly made by P.W.Bearman, B.E.Lee, Y.Nakamura, B.J.Vickery, G.V.Parkinson, A.R.Barriga and J.A.Robertson. Besides these, findings of several other researchers are also included in this chapter.

In the chapter 3 mainly an account of the experimental arrangement and procedure adopted for the investigation are presented. It includes the description of the wind tunnel, the constructional details of the test section

and the rectangular cylinders used for the study. The experiment was conducted in the wind tunnel for only two dimensional uniform cross flow keeping the velocity and turbulence intensity constant.

Chapter 4 presents the analysis concerning the results of the experimental results are presented in the graphical form. In few cases the existing experimental results of different researchers are correlated with the present one.

Finally, the conclusions which are drawn from the present investigation are given in the chapter 5. This chapter also includes an outline regarding further research in this field.

CHAPTER 2

REVIEW OF LITERATURES

Arising from the increasing practical importance of bluff body aerodynamics, there have been, over the past few decades, an enormous increase in research works concerning laboratory simulations, full-scale measurements and more recently, numerical calculations and theoretical predictions for flows over a wide variety of bluff bodies. It is true that researchers from all over the world have contributed greatly to the knowledge of flow over bluff bodies but the major part of the reported works are of fundamental nature involving the flow over a single body. Most of the researchers have conducted research works on either single cylindrical cylinder or a square section cylinder with various flow parameters. The following sections give the brief descriptions of the works presented by selected researchers like P.W.Bearman, B.E.Lee, B.J.Vickery, Y.Nakamura, A.R.Barriga, I.P.Castro, J.A.Roberson, G.V.Parkinson and others.

2.1 Literature concerning Single Body

P.W.BEARMAN AND D.M.TRUEMAN[3] investigated the base pressure coefficient, drag coefficient and Strouhal number of rectangular cylinders with one face normal to the flow direction. They found that when $d/h = 0.62$, where d is section depth and h is section width normal to the wind direction, the drag coefficient was maximum (about 2.94). By introducing a splitter plate into the wake region they found that the increased drag effect was completely eliminated. This finding demonstrated that the high drag was associated with the regular shedding of vortices. They also showed that the further the vor-

tices could be persuaded to form away from the body, the higher the base pressure. They suggested that for higher values of $d/h (> 0,6)$ the vortices were forced to form further downstream because of the influence of the trailing edge corners.

YASUHARU NAKAMURA AND YUJIOHYA[33] attempted to study vortex shedding from square prisms placed normal to smooth and turbulent approaching flows. They made flow visualization and measured the velocity and pressure for the flow past prisms of variable length with square section. They found that square prisms shed vortices in one of the two fixed wake planes which were parallel with the plate sides. The plane of shedding was switched irregularly from one to the other. They further showed that the vortex shedding from a square prism with $d/h = 0.5$ and a cube was similar, while for a square prism with $d/h = 2.0$, no such vortex shedding was observed.

R.W.DAVIS AND E.F.MOORE[8] carried out a numerical study of vortex shedding from rectangular cylinders. They attempted to present numerical solutions for two-dimensional time dependent flow about rectangles in infinite domains. They investigated the initiation and subsequent development of the vortex shedding phenomena for Reynolds number varying from 100 to 2800. They found that the properties of these vortices were strongly dependent on the Reynolds number. Lift, drag and Strouhal number were also found to be influenced by Reynolds number. The computer simulation described in the paper was carried out on a UNIVAC 1108.

Y.NAKAMURA AND T.MATSUKAWA[31] experimentally investigated the vortex excitation of rectangular cylinders with a long side normal to the flow in a mode of lateral translation using free and forced oscillation methods. The rectangular cylinders had side ratios of 0.2, 0.4 and 0.6. The forced oscillation experiments included measurements of the fluctuating lift-force at

amplitudes upto 10% of the length of the long side. They presented the results of the measurement of the mean base pressure, the fluctuating lift force and the velocity fluctuation in the near wake on forced oscillating rectangular cylinders along with the results concerning the rate of growth of oscillation on freely oscillating rectangular cylinders. They found that the vortex excitation of a rectangular cylinder was strongly dependent on the side ratio. They concluded that the critical change of the mean base pressure of an oscillating rectangular cylinder with increasing side ratio was closely correlated with the vortex excitation characteristics.

ATSUSHI OKAJIMA[35] conducted experiments in a wind tunnel and in a water tank on the vortex shedding frequencies of various rectangular cylinders. He presented results that showed how Strouhal number varied with width to height ratio of the cylinders for Reynolds number between 70 and 2×10^4 . He found that there existed a certain range of Reynolds number for the cylinders with the width to height ratios of 2 and 3 where flow pattern abruptly changed with a sudden discontinuity in Strouhal number. For Reynolds number below this region, the flow separated at the leading edges, reattached on either the upper or lower surfaces of the cylinder during a period of vortex shedding. Again for Reynolds number beyond it the flow fully detached itself from the cylinder.

B.E.LEE[22] made an elaborate study of the effect of turbulence on the surface pressure field of a square prism. He presented measurements of the mean and fluctuating pressures on a square cylinder placed in a two-dimensional uniform and turbulent flow. It was observed that the addition of turbulence to the flow raised the base pressure and reduced the drag of the cylinder. He suggested that this phenomena was attributable to the manner in which the increased turbulence intensity thickened the shear layers, which

caused them to be deflected by the downstream corners of the body and resulted in the downstream movement of the vortex formation region. The strength of the vortex shedding was shown to be reduced as the intensity of the incident turbulence was increased. Measurement of drag at various angle of attack (0° to 45°) showed that with increase in turbulence level the minimum drag occurred at smaller values of angle of attack.

J.A.ROBERSON,C.T.CROWE AND R.TSENG[40] measured pressure distribution on rectangular rods placed in a cross flow with the rods oriented at small angles of attack with respect to the wind direction. The Reynolds number based on the minimum dimension of the rod was 4×10^4 and the turbulence intensity of the cross flow ranged between 1% and 10%. They concluded that the free-stream turbulence had a significant effect on the pressure distribution about bodies of rectangular cross-section. With small angle of attack these bodies had a significantly lower pressure on their windward side wall than did the same bodies with zero angle of attack.

To study the pressure distribution on bodies that more nearly represent building configurations, tests were made on bodies of square cross section placed on the floor of the wind tunnel. It was found that decreasing relative height of the body had an attenuating effect on the negative pressure on the windward sidewall and it also increased the critical angle of attack.

J.A.ROBERSON,CHI YU LIN,G.S.RUTHERFORD AND M.D.STINE[39] carried out experiments on circular cylinders, spool shaped bodies, cup-shaped bodies, square rods and rectangular rods to observe the effect of turbulence on the drag of these bodies. For square rods with their axes parallel to the flow direction it was found the C_D decreased approximately 25% when the turbulence intensity increased from 1% to 10%. Two rectangular rods were used; one had a square cross section and the other had a length (in the free stream direction)

to breadth ratio of two ($L/B=2$). The drag was measured with the axes of the rectangular rods oriented normal to the free stream direction. It was noted that on the sides of the square rod the pressure change with a change in turbulence intensity was about the same as for the rear face; but for the rectangular rod, the change in pressure on the sides was large, but small on the rear face. They concluded that bodies which have shapes such that reattachment of the flow is not a factor, experience an increase in C_D with increased turbulence intensity. On the other hand bodies for which reattachment or near reattachment of flow occurs with increased turbulence may experience either a decrease or increase in C_D with increased turbulence intensity depending upon the shape of the body.

A.R.BARRIGA,C.T.CROWE AND J.A.ROBERSON[3] studied the effects of angle of attack, turbulence intensity and scale on the pressure distribution of a single square cylinder placed in a turbulent cross flow. They found that when the square cylinder was positioned in a cross flow with one face normal to the flow direction, only drag force was produced; but in the same flow a negative lift force was developed at small positive angle of attack, the magnitude of which depended on the turbulence characteristics of the cross flow. It was suggested that the negative lateral force on the square cylinder oriented at a small positive angle of attack was due to the relatively large negative pressure co-efficient in the separated zone on the windward sidewall. It was also concluded that the effect of turbulence intensity was to decrease the pressure near the front corner of the windward sidewall and promote flow reattachment near the rear, giving rise to a very significant increase in aerodynamic moment.

Y.NAKAMURA AND Y.OHYA[32] studied the effects of turbulence on the mean

flow past square rods. Measurements were made on square rods with different lengths with their square face normal to the flow to investigate the effects of turbulence intensity and scale on the mean flow characteristics. The turbulence intensity varied from 3.5% to 13% and the length-to-size ratio of d/h of the rods ranged from 0.1 to 2.0 where d was the length of the rod. It was found out that there were two main effects of turbulence on the mean flow past a three-dimensional sharp edged bluff body. Small-scale turbulence increased the growth rate of the shear layer, while large-scale turbulence enhanced the roll up of the shear layer. The consequences of these depended on the shape of the bluff body. For a square plate, both small and large-scale turbulence reduced the size of the base cavity. As the length of the square rod was increased beyond the critical (0.6 times the height), the shear-layer-edge direct interaction controlled the near wake, eventually leading to flow reattachment. The effect of small-scale turbulence was to promote the shear-layer direct interaction.

B.J.VICKERY[49] presents in his paper the results of the measurements of fluctuating lift and drag on a long square cylinder. He attempted to establish a correlation of lift along the cylinder and the distribution of fluctuating pressure on a cross-section. It was found that the magnitude of the fluctuating lift was considerably greater than that for a circular cross section and the spanwise correlation much stronger. It was also reported that the presence of large scale turbulence in the stream had a remarkable influence on both the steady and the fluctuating forces. At small angle of attack (less than 10°) turbulence caused a reduction in base suction and a decrease in fluctuating lift of about 50%.

B.R.BOSTOCK AND W.A.MAIR[6] studied the pressure distributions and forces on rectangular and D-shaped cylinders placed in two dimensional flow,

at Reynolds number 1.9×10^5 . It was found that for rectangular cylinders a maximum drag coefficient was obtained when the height h (normal to the stream) of the section was about 1.5 times the width d . Reattachments on the sides of the cylinders occurred only for h/d less than 0.35.

HIROSHI SAKAMOTO AND MIKIO ARIE[42] collected experimental data on the vortex shedding frequency behind a vertical rectangular prism and a vertical circular cylinder attached to a plane wall and immersed in a turbulent boundary layer. They tried to investigate the effects of the aspect ratio (height/width) of these bodies and the boundary layer characteristics on the vortex shedding frequency. Measurements revealed that two types of vortex were formed behind the body, depending on the aspect ratio; they were the arch-type vortex and the karman-type vortex. The arch-type vortex appeared at an aspect ratio less than 2.0 and 2.5 for rectangular and circular cylinders respectively. The karman-type vortex appeared for the aspect ratio greater than the above values.

The whole experiment was conducted at a turbulence level of 0.2% and free stream velocity of 20m/sec. The aspect ratio was varied between 0.5 to 8.0.

I.P.CASTRO AND A.G.ROBINS[7] describe in their paper the flow around surface mounted cubes in both uniform, irrotational and sheared, turbulent flows. The shear flow was a simulated atmospheric boundary layer with a height ten times the body dimension. They presented measurements of body surface pressures and mean and fluctuating velocities within the wake region. These measurements reflected the effects of upstream turbulence and shear on the wake flow. It was found that in the reversed flow region directly behind the body the addition of upstream turbulence and shear considerably reduced the size of the cavity zone. Unlike the case of uniform flow the separating shear

layers reattached to the body surface. Measurements for a variety of cube size/boundary layer height ratios further revealed that reattachment occurred even for cube heights larger than the boundary layer height. They found that in the case of uniform flow approaching the cube at 45° , the near wake and pressure field were dominated by strong vortices shed from the top edges of the body.

A.LANEVILLE, I.S.GARTSHORE AND G.V.PARKINSON[19] explain in their paper some effects of turbulence on bluff bodies. The bluff bodies include square and rectangular prisms.

C.K.HUA[5] made measurements of fluctuating lift and the oscillating amplitudes on a square cylinder in a wind tunnel test. He reported that the wind pressure distributions and the lift on the stationary cylinder normal to the wind. Also the lift force was proportional to the square of its amplitude.

2.2 Literatures concerning Multiple Bodies

J.LEUTHEUSSER[23] made wind tunnel tests on scale models of typical building configurations. The experiment was conducted on four models each with different height and cross section. He found out the static wind loading on each of the buildings in free standing condition and as a member of a group of buildings. He concluded that the wind loading of a building was less severe when it formed a part of a group than when it was free standing.

MASANORI HAYASHI, AKIRASAKURAI AND YUJIOHYA[14] made an experimental investigation into the wake characteristics of a group of flat plates, consisting of two, three or four plates placed side by side normal to the flow direction. They found that when the ratio of the split width to the plate width(split ratio) of a row of flat plates was less than about 2, the flows through the gaps were biased either upward or downward in a stable way, lead-

ing to multiple flow patterns for a single split ratio value. The plates on the biased side showed high drag and regular vortex shedding, while those on the unbiased side showed the opposite. They suggested that the origin of biasing was strongly related to the vortex shedding of each plate of a row. The experiment was conducted for Reynolds number of $(1.3 - 1.9) \times 10^4$.

K.KOEING AND A.ROSHKO[18] describes in their paper an experimental investigation of the shielding effects of various disks placed co-axially upstream of an axisymmetric flat faced cylinder. For certain combinations of the diameter and gap ratios they observed a considerable decrease in the drag of such a system. By flow visualization technique they showed that for such optimum shielding the upstream surface which separated from the disk reattached smoothly onto the front edge on the downstream cylinder.

P.W.BEARMAN AND A.J.WADCOCK[5] present in their paper how the flows around two circular cylinders, displaced in a plane normal to the free stream, interact as the two bodies are brought close together. Surface pressure measurements at a Reynolds number of 2.5×10^4 based on the diameter(D) of a single cylinder, showed the presence of a mean repulsive force between the cylinders. At gaps between $0.1D$ and $1D$ a marked asymmetry in the flow was observed with the two cylinders experiencing different drags and base pressures. The base pressure was found to change from one steady value to another or simply fluctuate between the two extremes. They also showed how mutual interference influenced the formation of vortex streets from the two cylinders.

CHAPTER 3

EXPERIMENTAL SET-UP

The objectives of the investigation of wind loading on the rectangular cylinders have been realized essentially with the help of a subsonic wind tunnel, four sets of rectangular cylinders and an inclined multimanometer. Mean pressure distribution around the rectangular bodies placed normal to the approaching uniform flow was measured with the help of the multimanometer. The following sections describe in detail regarding the experimental set-up and techniques adopted for the investigation.

3.1 The Wind Tunnel

The open circuit subsonic wind tunnel was 16.15m(53ft) long with a test section of 45.72cm x 45.72cm (18in x 18in) cross-section. Figure 3.1 depicts the wind tunnel used for the experiment. The successive sections of the wind tunnel comprised of a filter-cum settling chamber, a bell mouth entry, an eddy breaker, a flow straightener, a 152.4cm(30inch) uniform perspex upstream section, test section, diverging section, two counter rotary axial flow fans, a flow controlling valve and finally a silencer. The central longitudinal axis of the wind tunnel was maintained at a constant height from the floor.

The filter-cum settling chamber was incorporated into the system to prevent foreign particles entering the tunnel and maintain uniform flow into the duct free from outside disturbances. The chamber was made of a rectangular wooden frame measuring 254cm x 152.4cm x 213.4cm covered with a layer of 2.54cm thick foam sheets. The exposed surface of the foam chamber was covered with cloth for extra protection against dust.

The entry nozzle, made of 18 SWG black sheet, was 118cm long with a contraction ratio of 10:3. Wire net with 2 holes/cm was fitted at the entrance of the nozzle to act as the primary eddy breaker. A honeycomb like flow straightener made of 15cm long, 2.54cm diameter PVC pipes was stacked at the 15cm long short entry section following the nozzle. Both ends of the honeycomb section was guarded by wire net with 2 holes/cm. This facility produced a more uniform and stable flow.

The diverging section of the wind tunnel was 396.24cm long and made of 15 SWG black sheet. The angle of divergence was 6° , which was done with a view to minimize expansion loss and reduce the possibility of flow separation. A foam made isolater was placed between the fan unit and the diverging section of the wind tunnel to prevent transmission of vibration towards the main test section.

The induced flow through the wind tunnel was produced by a two-stage contra-rotating axial flow fan (Woods of Colchester Ltd., England, Type 38 JTE) of capacity 30,000 cfm at the head of 15.24cm of water and rpm 1475. A butterfly valve, actuated by a screw thread mechanism, was placed behind the fan and used to control the flow. Finally a silencer was fitted at the end of the tunnel in order to reduce the noise of the system.

3.2 The Test Section

The constructional details of the test section are shown in the figures 3.2 and 3.3. The length of the test section was 1.52m and it was positioned adjacent to the 76.2cm upstream perspex section. The roof and floor of the test section was made of plywood. One side wall was made of perspex. The other side wall was made in such a way as to fulfill the requirements of the experimental procedure. The mid portion of this side of length 43.8cm, was made

of wood and the remaining end portions were made of plywood. The sliding doors of the wooden vertical side wall as shown in the figure 3.2 were provided with the facility for transverse movement of the rectangular cylinders in a plane normal to the flow. The longitudinal movement (along the flow direction) of the centrally mounted cylinders was made possible by the 3cm wide and 27cm long slot shown in the same figure 3.2. This figure also shows wooden blocks of lengths 3cm, 6cm and 12cm and of width 3cm each which were used to fix the centrally mounted cylinders at different longitudinal positions along the length of the slot. The corresponding holes of 1.3cm diameter to mount the cylinders were made on the opposite side perspex wall as shown in figure 3.3. There were four removable perspex plates (figure 3.3), each of which included 6 holes in order to fix the cylinders for different transverse spacings. These plates were made as a part of the vertical perspex side wall and positioned towards the downstream side.

3.3 The Cylinders

The twelve cylinders of rectangular section were made of perspex of which there were four sets of cylinders with three identical ones in each set. The figure 3.4 shows the constructional details of a cylinder. Each of the cylinders was constructed identically. The side dimensions of the cylinders in each set were $D= 3\text{cm}$ each and $H= 3.75, 4.5, 5.25$ and 6.0cm . 4mm thick and 45.72cm long perspex plates with the appropriate side dimensions were joined to form the shape of hollow rectangular cylinders. One end was closed by inserting a solid wooden block and the other end by inserting another wooden hollow block with 16mm through hole. On either side of the cylinders there were 30mm long projected circular portion in order to mount the cylinder as shown in the figure 3.4. The extreme end of the 13mm diameter projected por-

tion of the cylinder (figure 3.4) was given a rectangular shape and allowed to pass through the identical rectangular hole of a graduated disc. This provision was needed to maintain angular orientation of the cylinders.

Each rectangular cylinder was tapped on two adjacent sides to measure pressure distribution. Because of space limitation it was not possible to accommodate all the tapings in a section perpendicular to the axis of the cylinder. As shown in figure 3.5 the tapings were placed in an inclined sectional plane within 2cm from the centre of the cylinder. It was assumed that for two dimensional flow, such placement of tapings would not effect the results. The end tapping points were made at equal distances from the corners and the interspace between the consecutive tapping points was kept at equal distance. In the figure 3.6 tapping points are shown.

The tapings were made with copper tubes of 1.5mm outer diameter and 10mm length which were press fitted to the tapping holes. Flexible plastic tubes of 1.6mm outer diameter were used to connect the tapings to the limbs of a multimanometer. Water was used as the manometric liquid:

3.4 Experimental Procedure

The test was conducted in two phases. In the first phase pressure distribution on the cylinders with side ratio $H/D= 1.25, 1.5, 1.75$ and 2.0 were measured separately for angles of attack varying from 0° to 45° . In the second phase three rectangular cylinders of identical dimension were mounted horizontally in the staggered form with one cylinder placed centrally in the upstream side and the other two placed symmetrically in the downstream side with respect to the tunnel axis. Pressure distribution around the cylinders were measured for various combination of lateral and longitudinal spacings of the cylinders. Four sets of measurements were taken for side ratios $H/D= 1.25,$

1.5, 1.75 and 2.0.

The flow velocity in the test section was kept constant at 18.3m/sec(60 fps). The Reynolds number based on the side dimension $D= 3\text{cm}$ was 3.45×10^4 . The turbulence intensity of the tunnel was approximately 0.33%.

Before measuring the pressure distribution the mean velocity was measured in a vertical plane 60cm upstream from the cylinders by means of a pitot static tube connected to an inclined manometer with water as the manometric fluid. The measured velocity distribution was uniform which can be seen from the figure 3.8. One may also observe from the figure that, there is a velocity gradient within 4.1cm from the tunnel surface.

3.4.1 Single Cylinder

The rectangular cylinder of side dimension $H= 3.75$ was mounted centrally in horizontal plane at a distance of 1.45m (57inch) downstream from the end of the throat of the entry nozzle. The 3cm face of the cylinder was oriented normal to the flow direction. For angular orientation of the cylinders the graduated disc was used. The mean pressure distribution on the body was recorded by means of an inclined multimanometer. A pitot static tube for indicating the free stream velocity and pressure was placed centrally and 60cm ahead from the center of the cylinder.

Since pressure tappings were made only on two perpendicular surfaces of the cylinder, two-fold readings had to be taken for a complete record of pressure distributions on four surfaces by alternately placing the front surface towards the upstream and downstream direction. Mean pressure distribution was recorded at angles of attack varying from 0° to 45° with a step of 5° . It was assumed that for the prescribed flow condition the recordings of pressure distribution in this way would not differ from the pressure recorded simul-

taneously on each surface.

Pressure distributions for each of the cylinders with side dimension $H=$ 4.5, 5.25 and 6.0cm were measured in a similar manner.

3.4.2 Cylinders in Group

Three rectangular cylinders, each of side $D=$ 3cm and $H=$ 3.75cm were placed in the staggered form as shown in the figure 3.7. They were so positioned that the 3cm side of each of the cylinders were kept normal to the approach velocity direction. Initially the cylinders were mounted in such a way that the transverse spacing between the downstream cylinders and the longitudinal spacing between the front surface of downstream cylinders and back surface of the upstream cylinder were $1D$. Since the top downstream cylinder(T) and the bottom downstream cylinder(B) were symmetrically placed, the pressure distributions were considered on the bottom cylinder only.

The transverse spacings(L_t) for the downstream cylinders were altered to $1D$, $2D$ and $4D$ and for each spacing L_t , the longitudinal spacing(L_l) were set at $1D$, $2D$, $3D$, $5D$ and $7D$. Mean pressure distributions were measured for the above mentioned 15 sets and at zero angle of attack only. Pressures were measured simultaneously for both the upstream and downstream cylinders.

Pressure distributions for the cylinders with side ratios of $H/D=$ 1.5, 1.75 and 2.0 were measured in a similar manner.

CHAPTER 4

RESULTS AND DISCUSSIONS

This chapter provides with the discussions of the results of experimental investigation conducted for the flows on rectangular cylinders. The results of the pressure distribution on a single cylinder at varying angles of attack and side ratios are analysed first. At zero angle of attack the discussions regarding the results of the pressure distribution on a group of cylinders for different longitudinal and transverse spacings are made. In addition, comparative study of the existing research works and the present investigation are presented.

4.1 Single Rectangular Cylinder

Distribution of mean pressure co-efficients and variations of the aerodynamic forces on a single rectangular cylinder at varying angle of attack from 0° to 45° with a step of 5° are analysed in the following sub-sections. The effects of variable side ratios are also considered for study.

It would be relevant to show the approximate flow pattern around a rectangular prism before discussing the results of the experimental investigation. One may observe from the figure 4.1(a) the nature of the flow pattern around a rectangular prism at zero angle of attack. It can be seen from this figure that, the separation points are fixed at the leading edges and the shear layers originating from the leading corners curve outwards and a wake region is formed behind the body. The nature of formation of vortex shedding may also be seen from the same figure. When oriented at a small angle of attack to the approach flow the separated shear layer reattaches to the

windward side of the prism to form a 'separation bubble' as shown in figure 4.1(b). The mean pressure along the side under the bubble is low; near the end it rises rapidly to peak at or near reattachment.

4.1.1 Pressure Distribution

Figures 4.2 to 4.5 show the effect of angle of attack on mean pressure co-efficients around the rectangular cylinders for side ratios of $H/D= 1.25, 1.5, 1.75$ and 2.0 respectively. It is evident from these figures that the overall patterns of the C_p -distribution curves for all the rectangular bodies on all the four surfaces are similar. The C_p -distributions on the front surface of the cylinder with side ratio of 1.25 (figure 4.2) reveal that a stagnation point is established at the midpoint for angle of attack of 0° . This stagnation point is shifted towards the bottom corner of the surface with increase in angle of attack.

The pressure distribution on the windward side (bottom surface) of the cylinder at zero degree angle of attack is almost uniform throughout the surface. As the angle of attack is increased the pressure gradually falls near the front corner and rises near the rear corner on the bottom surface in comparison to that at angle of attack of 0° . This tendency is observed upto the angle of attack of 15° . The increase of pressure in the rear corner indicates the appearance of reattachment. The figure 4.2 reveals that as the angle of attack is increased further, the location of the highest pressure at each angle gradually shifts towards the front corner with increasing magnitude.

On the leeward side (top surface) of the cylinder as the figure 4.2 shows, an almost uniform pressure distribution exists over the whole length of the side for each angle of attack. From this figure one may note that as the angle of attack increases from 0° to 10° the values of C_p increases but with

further rise of angle of attack value, it starts to decrease. It may be observed that the pressure distributions on the back surface reveal a similar trend.

In the case of a sharp edged body like a rectangular cylinder, the separation points are fixed at the leading edges and thus the shear layers originating at the front corner curve outward and there appear the formation of familiar vortex shedding in the wake region behind the body. The free shear layers are basically unstable and roll up to form discrete vortices. The growing vortices draw in fluid from the base region and it is suggested that it is this continual entrainment process that sustain the low back pressure. In fact the magnitude of the back pressure is determined almost solely by the manner in which the shear layers leave the body and roll up to form discrete vortices. Thus a low base pressure is associated with vortex formation close to the body while a high base pressure (less negative value) is caused by vortex formation further away. The rise in pressure with increase of angle of attack in the lower range at the back surface of the rectangular body as the figure 4.2 shows, happens due to vortex formation at larger distance from the back side and the fall in pressure with further increase of angle of attack occurs due to vortex formation at smaller distance from the back surface.

The nature of the C_p -distribution curves which are presented in the figures 4.3 to 4.5 are similar to that of the figure 4.2. The patterns of the curves shown in the figures 4.3 to 4.5 may be explained in a similar manner as in the case of the figure 4.2.

The effect of side ratios (H/D) on the C_p -distributions for windward side(bottom surface) of rectangular cylinders at angles of attack of 0° , 5° , 10° , 15° and 30° are shown in the figure 4.6. It is clearly seen from the figure 4.6(a) that there is rise in pressure with the increase in the side

ratio(H/D) of rectangular cylinders at 0° angle of attack. Due to the increase of side ratio of the cylinder, the curvature of the shear layer originating from the front surface corner probably decreases which results in the rise of pressure. From figure 4.6(b) one may observe that there is also rise of pressure as the side ratio value increases. This rise of pressure occurs at a higher rate towards the rear corner of the surface. Figure 4.6(c) reveals that reattachment of flow towards the rear corner appear for the cylinder with side ratio of $H/D= 1.75$ and 2.0 at 10° angle of attack. Also the location of the minimum value of C_p shifts towards the front corner with the increase of side ratios of the cylinders. Reattachment of flow towards the rear corner of the bottom surface is prominent at all side ratios of the cylinders for 15° angle of attack as shown in the figure 4.6(d). One may observe that the peak C_p -values are shifted towards the front corner with the increase in the side ratio of the rectangular cylinders. At 30° angle of attack it is seen that for side ratio $H/D= 1.75$ and 2.0 the peak C_p -value is almost at the front corner suggesting separated flow.

The effect of side ratios on C_p -distributions on the back surface of cylinder at angles of attack of 0° , 10° , 20° , 30° and 45° are shown in the figure 4.7. It is seen that at 0° angle of attack (figure 4.7a) minimum C_p -values exists for side ratio $H/D= 1.25$ and it rises with the increase in side ratio. But with the increase in angle of attack it is seen that ultimately at 45° angle of attack (figure 4.7e) highest C_p -values occur for side ratio $H/D= 2.0$. However, from figure 4.7(d) it can be observed that at 30° angle of attack the C_p -distributions for all side ratios are very close.

The C_p -distribution curves on the windward side of a square cylinder at various angles of attack obtained by J.M.Robertson[41] for turbulence intensity of 0.33% and free stream velocity of 18m/sec are compared with those ob-

tained for the rectangular cylinder with side ratio of $H/D = 1.25$. in the figure 4.8. Since the experiment was not conducted for the side ratio(H/D) of 1.0, the experimental results on the rectangular cylinder with the closer side ratio of 1.25 from the present investigation are compared with the existing experimental results of side ratio(H/D) of 1.0. It is assumed that this correlation would give an approximate idea regarding the proximity of the present experimental results with the existing one. It is observed from the figure that the nature of pressure distribution at various angles of attack are quite similar but the C_p -values of the present experiment are higher for each angle of attack. It is seen from the trend of the curves in the previous figure 4.6 that in general due to the rise of side ratio the C_p -values rises which obviously justifies the nature of the correlation shown in the figure 4.8.

4.1.2 Aerodynamic Forces

The variation of drag co-efficient(C_D) for different side ratios(H/D) with angles of attack from 0° to 45° is shown in the figure 4.9. It can be seen from this figure that for all side ratios the general trend of drag variation occur in such a way that with the increase of angle of attack the drag co-efficient falls and becomes minimum in the region of angle of attack 8° to 12° and subsequently with further increase of angle of attack its value rises sharply upto the angle of attack of 45° . Furthermore, it can be seen from this figure that there occur remarkable variation of the drag co-efficients for the different side ratios of the cylinders. It is already mentioned that as the angle of attack increases the vortex formation occurs at larger distance thereby creating higher back pressure which is mainly the cause of lower drag with increased value of angle of attack. For further increase of angle of attack vortex formation appear closer to the back surface

of the body making the back pressure lower which is mainly the reason of higher drag for the increased value of angle of attack in the higher range. In the lower range of angle of attack, as the side ratio of the cylinder increases, reattachment of the shear layer occurs towards the rear corner which probably forces the vortices to form further downstream thereby creating higher back pressure and consequently lower drag as the figure 4.9 shows.

Comparison is also made in the figure 4.9 with the experimental results presented by A.C.Mandal[26] for a square section cylinder placed in a uniform flow with a turbulence intensity of 0.4%. The variation of drag co-efficient for side ratio $H/D=1$ follows the general trend already observed in case of the other cylinders. However, a good correlation is observed for the cylinders with side ratios of $H/D=1.25$ and 1.0 .

The variation of lift co-efficient(C_L) with angle of attack for different side ratios(H/D) is shown in the figure 4.10. The general trend in the variation of lift is similar to that of drag with angle of attack. The variation of lift co-efficient presented by A.C.Mandal[26] for side ratio of $H/D=1$ shown in this figure also follows a similar trend. The high negative lift at small angle of attack is associated with the formation of large enclosed separation bubble on the bottom surface of the cylinder which caused higher local suction than those on the top surface. As mentioned earlier the reattachment point on the bottom surface shifts towards the front corner with increase in the angle of attack thereby reducing the size of the separation bubble. This results in rise of lift co-efficient for further increase in angle of attack. However, beyond 25° angle of attack no appreciable change in lift occurs with increase in angle of attack for all the cylinders.

Figure 4.11 shows the variation of total force co-efficients(C_F) with angle of attack for different side ratios including that presented by

A.C.Mandal[25] for a square section cylinder. It is observed from this figure that around the angle of attack of 10° , there appear the minimum value of total force co-efficient. The trend of the curves in this figure may be explained from the figures 4.9 and 4.10.

4.1.3 Effect of Side Ratio on Drag

The variation of drag co-efficient with side ratios at an angle of attack of 0° is shown in the figure 4.12. Comparison is also made in this figure with the experimental results presented by P.W.Bearman and Trueman[4] for turbulence intensity of 0.3% and those by Bostock[6]. The experimental results provided by P.W.Bearman was for the range of side ratios of 0.2 to 1.25 while the results available for the present study is from 0.5 to 2.0, and hence comparison of drag beyond H/D of 1.25 is not included. It can be said that there is good correlation of the results within the common range of side ratios. It may be mentioned that the level of turbulence from the results produced by Bostock is unknown though the correlation is good.

It is seen from the figure 4.12 that drag rises to a maximum value with increase in side ratio upto about $H/D = 0.6$ and then it rapidly falls with further increase in side ratio. Maximum C_D found by Bearman and Trueman was about 2.94 when H/D was just over 0.6. The maximum value of C_D found in the present study is 2.85. The rise in drag co-efficient in the range of small side ratios is probably due to the reduction in the size of the separated wake cavity with increase in side ratio leading to gradual decrease in back pressure and thus the drag co-efficient is increased. It may be mentioned here that due to the rise of side ratio in the smaller range, there appear no reattachment on the side face of the body and hence the distance of the vortex formation is not shifted towards the downstream side; on the contrary due to the increase of

side ratio the distance between the back surface and the vortex formation become shorter. According to the figure the fall in drag for further rise in side ratio is associated with the direct interference of the downstream edge with the shear layer causing reattachment and thus the vortex formation is delayed further downstream.

4.2 Staggered Rectangular Cylinders

The distribution of mean pressure co-efficients and variations of the aerodynamic forces on the rectangular cylinders arranged in the staggered form at 0° angle of attack are presented in the following sub-sections. The effect of variable side ratios are also taken into account for analysis.

4.2.1 Pressure Distribution on Upstream Cylinder

The pressure distribution around the upstream cylinder with side ratio of $H/D = 1.25$ for varying longitudinal spacing L_1 keeping the transverse spacing constant at $L_t = 1D$ is shown in the figure 4.13. It is observed from this figure that for each longitudinal spacing L_1 , the pressure distributions on the top and bottom surfaces are symmetrical. It may be noted that at $L_1 = 7D$, the pressure on the back, top and bottom surfaces are lowest. As the upstream cylinder is brought closer to the downstream cylinders the pressures tend to increase on all these surfaces upto the spacing $L_1 = 1D$. However, there is no change in the distribution of pressures on the front face for all variations of longitudinal spacing L_1 for obvious reasons.

As a result of the interference due to the proximity of the cylinders, the flow becomes turbulent. This leads to the exchange of momentum between the fluid particles as a result of which rapid pressure recovery occurs on the top, bottom and back surfaces of the upstream cylinder. With the increase in

distance(L_1) this effect is minimized. At $L_1 = 7D$ it becomes very small and the pressure distributions at this distance ($L_1 = 7D$) approaches to those on an isolated cylinder.

The figure 4.14 shows the effect of longitudinal spacing(L_1) on mean pressure co-efficients for upstream cylinder at constant transverse spacing of $L_t = 2D$. It can be noticed that pressure for $L_1 = 2D$ are appreciably higher than those at $L_1 = 1D$ and even the pressures for $L_1 = 3D$ are slightly higher on the side walls. For transverse spacing of $L_t = 2D$ the downstream cylinders probably interfere very less with the wake created by the upstream cylinder when $L_1 = 1D$. At $L_1 = 2D$ the interference is remarkably higher thereby making higher pressure recovery while with further increase of L_1 the interference gradually diminishes.

The C_p -distributions with different longitudinal spacings for constant transverse spacing(L_t) of $4D$ are shown in the figure 4.15. It is revealed that low C_p values exist for spacing of $L_1 = 1D$ on both the top and bottom walls but the variations are not marked for greater longitudinal distance. It is observed from the pressure distribution curves on the top and bottom surfaces that except at $L_t = 1D$, there appear considerable interference in the flow.

The figures 4.16 to 4.18, 4.19 to 4.21 and 4.22 to 4.24 show the C_p -distributions for the side ratio(H/D) of 1.5, 1.75 and 2.0 respectively. For each side ratio pressure distributions are given with three transverse spacings $L_t = 1D$, $2D$ and $4D$. For transverse spacings of $1D$ and $2D$, more or less similar pattern of C_p -distributions are observed for the cylinders with side ratios of 1.25, 1.5, 1.75 and 2.0. But for $L_t = 4D$ a marked variation in the distribution of pressure is observed among the cylinders. One may notice from the figures 4.18, 4.21 and 4.24 that there are high negative value C_p near the upstream corner while there appear substantial pressure recovery towards the

downstream corner of the top and bottom surfaces at longitudinal spacing of $1D$. However, similar nature is also observed at longitudinal spacing of $2D$ for cylinders with side ratios of 1.75 and 2.0 only. Probably the turbulence intensity of the flow is increased significantly due to the interference effect produced by downstream cylinder at L_t of $4D$. It may be mentioned that similar nature of curve was obtained by Barriga[3] with 10% turbulence intensity.

4.2.2 Variation of Drag for Upstream Cylinder

The variation of drag co-efficient with longitudinal spacings on upstream cylinder for different side ratios is shown in figure 4.25, keeping the transverse spacing(L_t) constant at $1D$. The figure reveals that with the increase of longitudinal spacing the drag co-efficient increases in the lower range, while in the higher range the change is not prominent. It is also observed from this figure that as the side ratio increases the drag decreases. The variation of drag co-efficient with longitudinal spacing on square section upstream cylinder presented by A.C.Mandal[26] is also shown in this figure for transverse spacing $L_t = 1D$. It is observed from this figure that in the higher range of longitudinal spacing the cylinder with side ratio(H/D) of 1.0 experience maximum drag. The pattern of the curves in this figure may be explained from the pressure distribution curves presented in the figures 4.13, 4.16, 4.19 and 4.22.

Figure 4.26 show the variation of drag co-efficient(C_D) for constant transverse spacing $L_t = 2D$. The trend in drag co-efficient is similar to that of spacing $L_t = 1D$ except that minimum drag co-efficient is observed close to longitudinal spacing of $L_1 = 2D$ for the cylinder with side ratio of $H/D = 1.25$. According to this figure nearly uniform drag is observed beyond spacing $L_1 = 3D$. It is also revealed from this figure that the drag is considerably lower

at spacing $L_1 = 1D$ and $2D$ compared to those at transverse spacing $L_t = 1D$ (figure 4.25). It is seen from this figure that the variation of drag coefficient with longitudinal spacing for a square section cylinder presented by A.C.Mandal[27] follows the general trend observed for the cylinders with higher side ratios.

Figure 4.27 show the variation of drag with longitudinal spacing for different side ratios of the cylinders at constant transverse spacing $L_t = 4D$. It is seen from this figure that drag falls to a minimum value close to spacing $L_1 = 2D$ for all the cylinders. Also, contrary to the previous figures, highest drag is observed for spacing $L_1 = 1D$. However, highest drag is observed beyond $L_1 = 3D$ for the cylinder with side ratio of $H/D = 1.25$. The drag changes very little beyond longitudinal spacing $L_1 = 3D$ for all the cylinders. It is seen from this figure that in case of square section cylinder[27] minimum drag occurs close to longitudinal spacing $L_1 = 2D$ and highest drag is observed beyond spacing $L_1 = 3D$. From figures 4.25 to 4.27 it is evident that the cylinder with side ratio of $H/D = 2.0$ experiences lowest drag at all combinations of longitudinal and transverse spacings.

4.2.3 Pressure Distribution on Downstream Cylinder

The C_p -distributions on the bottom downstream cylinder with side ratio of $H/D = 1.25$ for varying longitudinal spacing (L_1) keeping the transverse spacing constant at $L_t = 1D$ is shown in the figure 4.28. It is observed from this figure that when $L_1 = 1D$ the value of C_p rises close to unity on the front surface near the bottom corner. For the spacings of $L_1 = 2D$ and $3D$ the pressures on the front surface are negative and show a rising tendency towards the bottom corner. For larger longitudinal spacings the pressures on the front surface are positive but they differ much from those on the front surface of an

isolated cylinder.

When the downstream cylinder is closer to the upstream one, the front face of that cylinder remains in the wake region created by the upstream body which is the cause of negative pressure on the front face. However, for spacing $L_1 = 1D$ the bottom corner of the downstream cylinder does not fall in the wake region of the upstream cylinder and thus a stagnation point is established near that corner.

Observing the pressure distribution on the top surface of the cylinder it is found that for spacing $L_1 = 2D$ and $3D$ nearly uniform distribution of pressure occur throughout the surface. However, for spacing $L_1 = 1D, 5D$ and $7D$ higher negative pressure at the front corner and pressure recovery at the rear corner is observed. The variation of C_p -distribution on the bottom surface is quite different. For longitudinal spacing of $L_1 = 1D$ uniform pressure exists throughout the surface. While for larger spacings pressure is very low at the front corner with rapid increase in pressure towards the rear corner indicating the tendency of reattachment.

The figure 4.28 also reveals that pressure distribution on the back surface of the cylinder for longitudinal spacing of $L_1 = 1D$ is low followed by a rise in pressure for spacings $L_1 = 2D$ and $3D$. However, for higher spacings again the value of pressure drop. It would be relevant to mention that due to the symmetry of flow the pressure distributions on the top downstream cylinder are identical.

The figures 4.29, 4.30 and 4.31 show the variation of C_p -distribution due to the effect of longitudinal spacings of $L_1 = 1D, 2D, 3D, 5D$ and $7D$ for downstream cylinder with side ratio (H/D) of 1.5, 1.75 and 2.0 respectively keeping the transverse spacing constant at $1D$. One may observe from the figures 4.28 to 4.31 that for all side ratios from 1.25 to 2.0, nearly similar

trend of pressure distribution appear. On the front surface of all the cylinders with side ratio of 1.5, 1.75 and 2.0 negative C_p -values are observed for $L_1 = 1D$ and $2D$ with a rise in pressure towards the bottom corner. While the same tendency was observed in case of the cylinder with side ratio of $H/D = 1.25$ for distance $L_1 = 2D$ and $3D$. However, the nature of pressure curve for spacing $L_1 = 1D$ is unique to the cylinder with $H/D = 1.25$. The figures 4.28 to 4.31 also reveal that another deviation from the general trend of pressure distribution occur which is uniform on the bottom surface at $L_1 = 1D$ for the cylinder with side ratio of 1.25.

The variation of C_p -distributions on the downstream cylinder with longitudinal spacing (L_1) for constant transverse spacing $L_t = 2D$ is shown in the figure 4.32. No negative C_p -value is observed on the front surface of this cylinder at all longitudinal spacings. Pressure on the front face is higher at small spacings ($L_1 = 1D, 2D$) and gradually decreases for larger spacings. This is probably because the downstream cylinders lie outside the influence of wake produced by the upstream cylinder at small spacings. However, as the longitudinal spacing is increased the front surface is effected by wake but in small amount.

Distribution of pressure on the top surface reveals that for longitudinal spacing of $L_1 = 1D$ and $2D$ tremendously high negative C_p exists towards the front corner with a sharp rise in pressure towards the rear suggesting reattachment. Figure 4.32 further shows that at longitudinal spacing of $L_1 = 3D, 5D$ and $7D$ pressure rises significantly at the front corner and continues to rise towards the rear.

As shown in the figure 4.32 the pressure curves on the bottom surface of the cylinder with side ratio of 1.25 are almost uniform for spacings $L_1 = 1D, 2D$ and $3D$. Further increase in the longitudinal spacing causes the pres-

sure to fall considerably near the front corner and rise towards the rear corner.

It can be seen from the figure 4.32 that as the longitudinal spacing(L_1) increases the C_p -values on the back surface rises. At the spacing $L_1 = 1D$ the front face of the bottom cylinder remains almost unaffected due to the wake generated by the upstream cylinder which may also be revealed from the C_p -distribution curve on the front face of this cylinder. Of course the top surface is in the wake region. Hence the C_p -values on the back surface at $L_1 = 1D$ is nearly similar to that of an isolated cylinder. However, with increase in longitudinal spacing the front face of the bottom cylinder fall in the wake region and the flow become probably more turbulent and the pressure at the back surface rises gradually.

The pressure distribution around the rectangular cylinders with side ratios of $H/D = 1.5, 1.75$ and 2.0 are shown in the figures 4.33, 4.34 and 4.35 respectively for the same transverse distance $L_t = 2D$. The pattern of C_p -distributions on the front surfaces of the cylinders are quite similar.

The nature of pressure distributions on the top surfaces with side ratios $1.5, 1.75$ and 2.0 are similar to those with side ratio $H/D = 1.25$. However, with side ratio(H/D) of 2.0 there occur a deviation of C_p -curve and it becomes rather of uniform nature for $L_1 = 2D$. It may be observed that at $L_1 = 1D$ and $H/D = 1.25$ there is the maximum negative C_p -value.

From the pressure distributions on the bottom surfaces of these cylinders as the figures 4.33, 4.34 and 4.35 shows, there exists low pressures near the front corner and pressure recovery takes place towards the rear for spacings $L_1 = 3D, 5D$ and $7D$. For small spacings pressure distribution for the cylinders with side ratios of $H/D = 1.25, 1.5$ and 2.0 are similar. However, for the cylinder with side ratio $H/D = 1.75$ significantly large negative C_p -value

occurs near the front corner at longitudinal spacing of $L_1 = 2D$ and at this spacing uniform pressure distributions are observed in the case of the other cylinders. Again for the cylinder with side ratio $H/D = 1.75$ lowest pressure on the back surface is observed for spacing $L_1 = 2D$. However, the nature of pressure distribution curves on the back surfaces of the other cylinders are more or less similar to that with $H/D = 1.25$. The pressure distributions on the front surfaces of each of the cylinders are of similar nature.

The figure 4.36 shows the pressure distributions about the rectangular cylinder with side ratio of $H/D = 1.25$ for constant transverse spacing of $L_t = 4D$. For all longitudinal spacings the C_p -distributions on the front face are very close to those for the isolated cylinder because the front face is almost out of the influence of wakes created by the upstream cylinder. The pressures on the top and bottom surfaces are very low but quite uniform for longitudinal spacings of $L_1 = 1D$ and $2D$. With the increase in longitudinal distance rapid rise of pressure takes place near the rear corner on the top surface. However, little change in C_p -distribution along the length of the bottom surface is observed with increase in longitudinal distance.

The C_p -distributions around the cylinders with side ratios of $H/D = 1.5$, 1.75 and 2.0 are shown in the figures 4.37, 4.38 and 4.39 respectively. The pressure distributions on the front surfaces are similar but with the side ratio of $H/D = 2.0$ the pressures are comparatively lower for larger longitudinal spacing suggesting relatively higher influence of wake produced by upstream cylinder. On the top surface of each cylinder low pressure exists near the front corner at all longitudinal spacings. However, rise in pressure towards the rear corner at all longitudinal spacings is observed only for the cylinders with side ratio of $H/D = 1.75$ and 2.0 . On the bottom surface reattachment tendency is observed with higher side ratios. The back surface pres-

sure increases with the increase in longitudinal distance in case of all the cylinders. As mentioned previously this may be due to increased turbulence effect.

4.2.4 Drag on Downstream Cylinder

The variation of drag co-efficients with longitudinal spacing(L_1) on downstream cylinder for different side ratios is shown in the figure 4.40 at constant transverse spacing of $L_t = 1D$. The figure also includes the variation of drag co-efficients with longitudinal spacing on downstream square section cylinder presented by A.C.Mandal[26] for the same transverse spacing. It is seen from this figure that for all the cylinders drag is low in the smaller range of longitudinal spacings while in the larger range it is high. However, for the cylinder with side ratio of $H/D = 1.25$ highest drag is observed at the lowest longitudinal spacing of $L_1 = 1D$ followed by a rapid fall in drag with small rise of L_1 . It would be interesting to note from this figure that as the side ratio increases the drag value at the lowest longitudinal spacing decreases. It can be seen from this figure that the variation of drag on square section cylinder follows the general trend observed for the cylinders with higher side ratios. From the nature of the pressure distribution curves presented in the figures 4.38 to 4.31, the patterns of the drag curves shown in the figure 4.40 may be explained.

The figure 4.41 show the variation of drag co-efficient with longitudinal spacing for constant transverse spacing of $L_t = 2D$. From this figure it is observed that low drag at large spacings(L_1) and high drag at small spacings are developed which is opposite to the nature of drag found for transverse spacing of $L_t = 1D$. This general trend is also observed in the case of cylinder with side ratio $H/D = 1.0$ presented by A.C.Mandal[27] which is shown in the same figure. However, comparison of the figures 4.40 and 4.41

shows that the drag for $L_t = 2D$ at any longitudinal spacing is always higher than that for $L_t = 1D$ at the corresponding longitudinal spacing. This behaviour of drag for the side ratios of 1.25, 1.5, 1.75 and 2.0 is easily understandable from the nature of pressure distributions on the front and back surfaces of the cylinders shown in the figures 4.32, 4.33, 4.34 and 4.35 respectively. From the figure 4.41 one may also notice that for the side ratio of 2.0 the nature of the drag curve deviate from the general trend of the drag curves for the other side ratios. For $H/D = 2.0$ at $L_1 = 2D$ drag rather increases slightly. High drag at spacing $L_1 = 2D$ is also observed for the cylinder with side ratio $H/D = 1.0$.

The variation of drag co-efficients with longitudinal spacing for constant transverse spacing of $L_t = 4D$ is shown in the figure 4.42. It is observed from this figure that the drag in general drops, as the longitudinal spacing increases. However, at $L_1 = 2D$ there occur slight deviation from the general trend of the curves. It may be noticed from this figure that the variation of drag on square section cylinder[27] follows the general trend more closely.

An overall observation from the figures 4.40, 4.41 and 4.42 can be made as that the cylinder with side ratio of $H/D = 2.0$ experiences minimum drag.

4.2.5 Lift on Downstream Cylinder

The variation of lift co-efficient with longitudinal spacing(L_1) on the downstream rectangular cylinders is shown in the figure 4.43 at constant transverse spacing of $L_t = 1D$. It is seen from this figure that negative lift exists on each of the cylinders for all longitudinal spacings and side ratios except for side ratio(H/D) of 1.25 at $L_1 = 1D$. The negative lift is due to the extremely low pressure region near the front corner of the bottom surface of all the cylinders for all longitudinal spacings as revealed from the figures

4.28, 4.29, 4.30 and 4.31. In contrast to this development A.C.Mandal[26] showed that square cylinder experienced a quite uniform positive lift at all longitudinal spacings which may be seen from this figure as well. However, the figure 4.43 shows that a uniform but negative lift is only produced on the cylinder with side ratio of $H/D= 2.0$ at all longitudinal spacings.

The figure 4.44 shows the variation of lift co-efficients with longitudinal spacing for constant transverse spacing of $L_t= 2D$. It is noted from this figure that the cylinders with side ratios of $H/D= 1.25$ and 1.5 experience positive lift in the lower range of longitudinal spacings while for the same range the cylinders with side ratios of 1.75 and 2.0 develop negative lift. The figure 4.44 reveals that close to the longitudinal spacing of $L_1= 2D$ a large positive lift is developed on the cylinder with side ratio of $H/D= 1.25$ whereas a high negative lift is produced on the cylinder with side ratio of $H/D= 1.75$. The large negative lift developed on the cylinder with side ratio of $H/D= 1.75$ is due to the tremendously high suction produced near the front corner of the bottom surface at spacing $L_1= 2D$ as shown in the figure 4.34. The reverse phenomena is observed on the top surface of the cylinder with side ratio of $H/D= 1.25$ at longitudinal spacings of $L_1= 1D$ and $2D$ as revealed from the figure 4.32. A.C.Mandal[27] in his paper showed that a large negative lift was developed on square section cylinder for longitudinal spacings of $L_1= 1D$ and $2D$ which can be seen from this figure.

The figure 4.45 reveals the variation of lift co-efficient with longitudinal spacing at constant transverse spacing of $L_t= 4D$. It is observed from this figure that positive lift is developed on all the cylinders at small spacings ($L_1=1D, 2D, 3D$) whereas negative lift is produced at larger spacings. The reason is easily understandable from the figures 4.36, 4.37, 4.38 and 4.39. Contrary to the present finding A.C.Mandal[27] showed that square sec-

tion cylinder experienced negative lift for almost all longitudinal spacings which can be observed from the figure 4.45.

4.3 Observation of Pressure Fluctuations

During recording of the pressure, fluctuation of liquid in the manometer limbs was always observed. Negligible fluctuation was observed for the test on a single cylinder oriented at an angle of attack of 0° . While in the higher range of angle of attack fluctuation of pressure slightly increased, specially on the windward surface; but the difference between the maximum and minimum liquid column observed in the manometer limb never exceeded 0.4cm(0.15inch). When three cylinders were considered, fluctuations increased appreciably on the downstream cylinder and the maximum fluctuation observed was of the order of 0.63cm (0.25inch). However, for this test, always mean pressure was recorded with careful observation.

4.4 Effect of Reynolds Number

Besides extremely low Reynolds number it has been shown by tests carried over a wide range of Reynolds number that the flow pattern around a sharp-edged body is relatively insensitive to Reynolds number. This is because the positions of the flow separations are fixed by the sharp edges. R.W.Davis[8] showed that for Reynolds number less than 1000 the flow around rectangular cylinders was strongly dependent on Reynolds number. In case of extremely low Reynolds number flow reattachment occurs immediately after separation from the front corner and finally it separates at the trailing edges. With an increase of Reynolds number flow separation occurs at the leading edges and henceforth flow pattern becomes independent of Reynolds number. However, in case of reattachment appearing for the change of angle of attack

and the side ratio of rectangular cylinder, the effect of Reynolds number may not be ignored.

4.5 Blockage Corrections

The presence of a body in the wind tunnel test section reduces the flow area and thereby increases the velocity of air as it flows around the body. This increase of velocity due to the presence of the body is called solid blocking. The wake behind a body has a mean velocity lower than the free stream. According to the law of continuity, the velocity outside the wake must be higher than free stream so that a constant volume of fluid may pass through the tunnel test section. According to Bernoulli's principle this increase in speed is balanced by a decrease in static pressure of the mainstream. Consequently, since the static pressure within the wake is governed by that of the steady airstream immediately adjacent to the boundary of the wake, the static pressure at the back surface of the body tends to be less than it would be if the airstream were unconfined. Due to this wake blocking and solid blocking, blockage corrections are required to obtain accurate values of non-dimensional co-efficients. Investigation of this effect has shown that sufficient accuracy in results are obtained for models occupying less than 10% of the tunnel working section area.

The total solid and wake blockage corrections are summed to get the total blockage corrections. According to Pope and Harper[38] the total blockage corrections to C_p would be approximately of the order of half times the blockage percentage. In the present study maximum blockage percentage was around 13.9% for the single cylinder with side ratio 2.0 at 45° angle of attack. The downstream cylinders in the staggered form occupied a blockage area of 13%. No blockage corrections were made because the corrections needed

are small and also any corrections would make the co-efficient 'less conservative(i.e. the value of C_p would be more positive).

CHAPTER 5

CONCLUSIONS AND RECOMMENDATIONS

This chapter presents the conclusions drawn from the experimental investigation of flow around rectangular cylinders. The scope of extension and development of the present study are also included in this chapter.

5.1 Conclusions

(1) At an angle of attack of 0° , no flow reattachment occurs on the surfaces of each isolated rectangular cylinder. However, the C_p -values on the top, bottom and back surfaces rises with the increase in side ratio of the rectangular cylinders.

(2) Flow reattachment occurs on the windward(bottom) surface of the rectangular cylinder at small angle of attack and the reattachment location shifts from the rear corner towards the front corner of the windward surface with increase in angle of attack.

(3) Flow reattachment commences at smaller angle of attack if the side ratio is increased.

(4) At small angle of attack the C_p -value decreases considerably near the front corner of the windward(bottom) surface of each cylinder and the negative peak value of C_p is shifted towards the front edge with increase in the side ratio.

(5) The minimum drag on the rectangular cylinders occur within 8° and 12° angle of attack for all side ratios. Also within this range of angle of attack total force developed on the rectangular cylinder is minimum for any side ratio.

(6) The drag on a rectangular cylinder oriented at 0° angle of attack rises with the increase in side ratio upto about 0,6, then decreases with further increase in the side ratio.

(7) Higher suction is developed near the frontal region of top and bottom surfaces of the upstream cylinder in a group at transverse spacing $L_t = 4D$ and longitudinal spacing $L_l = 1D$.

(8) The C_p -distributions on the front face of the downstream cylinders with side ratios of $H/D = 1.5, 1.75$ and 2.0 are negative for $L_t = 1D$ and $L_l = 1D$ and $2D$. However, in case of the cylinder with side ratio of $H/D = 1.25$ and at $L_t = 1D$, a stagnation point is established at the bottom corner of the front face for $L_l = 1D$, while negative C_p is developed for spacing $L_l = 2D$ and $3D$.

(9) The C_p -values are considerably low near the frontal region of the bottom surface of the downstream cylinders with side ratios of $H/D = 1.5, 1.75$ and 2.0 for all longitudinal spacings (L_l) when transverse spacing $L_t = 1D$.

(10) Very high negative pressure is developed on the top surface of the downstream cylinder for all side ratios at $L_t = 2D$ and $L_l = 1D$. The maximum negative C_p occur at H/D of 1.25 which is -2.85 .

(11) In the staggered form drag is lower on rectangular cylinders with higher side ratios.

(12) The drag on an isolated cylinder is higher in general than that on the same cylinder while it becomes part of a group.

5.2 Recommendations

(1) The same experiment can be done with flow visualization technique to get a better understanding about the formation of wakes and vortex shedding pattern.

(2) Experiment can be performed on surface mounted rectangular cylinders within the boundary layer.

(3) Investigation of flow around staggered rectangular cylinders at different angles of attack may be done.

(4) The effect of surface roughness on the flow over isolated and group of rectangular cylinders can be investigated.

(5) The effect of Reynolds number on staggered cylinders with varying side ratios may be investigated.

(6) Building models of various other shapes and sizes can be brought under this kind of investigation.

REFERENCES

REFERENCES

- [1] Achenback, E. "Distribution of Local Pressure and Skin Friction Around a Circular Cylinder in Cross Flow up to $Re = 5 \times 10^6$ ", *Journal of Fluid Mechanics*, vol.34, 1968, p.625-639.
- [2] Baines, W.D., "Effects of Velocity Distribution on Wind Loads and Flow Patterns on Buildings", *Proceedings of a Symposium on Wind Effects on Buildings and Structures*, U.K., 1963, p.197-225.
- [3] Barriga, A.R., Crowe, C.T. and Roberson, J.A., "Pressure Distribution on a Square Cylinder at a Small Angle of Attack in a Turbulent Cross Flow", *Proceedings of the 4th International Conference on Wind Effects on Buildings and Structures*, London, U.K., 1975, p.89-93.
- [4] Bearman, P.W. and Trueman, D.M., "An Investigation of the Flow Around Rectangular Cylinders", *The Aeronautical Quarterly*, vol.23, 1972, p.229-237.
- [5] Bearman, P.W. and Wadcock, A.J., "The Interaction Between a Pair of Circular Cylinders Normal to a Stream", *Journal of Fluid Mechanics*, vol.61 1973, p.499-511.
- [6] Bostock, B.R. and Mair, W.A., "Pressure Distributions and Forces on Rectangular and D-shaped Cylinders", *The Aeronautical Quarterly*, vol.23, 1972, p.1-5.
- [7] Castro, I.P. and Robins, A.G., "The Flow Around a Surface Mounted Cube in Uniform and Turbulent Streams", *Journal of Fluid Mechanics*, vol. 79 1977, p. 307-335.
- [8] Davis, R.W. and Moore, E.F., "A Numerical Study of Vortex Shedding from Rectangulars", *Journal of Fluid Mechanics*, vol.116, p.475-506.
- [9] Faruque, O., "Experimental Investigation of Two Dimensional Wakes Behind Flat Plates", *M.Sc.Thesis*, BUET, November, 1983.
- [10] Frank, N., "Model Law and Experimental Technique for Determination of Wind Loads on Buildings", *Proceedings of the 1st International Conference on Wind Effects on Buildings and Structures*, Teddington, London, 1963 p. 181-189.
- [11] Gandemer, J., "Wind Environment Around Buildings: Aerodynamic Concepts", *Proceedings of the 4th International Conference on Wind Effects on Buildings and Structures*. London, U.K., 1975, p.423-432.

- [12] Gerrard, J.H., "The Mechanics of the Formation Region of Vortices Behind Bluff Bodies", *Journal of Fluid Mechanics*, vol.25, 1966, p.401-413.
- [13] Hasan, A., "Study of Turbulent Boundary Layer in a Step Change from Smooth to Rough Surface", *M.Sc. Thesis*, BUET, 1984.
- [14] Hayashi, M., Akirasakurai and Yujiohya, "Wake Interference of a Row of Normal Flat Plates Arranged side by side in a Uniform Flow", *Journal of Fluid Mechanics*, vol.164, 1986, p. 1-25.
- [15] Hua, C.K., "The Behaviour of Lift Fluctuations on the Square Cylinders in the Wind Tunnel Test", *Proceedings of the 3rd International Conference on Wind Effects on Buildings and Structures, Tokyo, Japan, 1971*, p. 911-920.
- [16] Huot, J.P., Rey, C. and Arby, H., "Experimental Analysis of the Pressure Field Induced on a Square Cylinder by a Turbulent Flow", *Journal of Fluid Mechanics*, vol.162, 1986, p.283-298.
- [17] Kelnhoffer, J., "Influence of a Neighbouring Building on Flat Roof Wind Loading", *Proceedings of the 3rd International Conference on Wind Effects on Buildings and Structures*, Tokyo, Japan, 1971, p.221-230.
- [18] Koenig, K. and Roshko, A., "An Experimental Study of Geometrical Effects on the Drag and Flow Field of two Bluff Bodies Separated by a Gap", *Journal of Fluid Mechanics*, vol.156, 1985, p.167-204.
- [19] Laneville, A., Gartshore, I.S. and Parkinson, G.V., "An Explanation of some Effects of Turbulence on Bluff Bodies". *Proceedings of the 4th International Conference on Wind Effects on Buildings and Structures, London, U.K., 1975*, p.333-341.
- [20] Laneville, A. and Parkinson, G.V., "Effects of Turbulence on Galloping of Bluff Cylinders", *Proceedings of the 3rd International Conference on Wind Effects on Buildings and Structures, Tokyo, Japan, 1971*, p.787-797.
- [21] Lawson, T.V., *Wind Effects on Buildings*, vol.1, Applied Science Publisher Ltd., London, 1980.
- [22] Lee, B.E., "The Effect of Turbulence on the Surface Pressure Field of a Square Prism", *Journal of Fluid Mechanics*, vol.69, 1975, p.263-282.
- [23] Leutheusser, J., "Static Wind Loadings of Grouped Buildings", *Proceedings of the 3rd International Conference on Wind Effects on Buildings and Structures, Tokyo, Japan, 1971*, p.211-220.
- [24] Macdonald, A.J., *Wind Loading on Buildings*, Applied Science Publishers

Ltd., London.

- [25] Mandal, A.C., "A Study of Wind Effects on Square Cylinders", *M.Sc. Thesis* BUET, 1979.
- [26] Mandal, A.C., Islam, O., "A Study of Wind Effect on a Group of Square Cylinders with Variable Longitudinal Spacings", *Mechanical Engineering Research Bulletin*, vol.3, No.1, 1980.
- [27] Mandal, A.C., Islam, O., "A Study of Wind Effect on a Group of Square Cylinders with Variable Transverse and Longitudinal Spacings", *Journal of the Institution of Engineers, Bangladesh*, vol.9, No.1, Jan. 1981.
- [28] Matsumoto, M., "The Dynamical Forces Acting on the Vibrating Square Prism in a Steady Flow", *Proceedings of the 3rd International Conference on Wind Effects on Buildings and Structures*, Tokyo, Japan, p.921-930
- [29] McLaren, F.G., Sherratt, A.F.C. and Morton, A.S., "Effect of Free Stream Turbulence on Drag Co-efficient of Bluff Sharp-Edged Cylinders", *Nature*, vol.224, No.5222, Nov.29, 1969, p.908-909.
- [30] Modi, V.J. and El-Sherbiny, S., "Wall Confinement Effect on Bluff Bodies in Turbulent Flows", *Proceedings of the 4th International Conference on Wind Effects on Buildings and Structures*, London, U.K., 1975, p. 121-132.
- [31] Nakamura, Y. and Matsukawa, T., "Vortex Excitation of Rectangular Cylinders with a Long Side Normal to the Flow", *Journal of Fluid Mechanics*, vol. 180, 1987, p.171-191.
- [32] Nakamura, Y. and Ohya, Y., "The Effects of Turbulence on the Mean Flow Past Square Rods", *Journal of Fluid Mechanics*, vol.137, 1983, p.331-345.
- [33] Nakamura, Y. and Yujiohya, "Vortex Shedding from Square Prisms in Smooth and Turbulent Flows", *Journal of Fluid Mechanics*, vol.164, 1986, p. 77-89.
- [34] Newberry, C.W., "The Measurements of Wind Pressures on Tall Buildings and Structures", *Proceedings of the 1st International Conference on Wind Effects of Buildings and Structures*, Teddington, U.K., p.113-149.
- [35] Okajima, A., "Strouhal Numbers of Rectangular Cylinders", *Journal of Fluid Mechanics*, vol.123, 1982, p.379-398.
- [36] Ower, E. and Pankhurst, R.C., *The Measurement of Air Flow*, Peragon Press Ltd., Oxford, 4th Edition, 1966.
- [37] Parkinson, G.V. and Modi, V.J., "Recent Research on Wind Effects on Bluff Two-Dimensional Bodies", *Proceedings of International Research Se-*

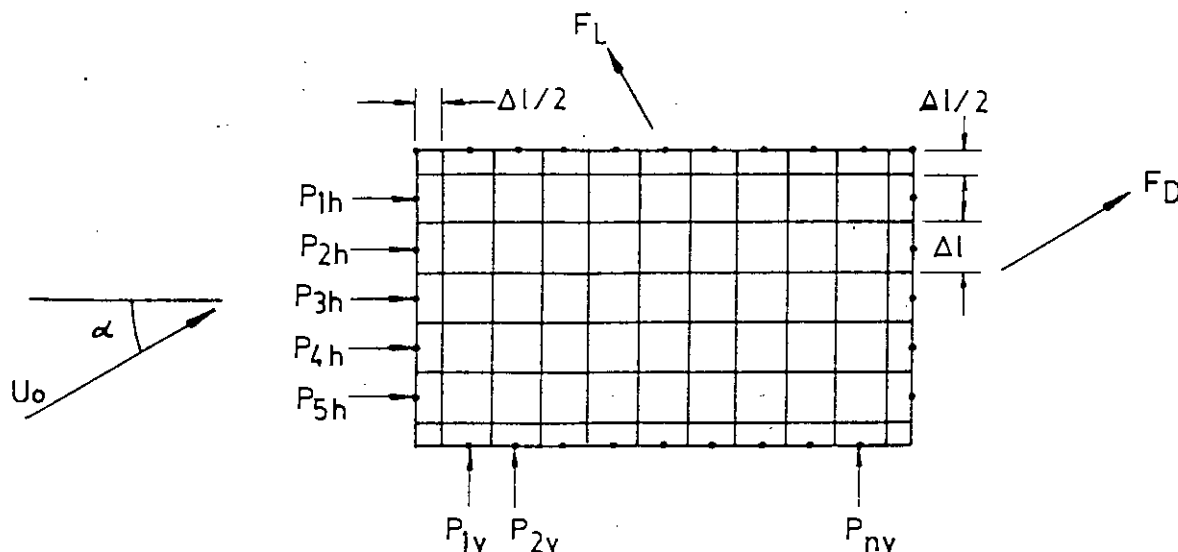
- minar, *Wind Effects on Buildings and Structures*, Ottawa, Canada, 1967, p. 485-514.
- [38] Pope, A. and Harper, J.J., *Low Speed Wind Tunnel Testing*, John Willy and Sons, New York, 1966.
- [39] Roberson, J.A., Lin, Chi Yu, Rutherford, G.S., "Turbulence Effects on Drag of Sharp-edged Bodies", *Journal of Hydraulics Division*, vol.98, No. HY7, p.1187-1201.
- [40] Roberson, J.A., Crowe, C.T., Tseng, R., "Pressure Distribution on Two and Three Dimensional Models at Small Angles of Attack in Turbulent Flow", *Proceedings of the 2nd U.S. National Conference on Wind Engineering Research*, June 22-25, Colorado, 1975.
- [41] Robertson, J.M., "Pressure Field at Reattachment of Separated Flows", *Proceedings of the 2nd U.S. National Conference on Wind Engineering Research*, June 22-25, 1975, Colorado.
- [42] Sakamoto, H. and Arie, M., "Vortex shedding from a Rectangular Prism and a Circular Cylinder Placed Vertically in Turbulent Boundary Layer", *Journal of Fluid Mechanics*, vol.126, 1983, p.147-165.
- [43] Schlichting, H., *Boundary Layer Theory*, Seventh Edition.
- [44] Scruton, C., "Introductory Review of Wind Effects on Buildings and Structures", *Proceedings of the 1st International Conference on Wind Effects on Buildings and Structures*, Teddington, U.K., 1963, p.9-25.
- [45] Simiu, E. and Scanlan, R.H., *Wind Effects on Structures: An Introduction to Wind Engineering*, John Wiley & Sons, New York.
- [46] West, G.S. and Apelt, C.J., "The Effects of Tunnel Blockage and Aspect Ratio on the Mean Flow Past a Circular Cylinder with Reynolds Number Between 10^4 to 10^5 ", *Journal of Fluid Mechanics*, 13 May, 1981.
- [47] Whitbread, R.E., "Model Simulation of Wind Effects on Structures", *Proceedings of the 1st International Conference on Wind Effects on Buildings and Structures*, Teddington, U.K., 1963, p.283-301.
- [48] Wiren, B.G., "A Wind Tunnel Study of Wind Velocities in Passages Between and Through Buildings", *Proceedings of the 4th International Conference on Wind Effects on Buildings and Structures*, London, U.K., 1975 p. 465-475.
- [49] Vickery, B.J., "Fluctuating Lift and Drag on a Long Cylinder of Square Cross-Section in a Smooth and in a Turbulent Stream", *Journal of Fluid Mechanics*, vol.25, part. 3, 1966, p.481-491.

APPENDICES

APPENDIX-A

Determination of Co-efficients

1. Determination of Lift and Drag co-efficients:



The section of the cylinder shown in the above figure is divided horizontally into five equal strips of width Δl with a tapping point at the mid point of each strip. Similarly it is divided vertically into n equal strips, where n is the number of tapping points on the bottom surface of the cylinders of different side ratios. $\Delta l/2$ is the remainder width of the section from the end corners both in the horizontal and vertical direction. It is assumed that the pressures at the mid point of these half-width strips are equal to the pressures at the tap pings nearest to the corners. The pressure distribution is assumed to be constant over a certain length at each section and therefore the area under each strip is Δl .

Let $P_{1h}, P_{2h}, \dots, P_{5h}$, and $P_{1v}, P_{2v}, \dots, P_{nv}$ be the pressure difference in meter of manometer liquid between the opposite surfaces of each strip along the horizontal and vertical directions respectively. By trapezoidal rule the total force per unit length can be taken as:

$$F_D = \gamma_w \times \Delta l \left[\frac{1}{2} P_{1h} + P_{2h} + \dots + \frac{1}{2} P_{5h} \right] \cos \alpha + \gamma_w \times \Delta l / 2 [P_{1h} + P_{5h}] \cos \alpha + \gamma_w \times \Delta l \left[\frac{1}{2} P_{1v} + P_{2v} + \dots + \frac{1}{2} P_{nv} \right] \sin \alpha + \gamma_w \Delta l / 2 [P_{1v} + P_{nv}] \sin \alpha \quad \dots(1)$$

$$\text{and } F_L = \gamma_w \times \Delta l \left[\frac{1}{2} P_{1h} + P_{2h} + \dots + \frac{1}{2} P_{5h} \right] \sin \alpha + \gamma_w \times \Delta l / 2 [P_{1h} + P_{5h}] \sin \alpha + \gamma_w \times \Delta l \left[\frac{1}{2} P_{1v} + P_{2v} + \dots + \frac{1}{2} P_{nv} \right] \cos \alpha + \gamma_w \times \Delta l / 2 [P_{1v} + P_{nv}] \cos \alpha \quad \dots(2)$$

where the terms for the half width strips are added algebraically.

$$\text{Now, } F_D = \gamma_w \times \Delta l \left[(P_{1h} + P_{2h} + \dots + P_{5h}) \cos \alpha + (P_{1v} + P_{2v} + P_{nv}) \sin \alpha \right] \\ = \gamma_w \Delta l \left[\Delta P_h \cos \alpha + \Delta P_v \sin \alpha \right]$$

where $\Delta P_h = P_{1h} + P_{2h} + \dots + P_{5h}$

$$\Delta P_v = P_{1v} + P_{2v} + \dots + P_{nv}$$

Equation (3) may be written in the form,

$$F_D = \gamma_w \Delta l \left[\Delta P_D \right]$$

where $\Delta P_D = \Delta P_h \cos \alpha + \Delta P_v \sin \alpha$

Similarly equation (2) may be reduced to the form,

$$F_L = \gamma_w \Delta l \left[\Delta P_L \right]$$

where $P_L = \Delta P_h \sin \alpha + \Delta P_v \cos \alpha$

By the definition of drag co-efficient,

$$C_D = F_D / \frac{1}{2} \rho A U_o^2 \\ = \gamma_w \Delta l \Delta P_D / \frac{1}{2} \rho 6 \Delta l U_o^2 \quad \text{where, } A = 6 \Delta l \\ = \gamma_w \Delta P_D / 3 \rho U_o^2 \quad (4)$$

Similarly lift co-efficient is given by,

$$C_L = F_L / \frac{1}{2} \rho A' U_o^2 \\ = \gamma_w \Delta l \Delta P_L / \frac{1}{2} \rho (n+1) \Delta l U_o^2 \quad \text{where } A' = (n+1) \Delta l \\ = \gamma_w \Delta P_L / \frac{1}{2} (n+1) \rho U_o^2 \quad (5)$$

At zero angle of incidence, i.e., when $\alpha = 0^\circ$, lift and drag coefficients are reduced to the forms,

$$C_D = \Delta P_h / 3 \rho U_o^2 \quad (6)$$

$$C_L = \Delta P_v / \frac{1}{2}(n+1) \rho U_o^2 \quad (7)$$

2. Pressure Co-efficient:

Pressure co-efficient is defined as $C_P = (P - P_o) / \frac{1}{2} \rho U_o^2$

3. Total Force Co-efficient:

Total force-co-efficient is defined as $C_F = \sqrt{(C_D^2 + C_L^2)}$

4. Calculation of Co-efficients:

$$\begin{aligned} \text{Since } U_o &= \sqrt{2gh_u} \\ &= \sqrt{(2g \gamma_w h_u / \gamma_a)} \end{aligned}$$

where h_u is the height of reference velocity head in the manometer limb and γ_w and γ_a are the specific weights of water and air respectively, we have

$$\frac{1}{2} \rho U_o^2 = \gamma_w h_u$$

$$\text{So that } C_P = (P - P_o) / \frac{1}{2} \rho U_o^2 = (h_p - h) / h_u \quad (8)$$

where h_p and h are the height of reference pressure head and local pressure head respectively in the manometer limb.

When the cylinder is oriented at 0° angle of attack we have for the front face

$$C_D = \gamma_w \Delta P_h / \frac{1}{2} \rho 6 U_o^2$$

$$\text{and } \Delta P_h = P_{1h} + P_{2h} + \dots + P_{5h}$$

$$= (h_1 - h_1') + (h_2 - h_2') + \dots + (h_5 - h_5')$$

where h_1 and h_1' are the local pressure heads on the front and back surface of the cylinder at tapping point number 1.

Now at tapping point number 1 we have coefficient of pressure on the front surface as

$$C_{p1} = h_p - h_1 / h_u \quad (9)$$

$$C_{p2} = h_p - h_2 / h_u \quad (10)$$

.

.

$$C_{p5} = h_p - h_5 / h_u \quad (13)$$

and similarly on the back surface pressure coefficients are

$$C_{p1}' = h_p - h_1' / h_u \quad (14)$$

$$C_{p2}' = h_p - h_2' / h_u \quad (15)$$

.

.

$$C_{p5}' = h_p - h_5' / h_u \quad (18)$$

Now the coefficient of drag can be written as

$$\begin{aligned} C_D &= \Sigma \gamma_w (h_n' - h_n) / \frac{1}{2} \rho U_o^2 \cdot 6 \\ &= \Sigma (h_n' - h_n) / 6 h_u \end{aligned} \quad (19)$$

From equations (9) to (13) and equations (14) to (18) it can be written in general that

$$h_n = h_p - C_{pn} h_u$$

$$h_n' = h_p - C_{pn}' h_u$$

and hence from equation (19) the drag coefficient becomes in terms of pressure coefficient as

$$\begin{aligned} C_D &= \Sigma [(h_p - C_{pn}' h_u) - (h_p - C_{pn})] / 6 h_u \\ &= \Sigma (C_{pn} - C_{pn}') / 6 \end{aligned} \quad (20)$$

Using equation (8) coefficient of pressure can be calculated directly from experimental values of pressure head and hence with the help of equation (20) coefficient of drag can be calculated directly from corresponding pressure coefficients.

APPENDIX-B

Uncertainty Analysis

Errors are introduced during measurement, due to atmospheric changes, measuring instruments, probe settings etc. Uncertainties thus may have crept into the measurements of pressure and it is analysed in the way suggested by Kline and McClintock.

Uncertainty for Pressure Measurement:

$$\text{If } u = f(\alpha_1, \alpha_2, \dots, \alpha_n) \quad (1)$$

$$\text{Then the mean } \mu_u = f(\bar{\alpha}_1, \bar{\alpha}_2, \dots, \bar{\alpha}_n) \quad (2)$$

$$\text{and the variance } \sigma_u^2 = \sum \left(\frac{\delta u}{\delta \alpha_i} \right)^2 \sigma_{\alpha_i} \quad (3)$$

In terms of objective coefficients of variance

$$\begin{aligned} \delta_u^2 &= \frac{\sigma_u^2}{\mu_u^2} = \sum \left(\frac{\delta u}{\delta \alpha_i} \cdot \frac{\bar{\alpha}_i}{\mu_u} \right)^2 \cdot \left(\frac{\sigma_{\alpha_i}}{\alpha_i} \right) \\ &\approx \sum_{i=1}^n \left(\frac{\delta u}{\delta \alpha_i} \cdot \frac{\bar{\alpha}_i}{\mu_u} \right)^2 \delta^2 \alpha_i \end{aligned} \quad (4)$$

where δ_u is the coefficient of variance and $\delta \alpha_i$ is the coefficient of variance of free variables α_i .

It may be noted that coefficient of variance is often used as measure of uncertainties.

The wall static pressures measured from the surface tappings were the gage pressure below atmospheric pressure. If P be the absolute static pressure and P_a be the atmospheric pressure, then the recorded pressure be

$$P_r = P_a - P \quad (5)$$

and the absolute static pressure

$$P = P_a - P_r \quad (6)$$

The recorded pressure is nothing but $\gamma_w h_w$. So that

$$\begin{aligned} P &= P_a - \gamma_w h_w \\ &= P_a - \gamma_w h_w / 100 \end{aligned} \quad (7)$$

where h_w is in cm of water.

Since the change of density of water is negligible, so the uncertainty in surface static pressure measurement is

$$\sigma_P = \left[\left(\frac{\delta P}{\delta P_a} \cdot \sigma_{P_a} \right)^2 + \left(\frac{\delta P}{\delta h_w} \cdot \sigma_{h_w} \right)^2 \right]^{1/2} \quad (8)$$

Now $\frac{\delta P}{\delta P_a} = 1$

$$\frac{\delta P}{\delta h_w} = - \gamma_w \times 1/100$$

$$\sigma_P = [\sigma_{P_a}^2 + \gamma_w^2 (1/100)^2 \cdot \sigma_{h_w}^2]^{1/2} \quad (9)$$

$$\frac{\sigma_P}{P} = \frac{[\sigma_{P_a}^2 + \gamma_w^2 (1/100)^2 \cdot \sigma_{h_w}^2]^{1/2}}{P_a - h_w \gamma_w \times 1/100}$$

But for a short interval $\sigma_{P_a} = 0$

Hence $\frac{\sigma_P}{P} = \frac{[\gamma_w (1/100) \sigma_{h_w}]}{P_a - h_w \gamma_w \times 1/100}$

Now $P = 101325 \text{ N/m}^2$

$$\gamma_w = 1000 \text{ kg/m}^3$$

$$h_w = 9.65 \text{ cm} \pm 0.63 \text{ cm of H}_2\text{O}$$

$$\sigma_p/P = 5.166 \times 10^{-5} \text{ i.e. } 0.005166\%$$

Uncertainty in Mean Velocity Measurement:

When air was flowing with a velocity of $U \text{ cm/sec}$ and a pitot static tube was placed parallel to the flow, the velocity was found from the dynamic head $h_u \text{ cm}$ of water recorded by the inclined manometer from the relation

$$u = \sqrt{2gh_u \gamma_w / \gamma_a} \quad (10)$$

where γ_w and γ_a are the specific weights of water and air respectively. If the sensing point of the pitot static tube had a misalignment of θ from the direction of flow due to adjustment error then the measured velocity would be

$$u = \sqrt{(2gh_u \gamma_w / \gamma_a)} \cdot \sec\theta \quad (11)$$

Using $P = \gamma_a RT$ where P , R and T are pressure, gas constant and absolute temperature of air respectively, then velocity u becomes

$$\begin{aligned} u &= \sqrt{(2gh_u \gamma_w RT / P)} \sec\theta \\ &= \sqrt{2gR\gamma_w} \times \sqrt{(h_u \cdot T / P)} \sec\theta \\ &= C \sqrt{(h_u T / P)} \sec\theta \end{aligned} \quad (12)$$

Here $u = f(T, P, h_u, \theta)$

So the uncertainty in velocity measurement can be expressed as

$$\sigma_u = \left(\frac{\delta u}{\delta P} \cdot \sigma_P \right)^2 + \left(\frac{\delta u}{\delta T} \cdot \sigma_T \right)^2 + \left(\frac{\delta u}{\delta h_u} \cdot \sigma_{h_u} \right)^2 + \left(\frac{\delta u}{\delta \theta} \cdot \sigma_\theta \right)^2 \quad (13)$$

Where σ_P , σ_T , σ_{h_u} and σ_θ are uncertainties associated with pressure,

temperature, manometer reading and alignment of the probe with the flow direction.

To get the uncertainties involved in the different variables the respective partial derivatives are now found out. Again writing equation (12) in the form

$$u = C\sqrt{(h_u \cdot T/P)} \cdot \sec\theta$$

The partial derivatives of U are found to be

$$\begin{aligned} \frac{\delta u}{\delta P} &= C\sqrt{h_u T} \cdot \sec\theta \cdot \left(-\frac{1}{2}P^{-3/2}\right) \\ &= -C/2\sqrt{h_u T/P^3} \cdot \sec\theta \end{aligned} \quad (14)$$

$$\begin{aligned} \frac{\delta u}{\delta T} &= C\sqrt{h_u/P} \cdot \sec\theta \cdot \frac{1}{2}T^{-\frac{1}{2}} \\ &= C/2\sqrt{h_u/TP} \cdot \sec\theta \end{aligned} \quad (15)$$

$$\frac{\delta u}{\delta h} = C\sqrt{T/P} \cdot \sec\theta \cdot \frac{1}{2}h_u^{-\frac{1}{2}} \quad (16)$$

and
$$\frac{\delta u}{\delta \theta} = C\sqrt{h_u T/P} \cdot \sec\theta \cdot \tan\theta \quad (17)$$

Putting these equations to equation (13) we get

$$\begin{aligned} \sigma_u &= [(-C/2\sqrt{h_u T/P^3} \cdot \sec\theta \cdot \sigma_P)^2 + (C/2\sec\theta\sqrt{h_u/TP} \cdot \sigma_T)^2 + (C/2\sqrt{T/Ph} \cdot \sec\theta \sigma_h)^2 \\ &\quad + (C\sqrt{h_u T/P} \cdot \sec\theta \cdot \tan\theta \cdot \sigma_\theta)^2]^{\frac{1}{2}} \\ &= [C^2/4 \cdot h_u T/P^3 (\sec\theta)^2 \cdot \sigma_P^2 + C^2/4 \cdot h_u/TP \cdot (\sec\theta)^2 \cdot \sigma_T^2 \\ &\quad + C^2/4 \cdot T/Ph \cdot \sec^2\theta \sigma_h^2 + C^2 h_u T/P \cdot \sec^2\theta \cdot \tan^2\theta \sigma_\theta^2]^{\frac{1}{2}} \\ &= C/2 \cos\theta [(h_u T/P^3) \sigma_P^2 + (h_u/TP) \sigma_T^2 + (T/Ph) \sigma_h^2 \\ &\quad + 4(h_u T/P) \sigma_\theta^2 \cdot \tan^2\theta]^{\frac{1}{2}} \end{aligned} \quad (18)$$

Now dividing equation (18) by equation (12) the uncertainty in velocity measurement takes the form

$$\frac{\sigma_u}{u} = \frac{1}{2} [\sigma_P^2/P^2 + \sigma_T^2/T^2 + \sigma_{h_u}^2/h_u^2 + 4\sigma_\theta^2 \cdot \tan^2\theta]^{\frac{1}{2}}$$

The direction is taken for objective uncertainties. There is also subjective uncertainties which is considered 5%, so the final uncertainties becomes

$$\frac{\sigma_u}{u} = \frac{1}{2} [\sigma_P^2/P^2 + \sigma_T^2/T^2 + \sigma_{h_u}^2/h_u^2 + 4\sigma_\theta^2 \cdot \tan^2\theta + \sigma_s^2]^{\frac{1}{2}}$$

Now during an experimental run, the following conditions were observed.

$$P = 76.2\text{cm} \pm 0.10\text{cm of Hg}$$

$$T = 82^\circ \pm 2^\circ\text{F}$$

$$h_u = 1.91\text{cm} \pm 0.0254\text{cm of water}$$

$$\theta = 0^\circ \pm 2^\circ$$

The corresponding uncertainty in velocity measurement becomes

$$\sigma_u/u = 0.0138 \text{ i.e., } 1.38\%$$

FIGURES

All measurements are in millimeter unless otherwise mentioned

- | | |
|-----------------------|----------------------|
| 1. SETTLING CHAMBER | 2. CONVERGING MOUTH |
| 3. HONEY COMB SECTION | 4. PERSPEX SECTION |
| 5. TEST SECTION | 6. WOOD SECTION |
| 7. WOOD SECTION | 8. DIVERGING SECTION |
| 9. FAN SECTION | 10. FAN SECTION |
| 11. BUTTERFLY SECTION | 12. SILENCER |

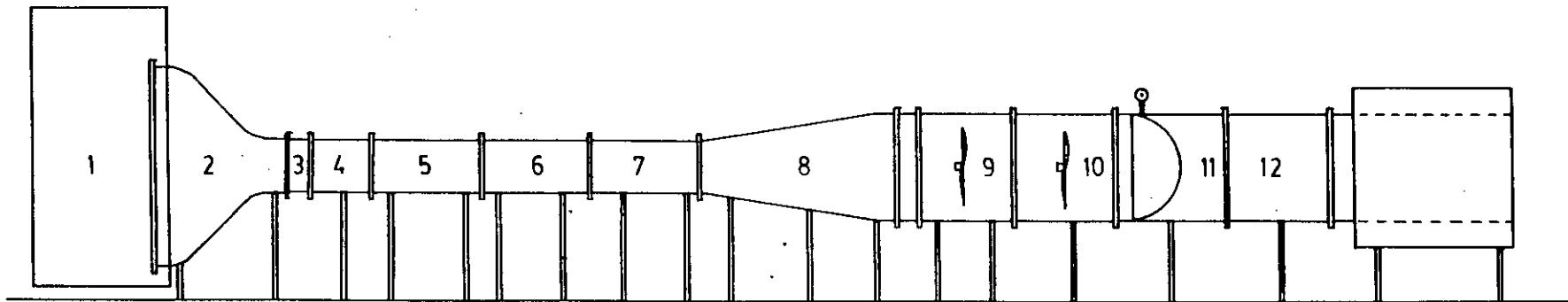


Figure 3.1: Schematic diagram of wind tunnel

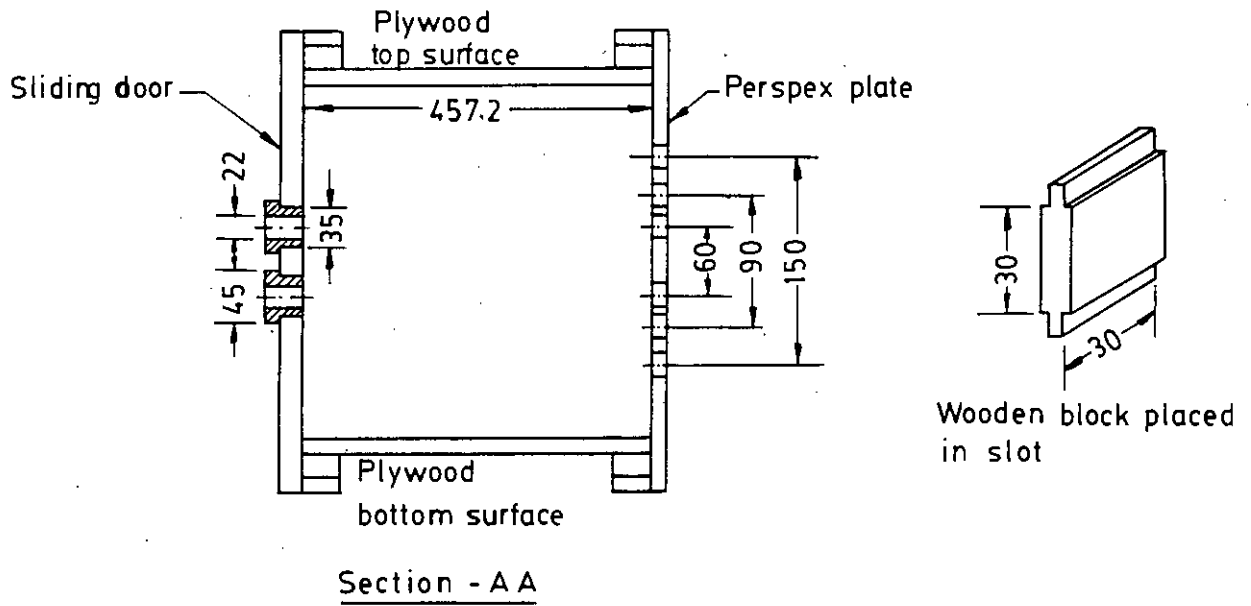
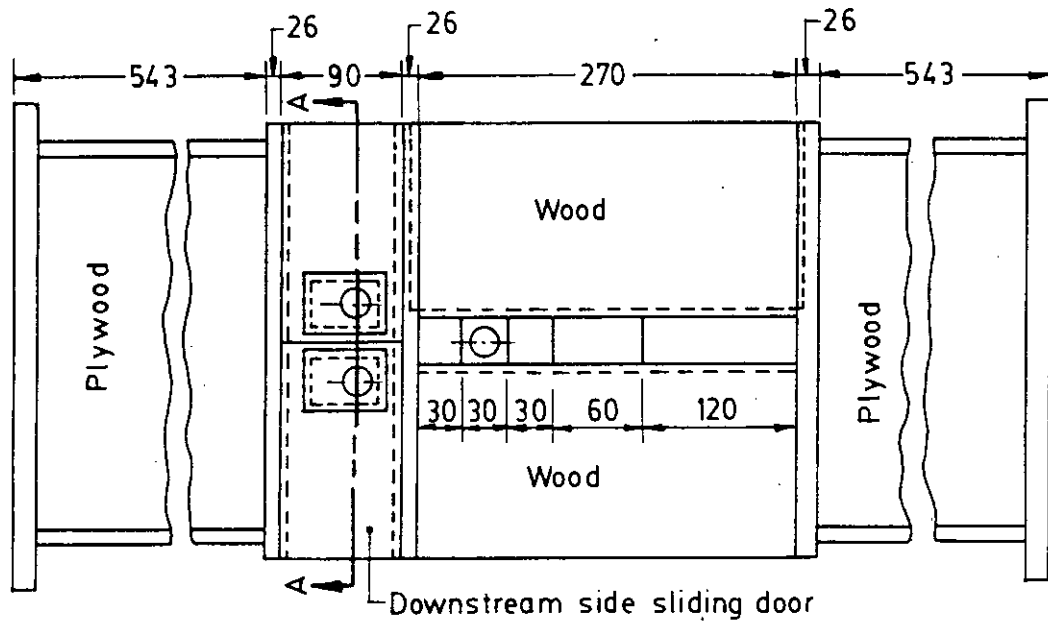
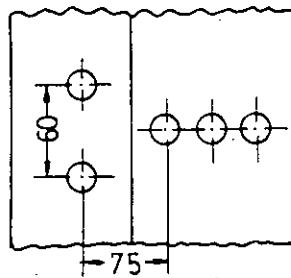
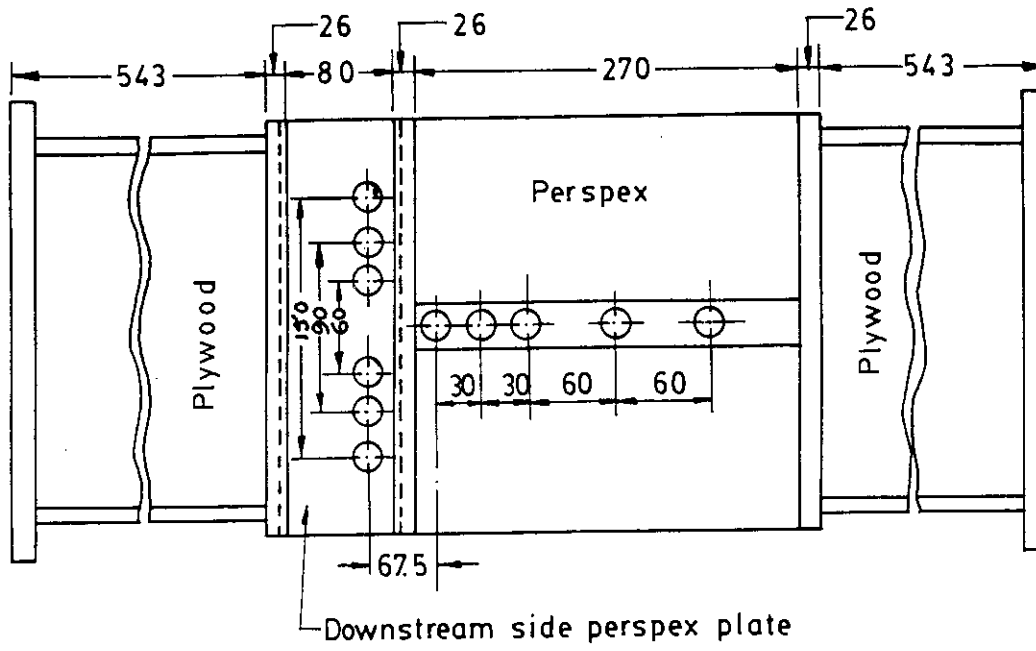
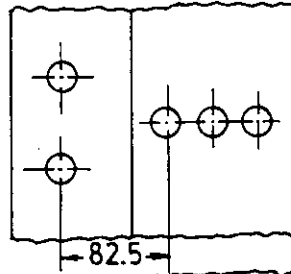


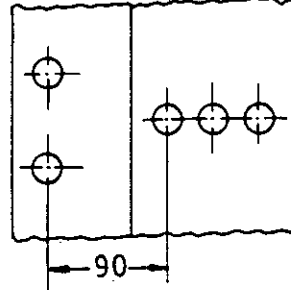
Figure 3.2 : Wooden vertical wall side of test section



Position of holes for mounting the cylinder with side ratio 1.5



Position of holes for mounting the cylinder with side ratio 1.75



Position of holes for mounting the cylinder with side ratio 2.0

Figure 3.3: Perspex vertical wall side of the test section

7/578

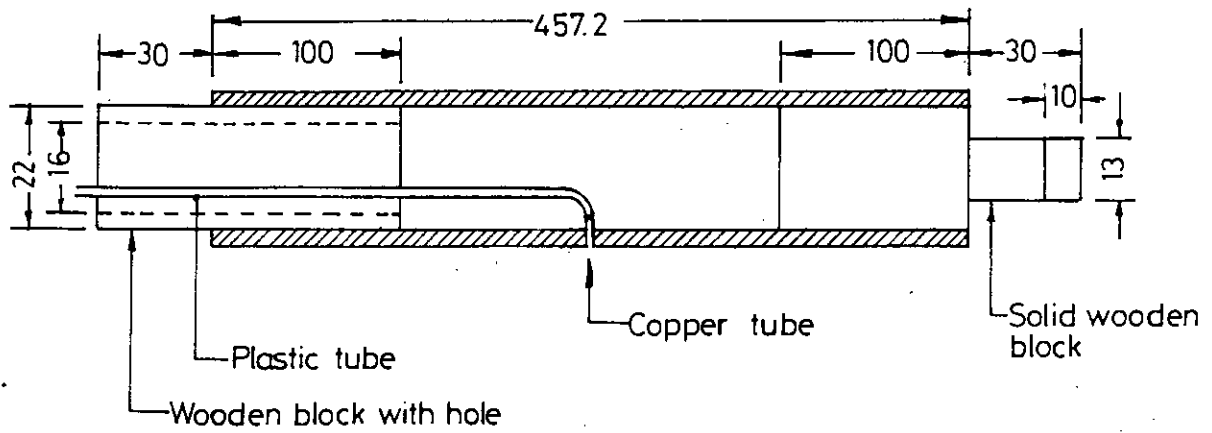


Figure 3.4: Sectional view of a specimen rectangular cylinder

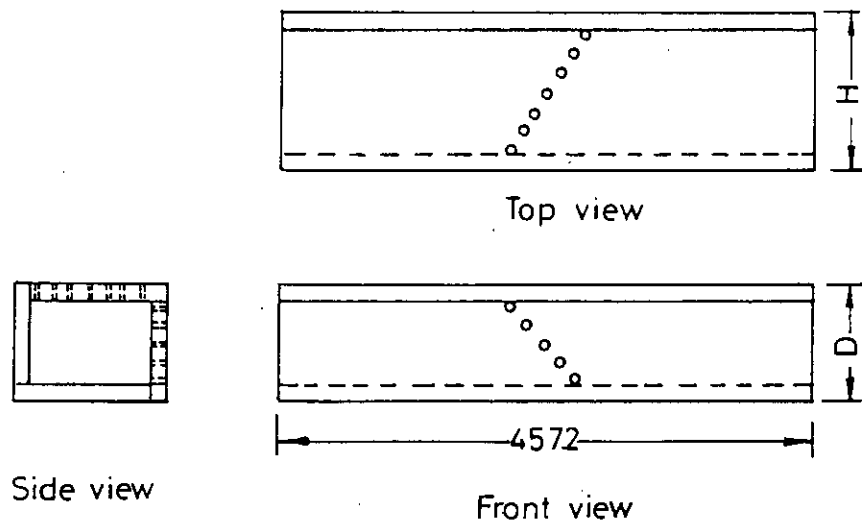


Figure 3.5: The arrangement of tapping points on adjacent sides

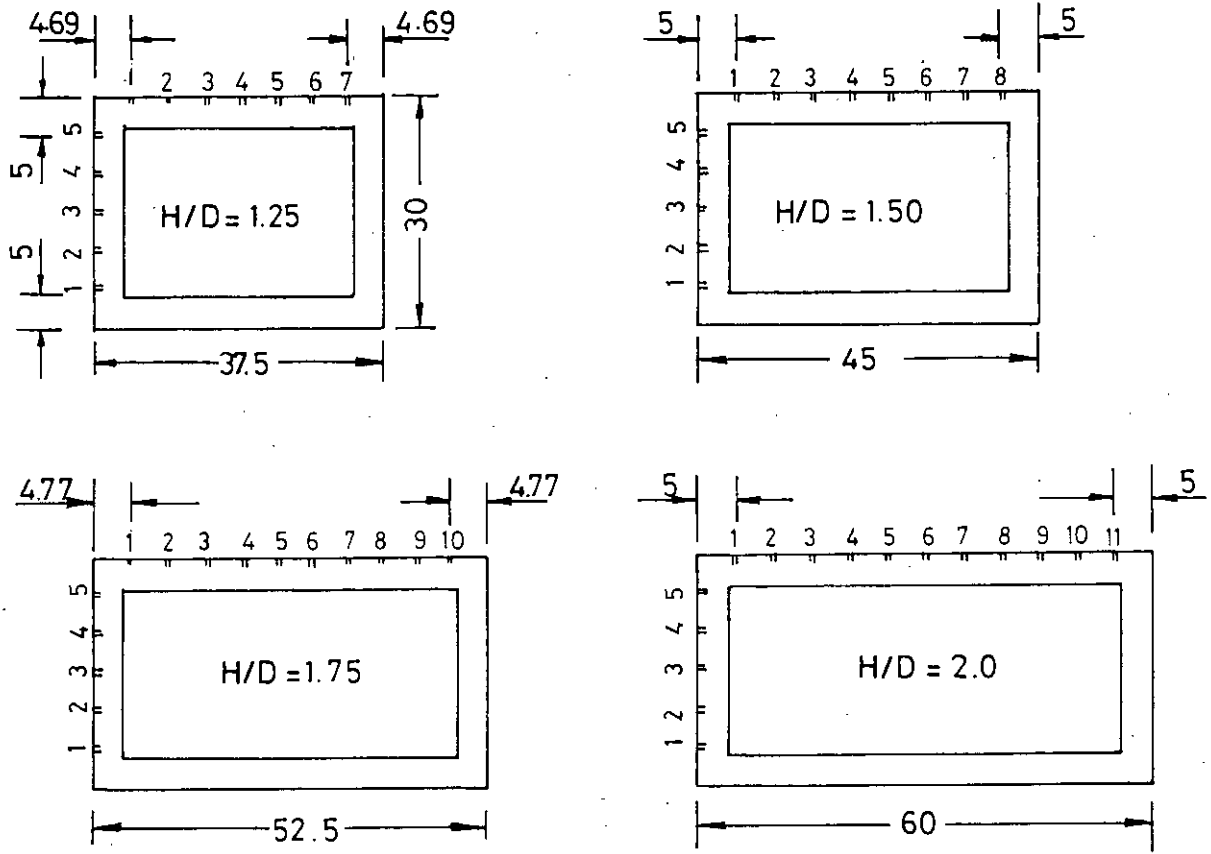


Figure 3.6: Cross section of rectangular cylinders from each set showing position of tapping points

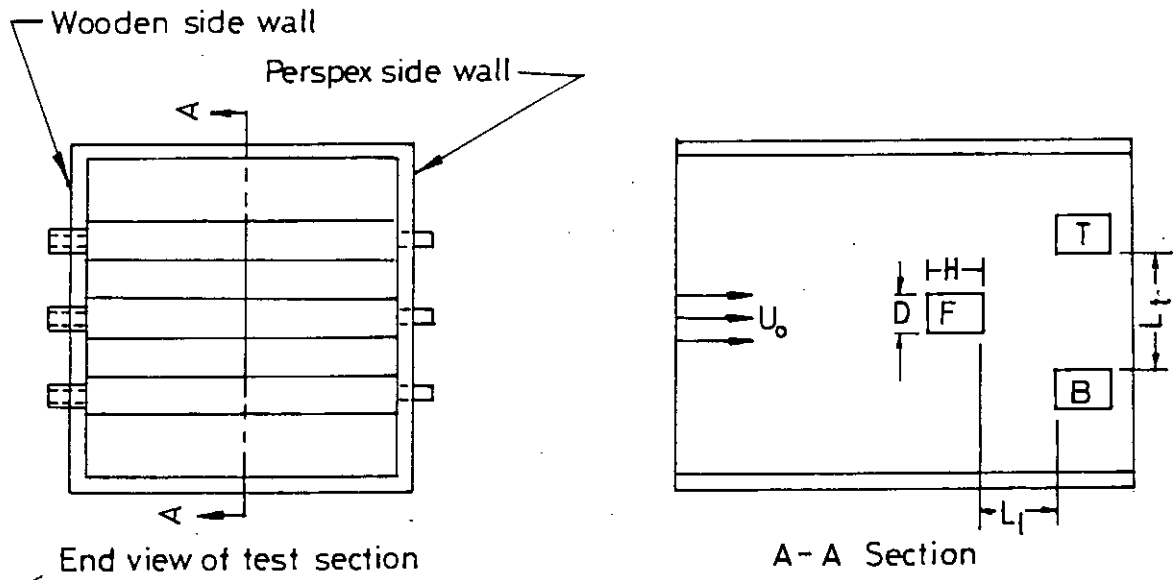


Figure 3.7: Tunnel test section showing the position of cylinders in staggered form

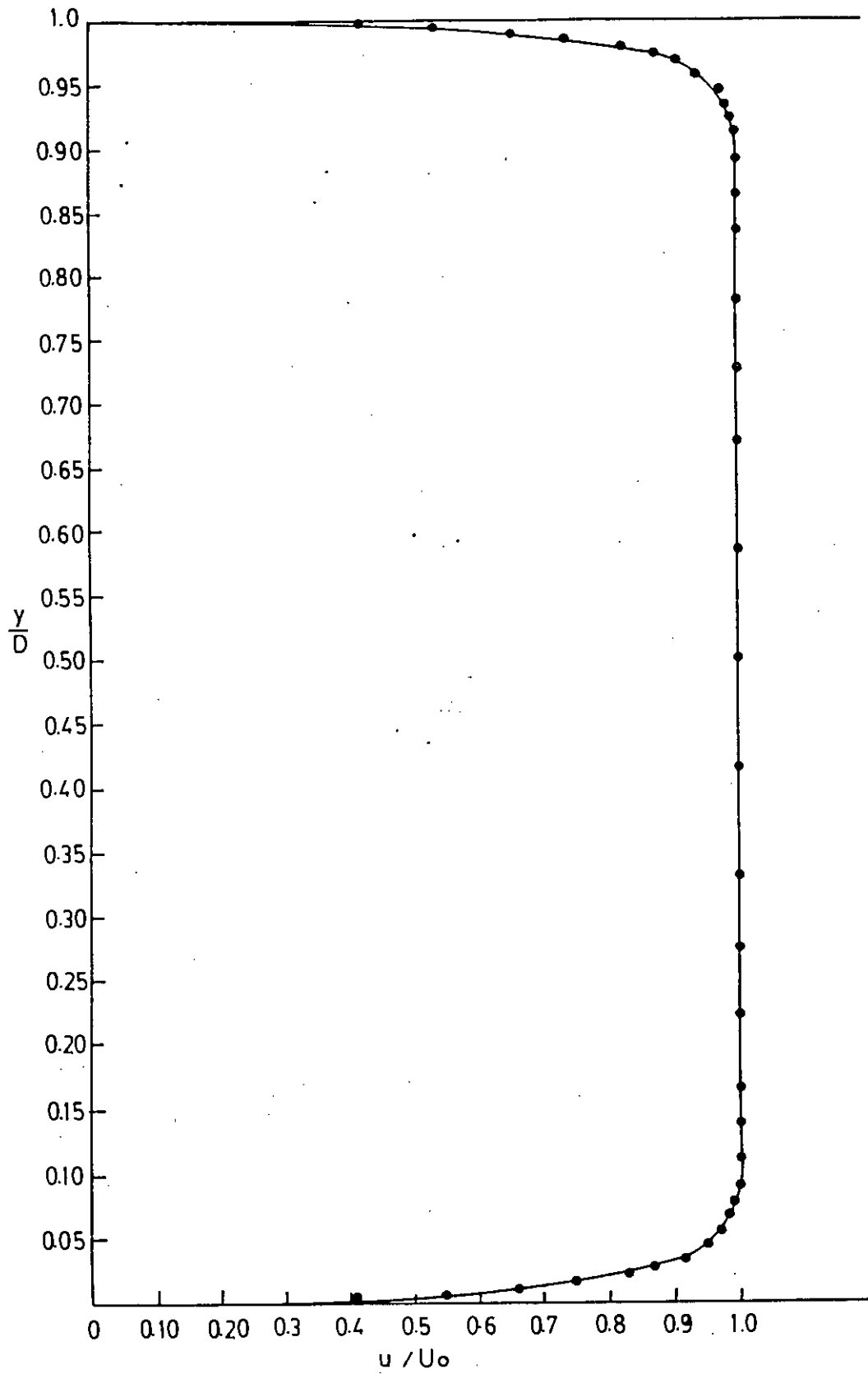


Figure 3.8 : Velocity distribution in upstream side of test section

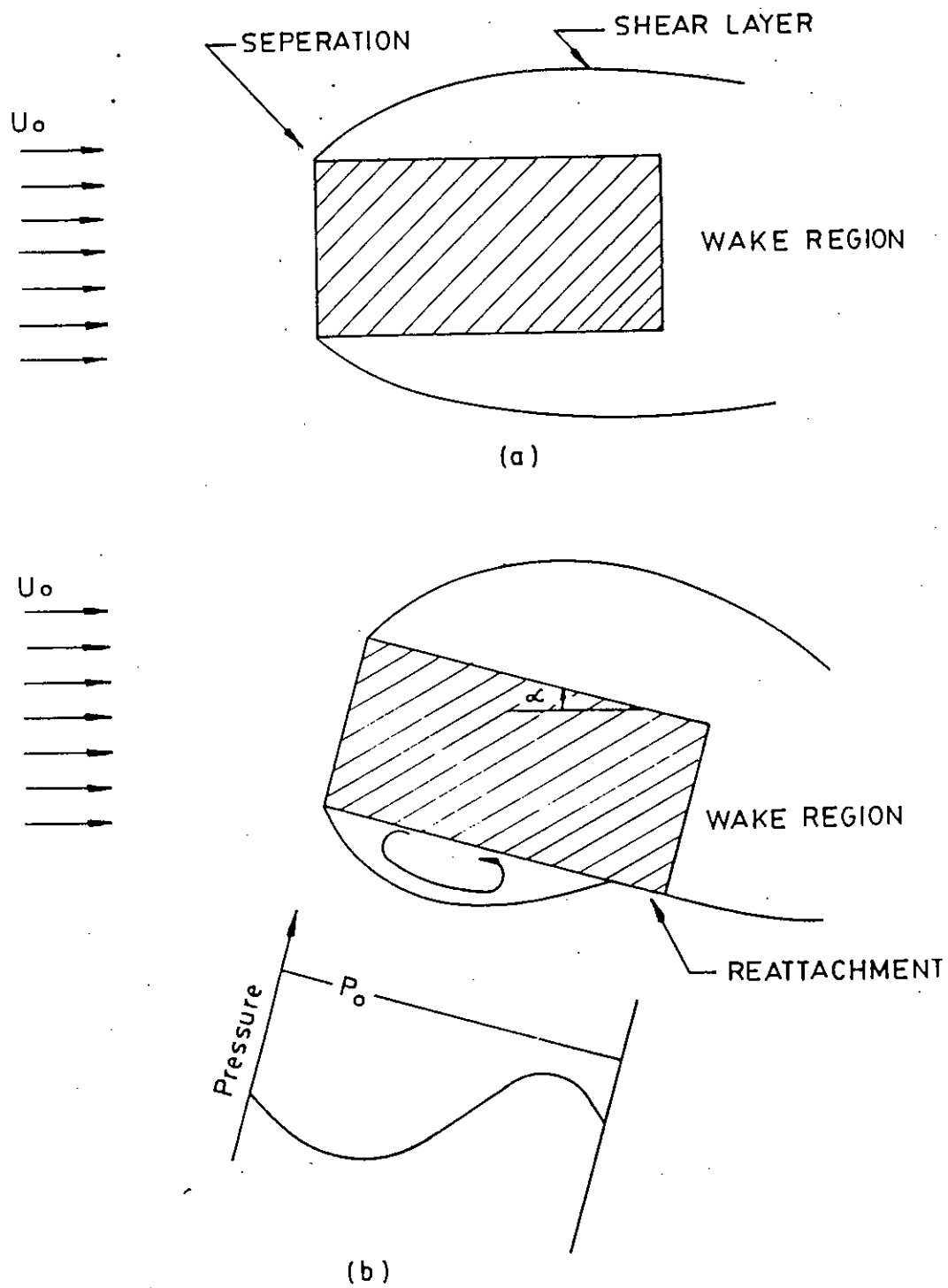


Figure 4.1: The nature of flow pattern around rectangular prisms

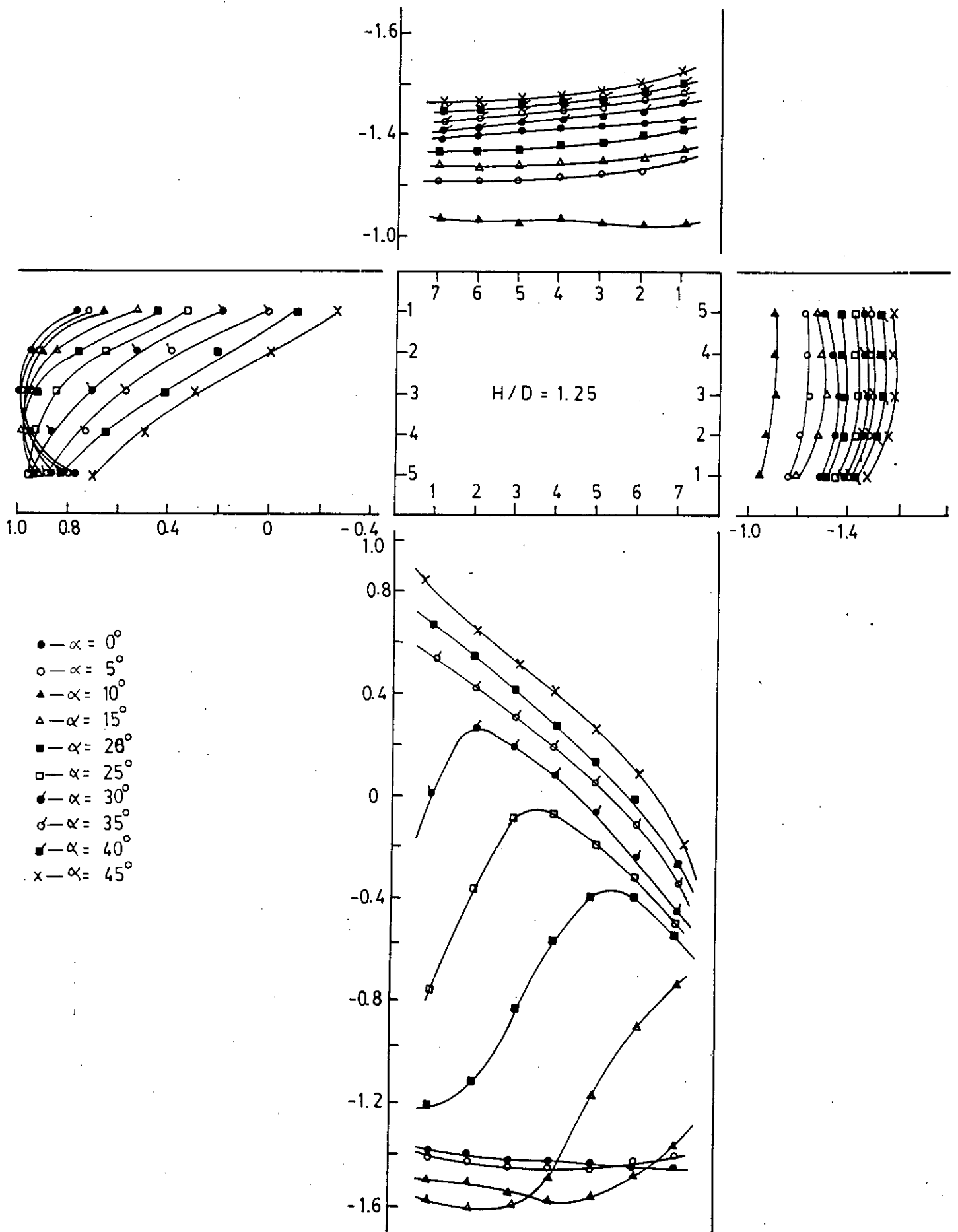


Figure 4-2: Effect of angle of attack (α) on C_p -distribution at side ratio (H/D) of 1.25

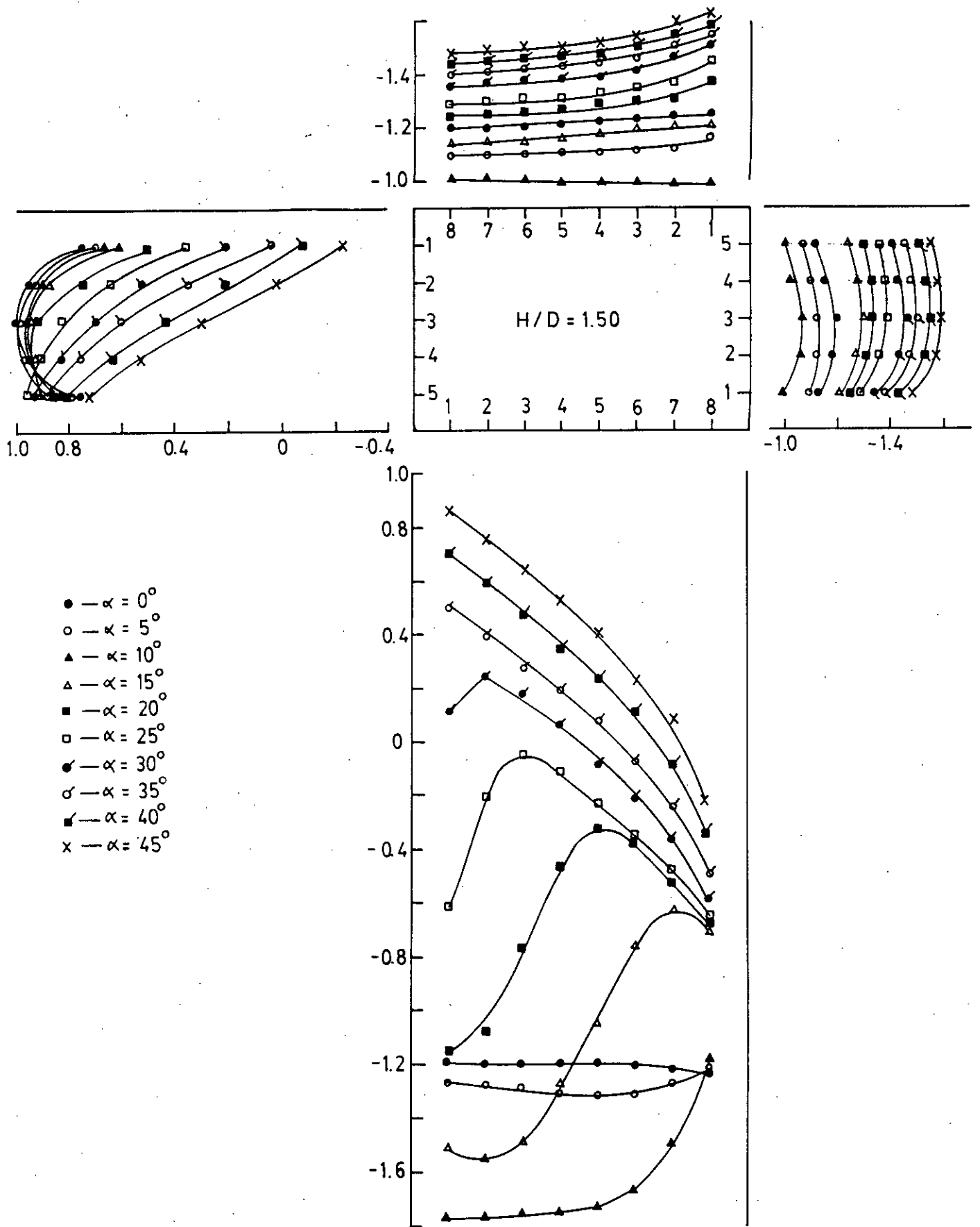


Figure 4-3 : Effect of angle of attack on C_p -distribution at side ratio (H/D) of 1.50

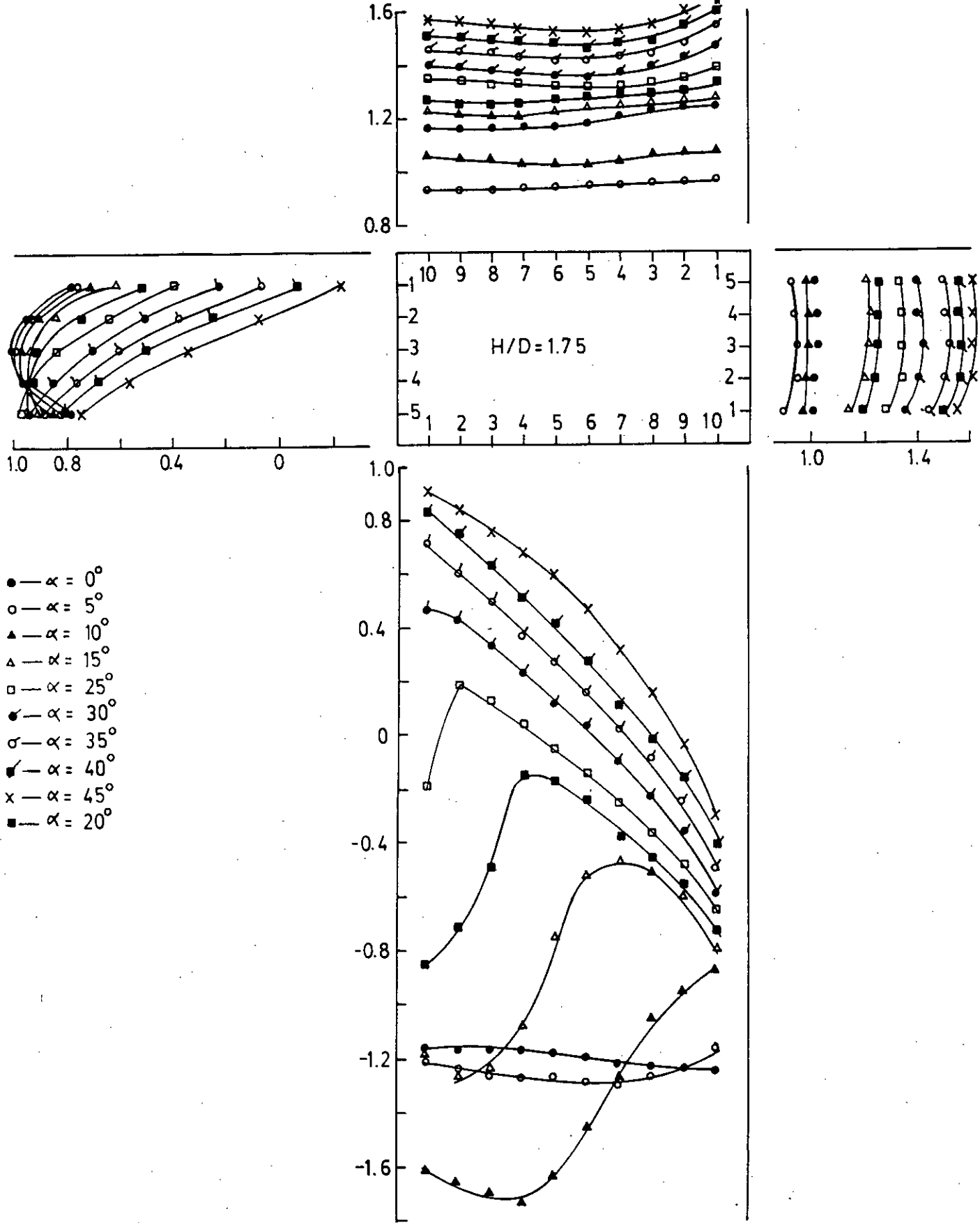


Figure 4-4 : Effect of angle of attack (α) on C_p -distributions at side ratio (H/D) of 1.75

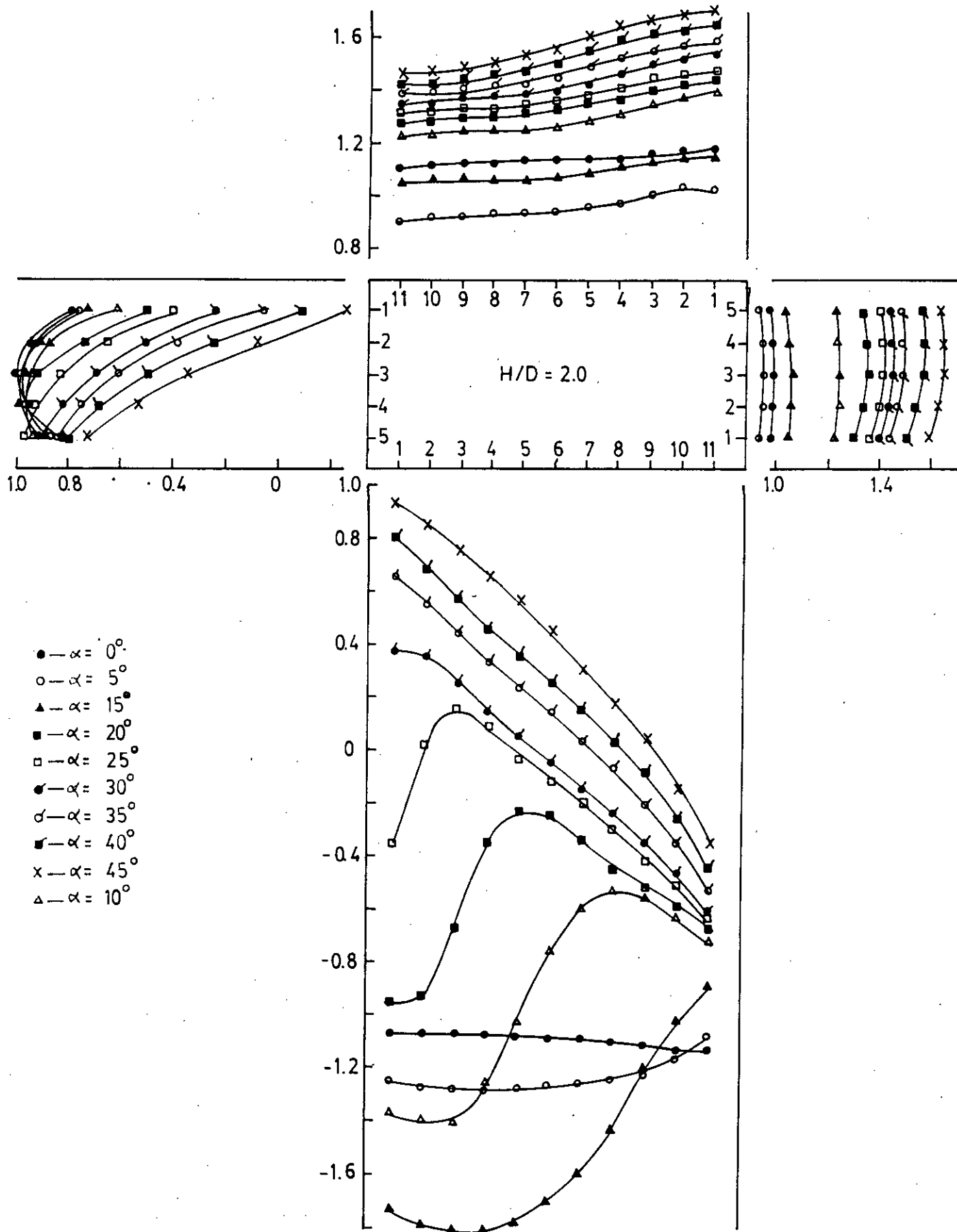


Figure 4-5: Effect of angle of attack (α) on C_p -distributions at side ratio (H/D) of 2.0

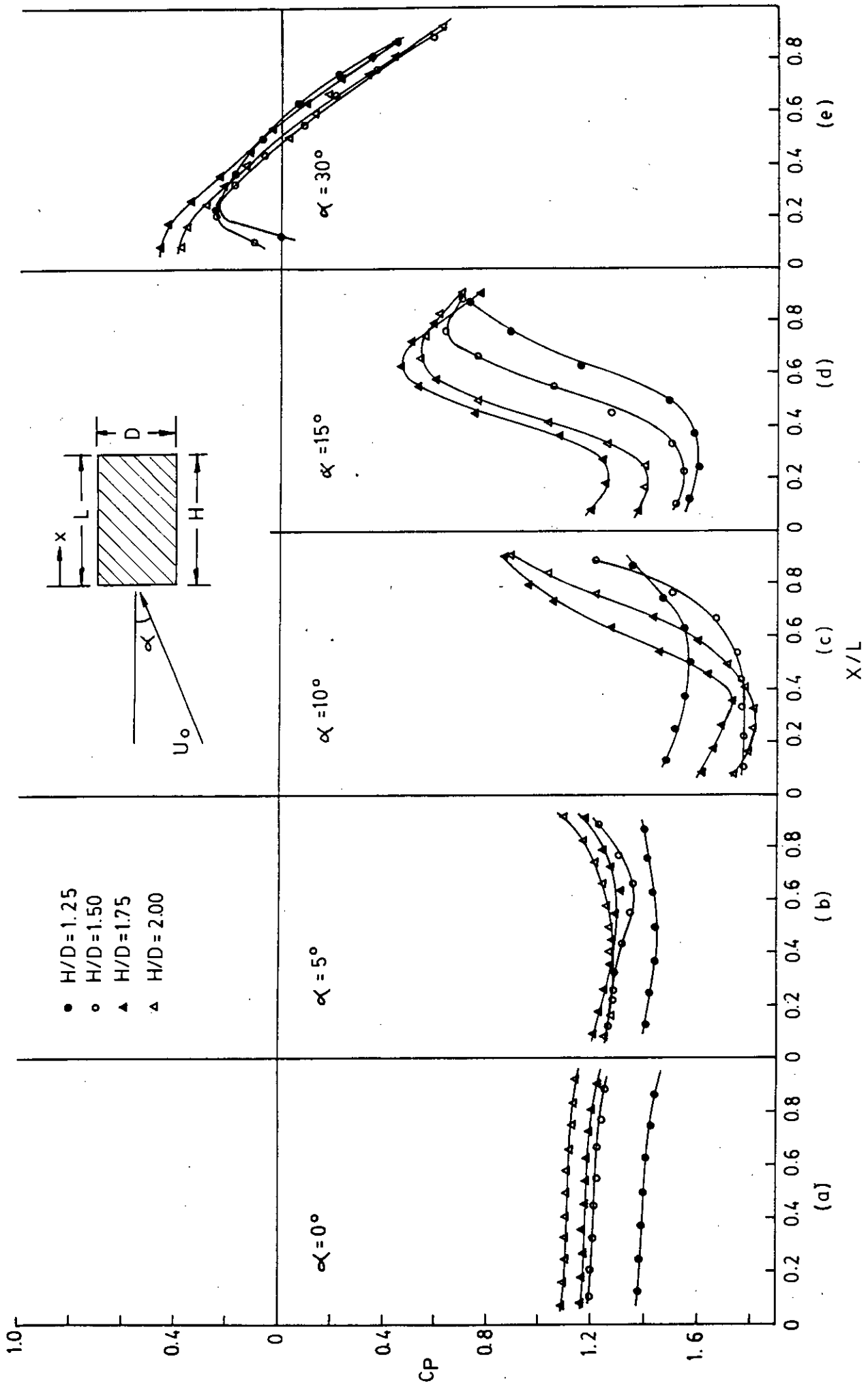


Figure 4.6 : Effect of side ratio (H/D) on Cp-distributions on the bottom surface at varying angle of attack

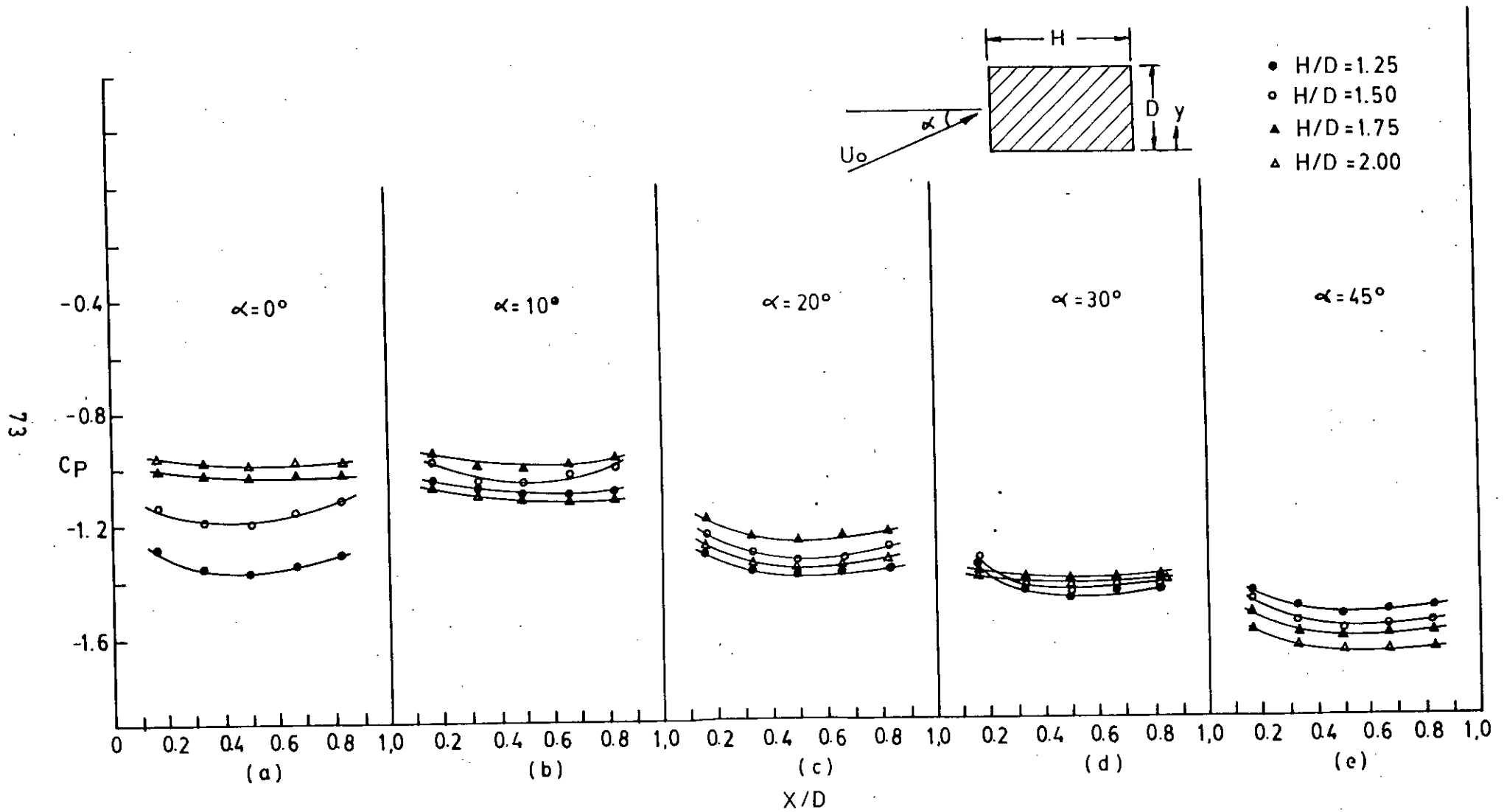


Figure 4.7: Effect of side ratio (H/D) on C_p -distributions on the bottom surface at varying angle of attack

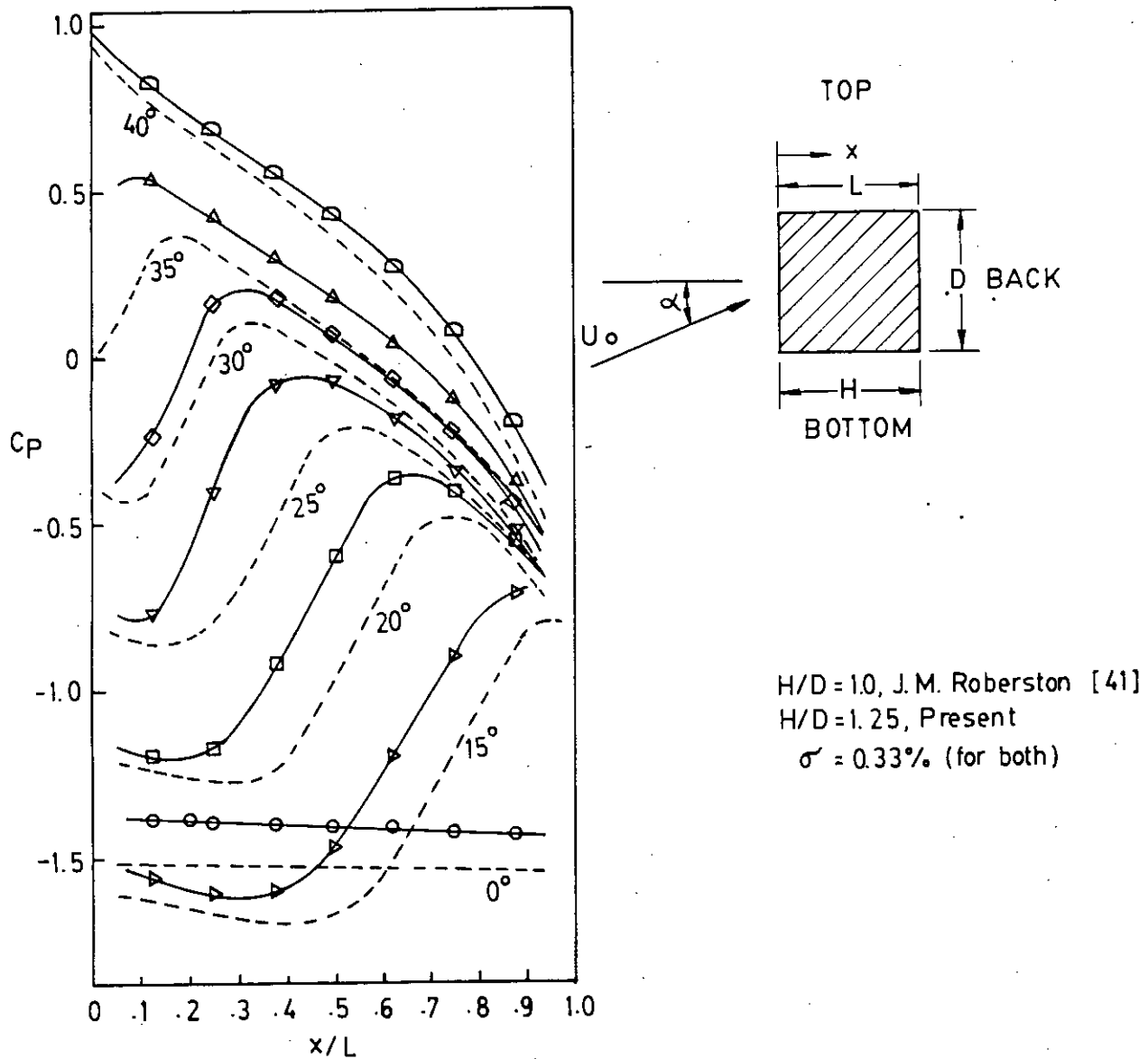


Figure 4-8 Comparisons of C_p -distribution at variable angle of attack on windward side

Present:	○	▷	◇	▽	□	△	◻
Robertson [41]:	-----						
α (deg)	: 0	15	20	25	30	35	45

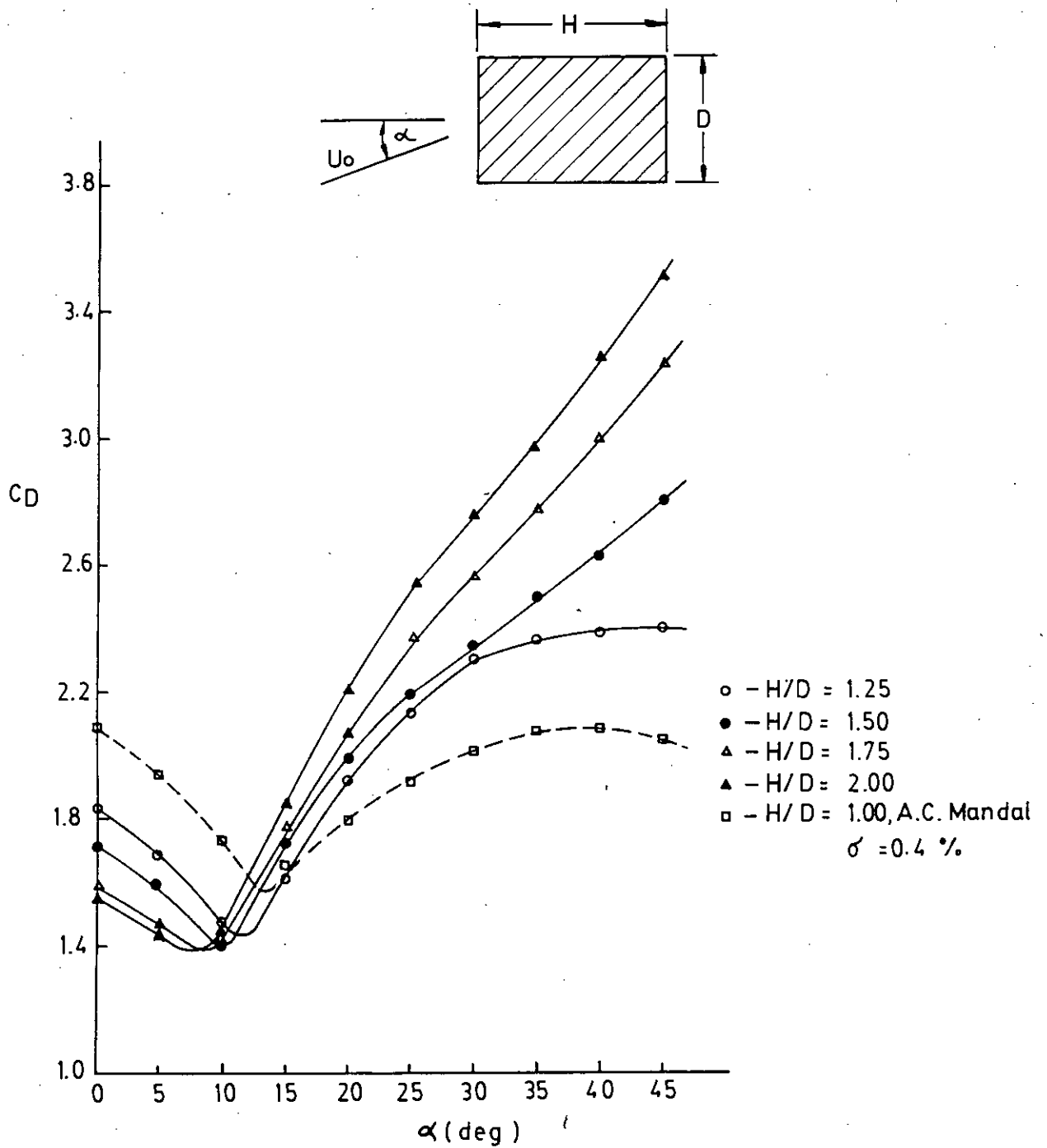
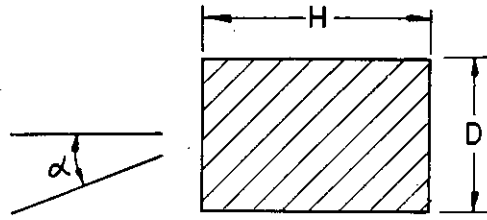


Figure 4.9 : Variation of drag coefficient (C_D) with angle of attack (α) for different side ratios (H/D)



- - $H/D = 1.25$
- - $H/D = 1.50$
- △ - $H/D = 1.75$
- ▲ - $H/D = 2.0$
- - $H/D = 1.0$, A.C. Mandal
 $\sigma = 0.4 \%$

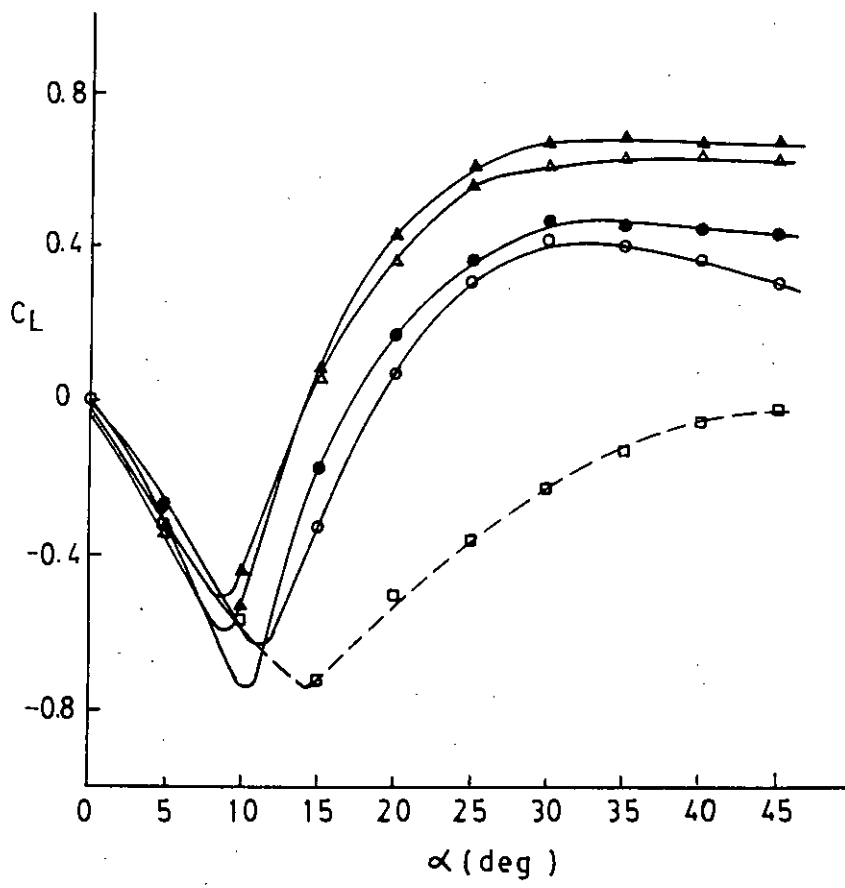


Figure 4.10 : Variation of lift coefficient (C_L) with angle of attack (α) for different side ratios (H/D)

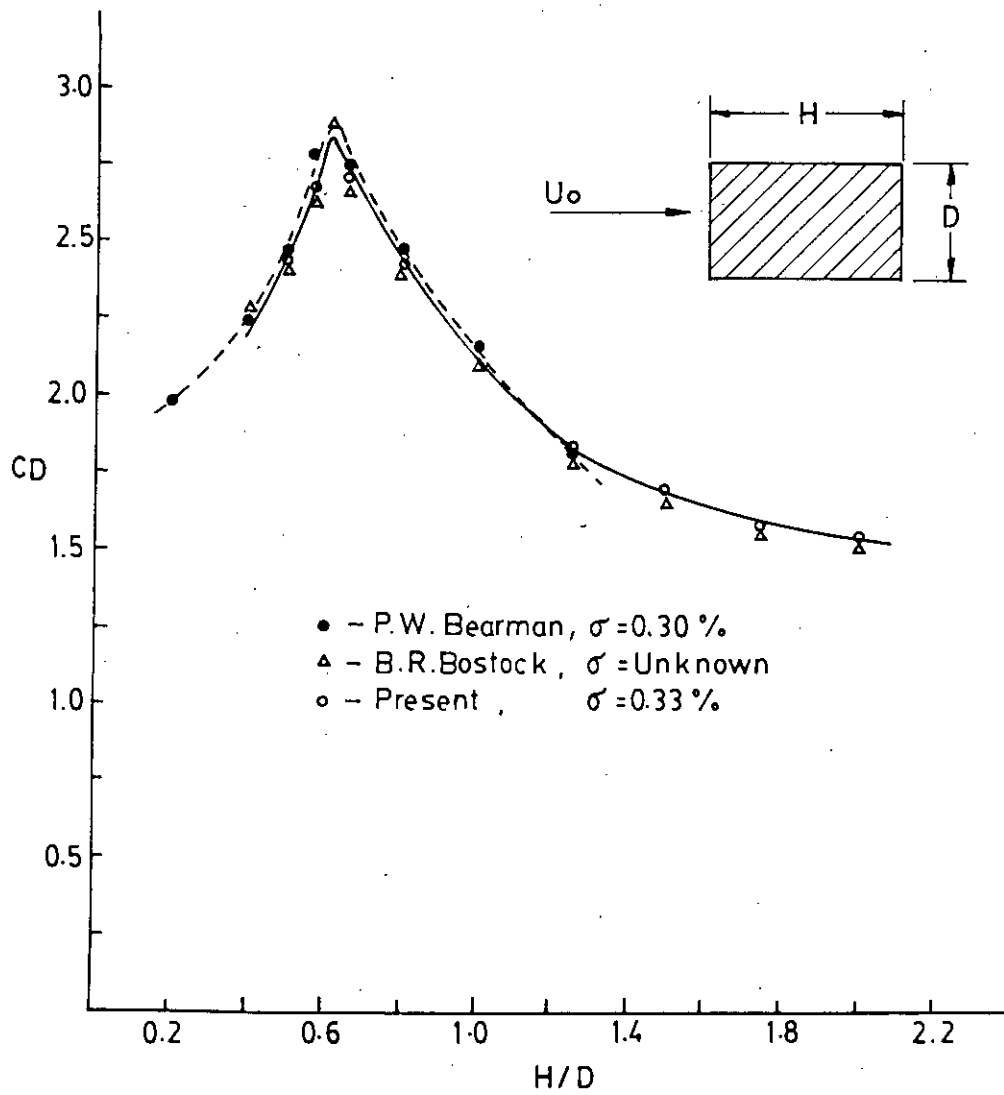


Figure 4-11: Variation of drag coefficients with side ratios at angle of attack of 0°

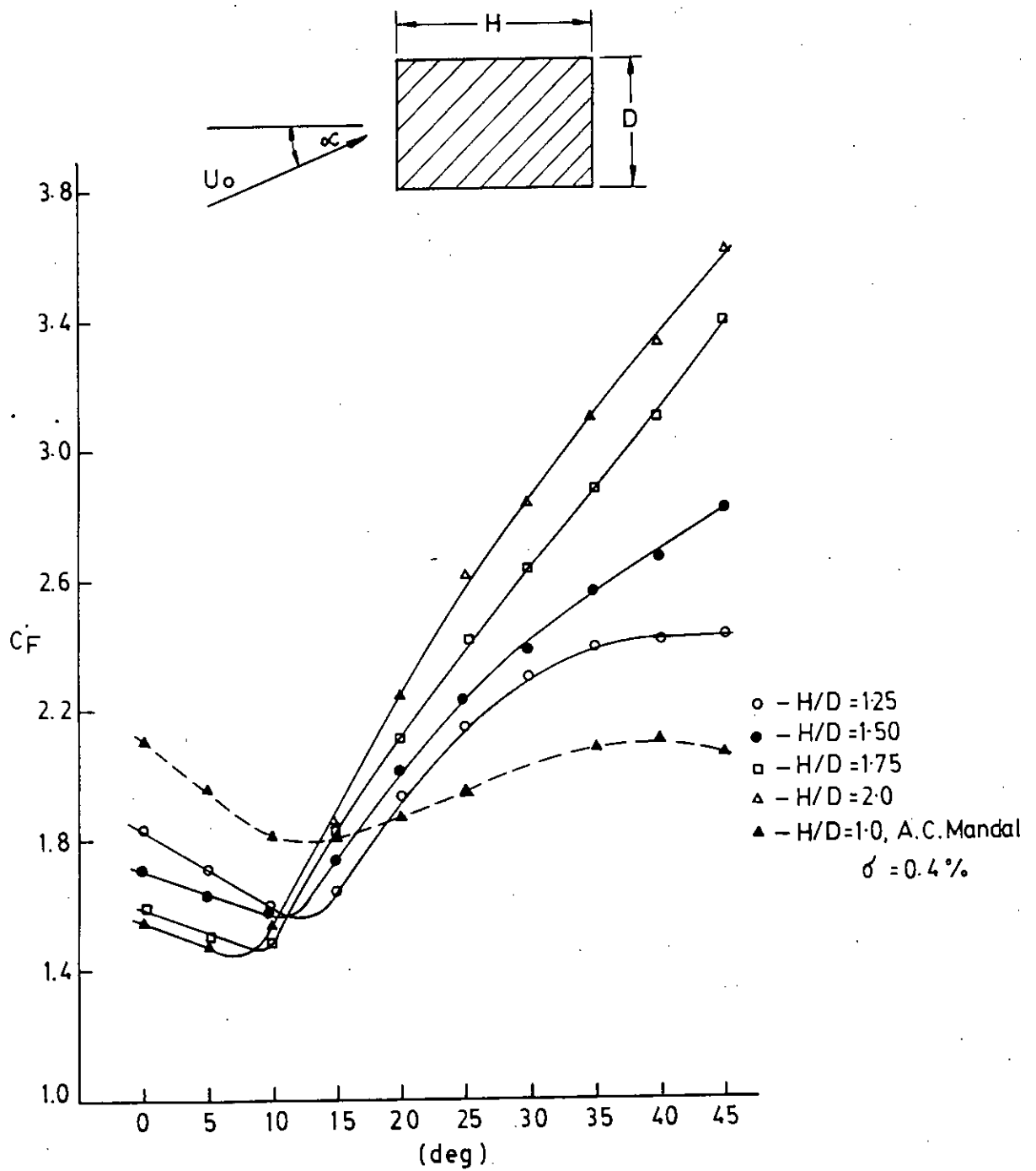


Figure 4.12: Variation of total force co-efficient (C_F) with angle of attack (α) for different side ratios (H/D)

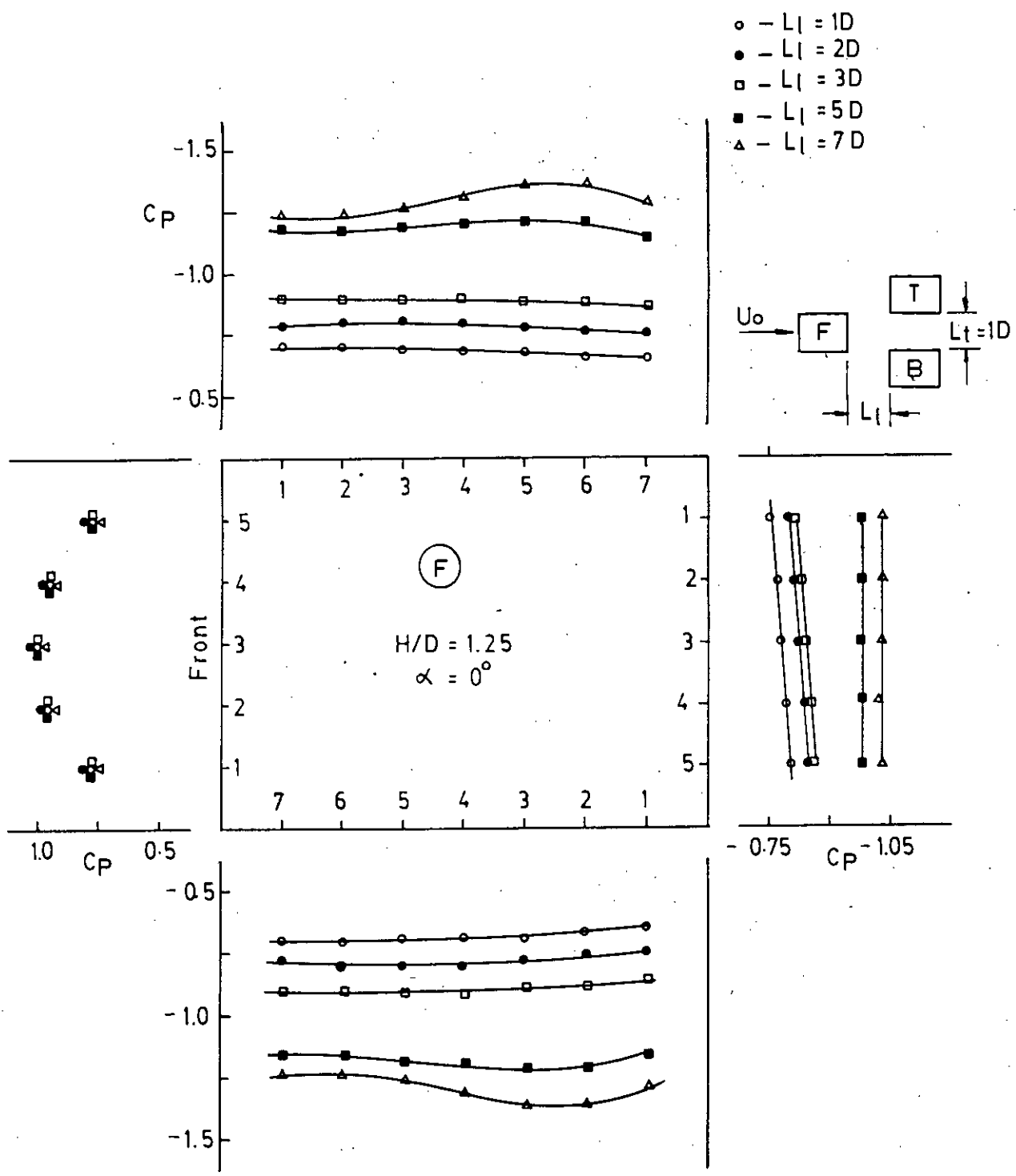


Figure 4-13: Effect of longitudinal spacing (L_l) on C_p -values for upstream cylinder with side ratio (H/D) of 1.25 keeping transverse spacing (L_t) constant at $1D$

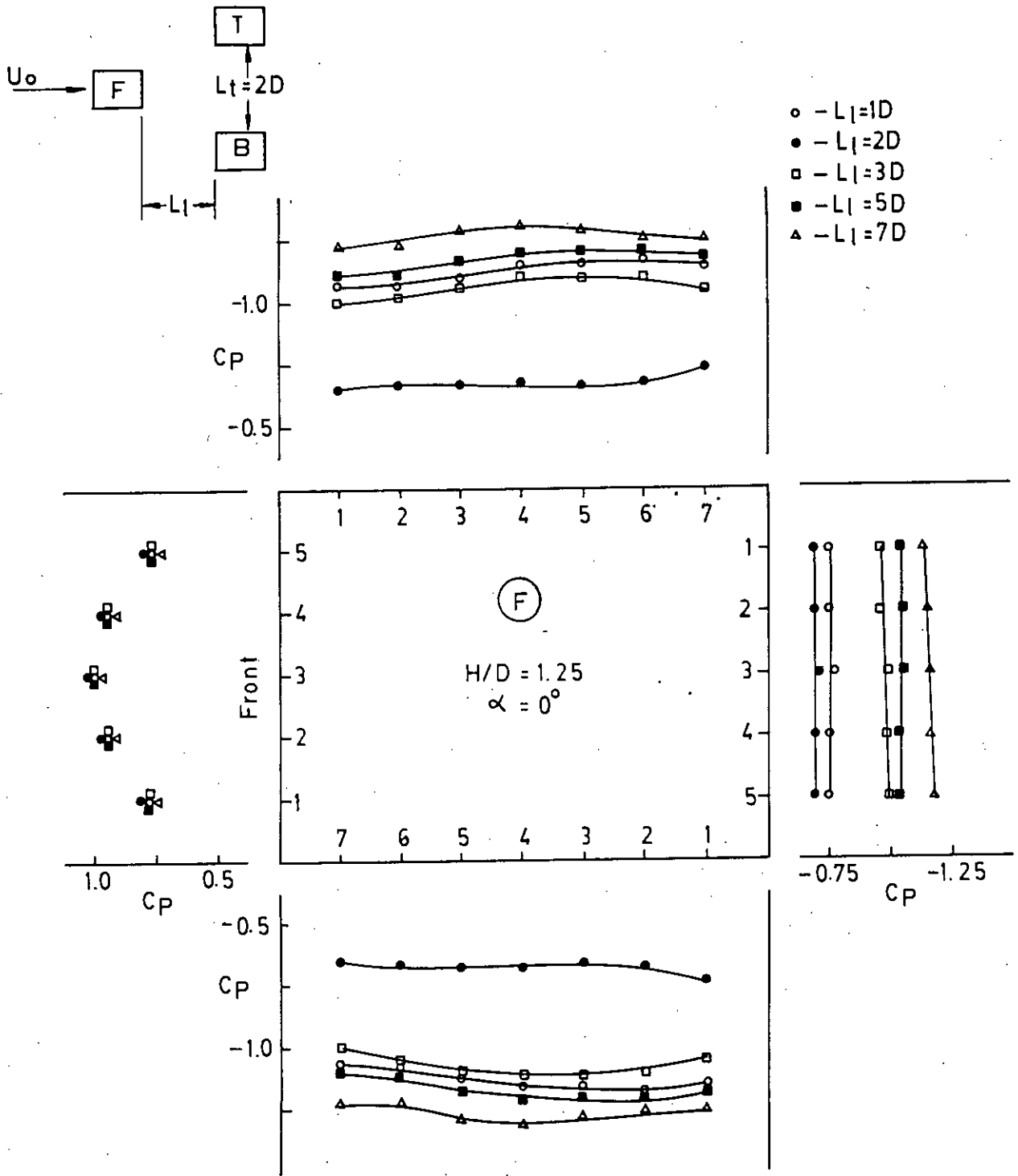


Figure 4.14: Effect of longitudinal spacing (L_1) on C_p -values for upstream cylinder with side ratio (H/D) of 1.25, keeping transverse spacing (L_t) constant at $2D$

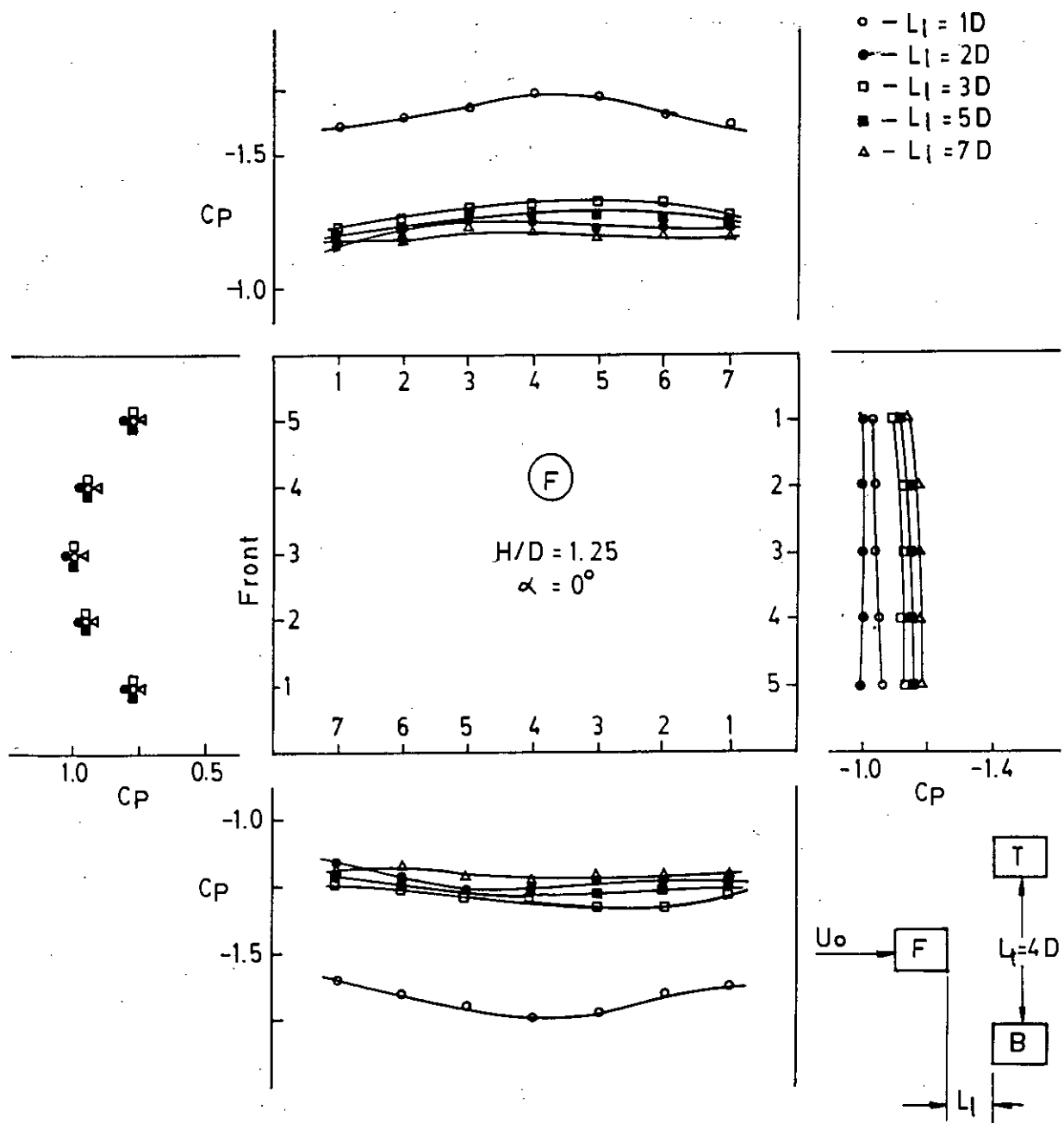


Figure 4-15: Effect of longitudinal spacing (L_l) on C_p -values for upstream cylinder with side ratio (H/D) of 1.25, keeping transverse spacing (L_t) constant at $4D$

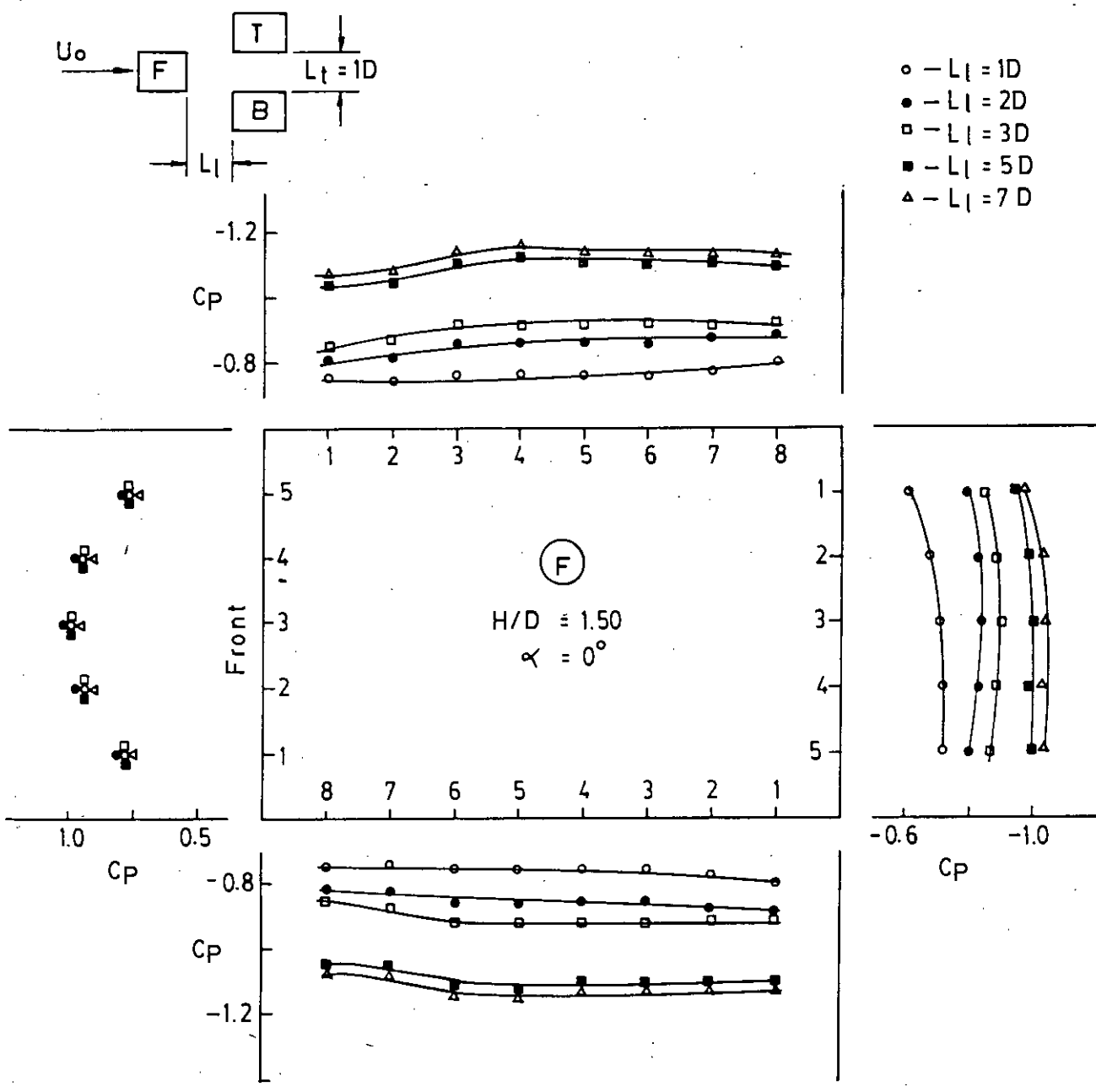


Figure 4-16: Effect of longitudinal spacing (L_l) on C_p -values for upstream cylinder with side ratio (H/D) of 1.50, keeping transverse spacing (L_t) constant at 1D

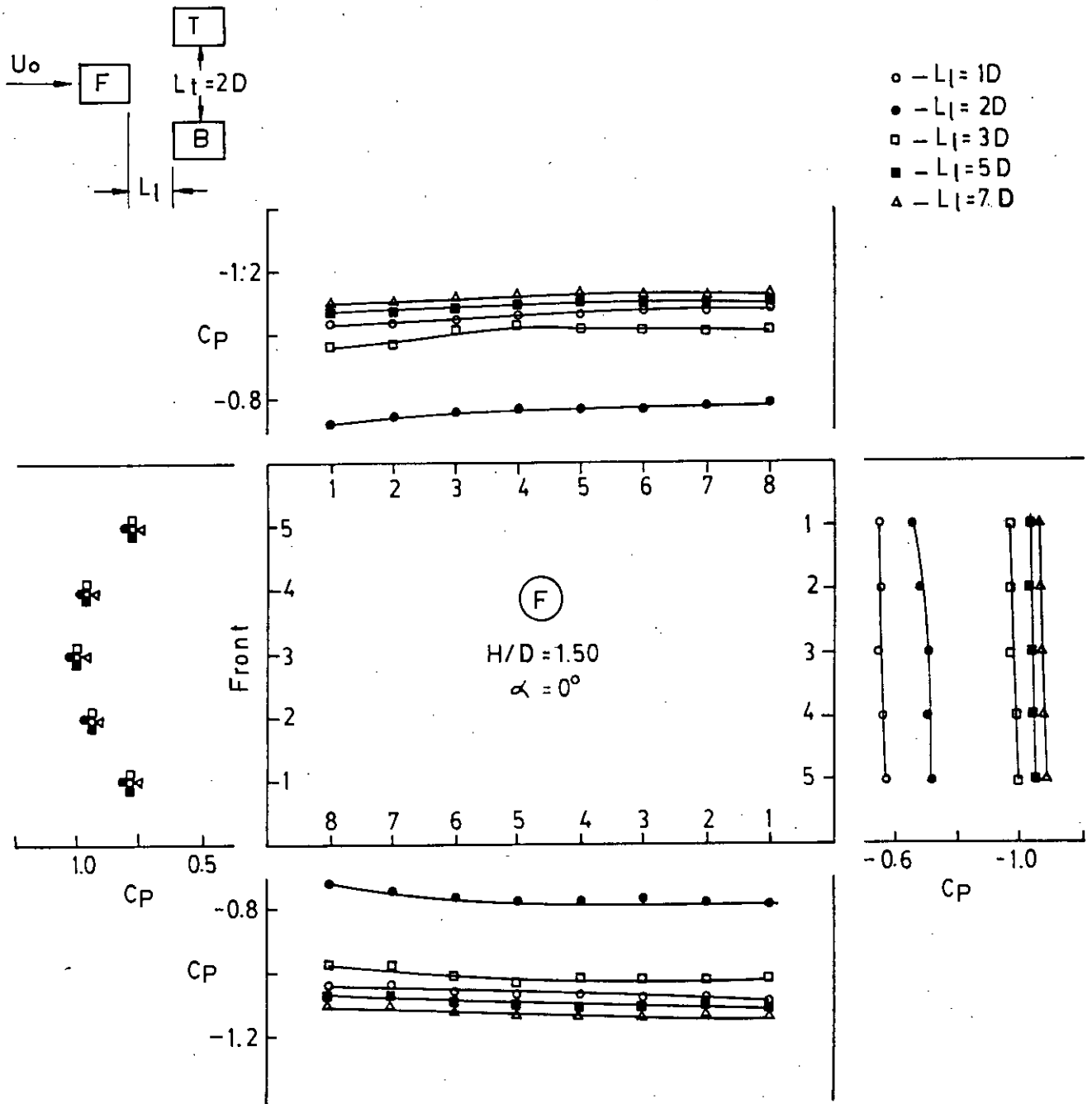


Figure 4-17: Effect of longitudinal spacing (L_1) on C_p -values for upstream cylinder with side ratio (H/D) of 1.50, keeping transverse spacing constant at $2D$

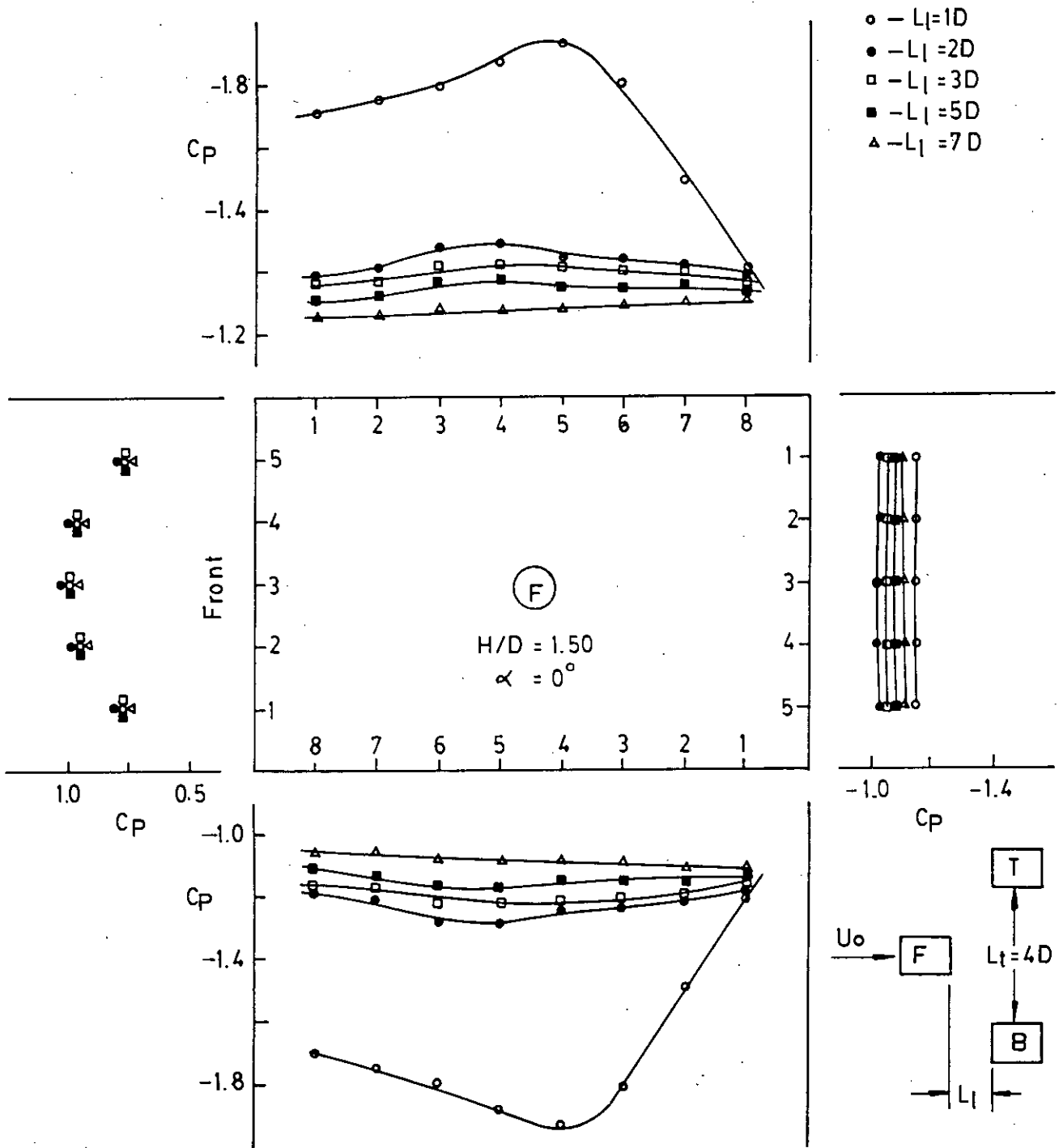


Figure 4-18 : Effect of longitudinal spacing (L_l) on C_p -values for upstream cylinder with side ratio (H/D) of 1.50, keeping transverse spacing (L_t) constant at $4D$

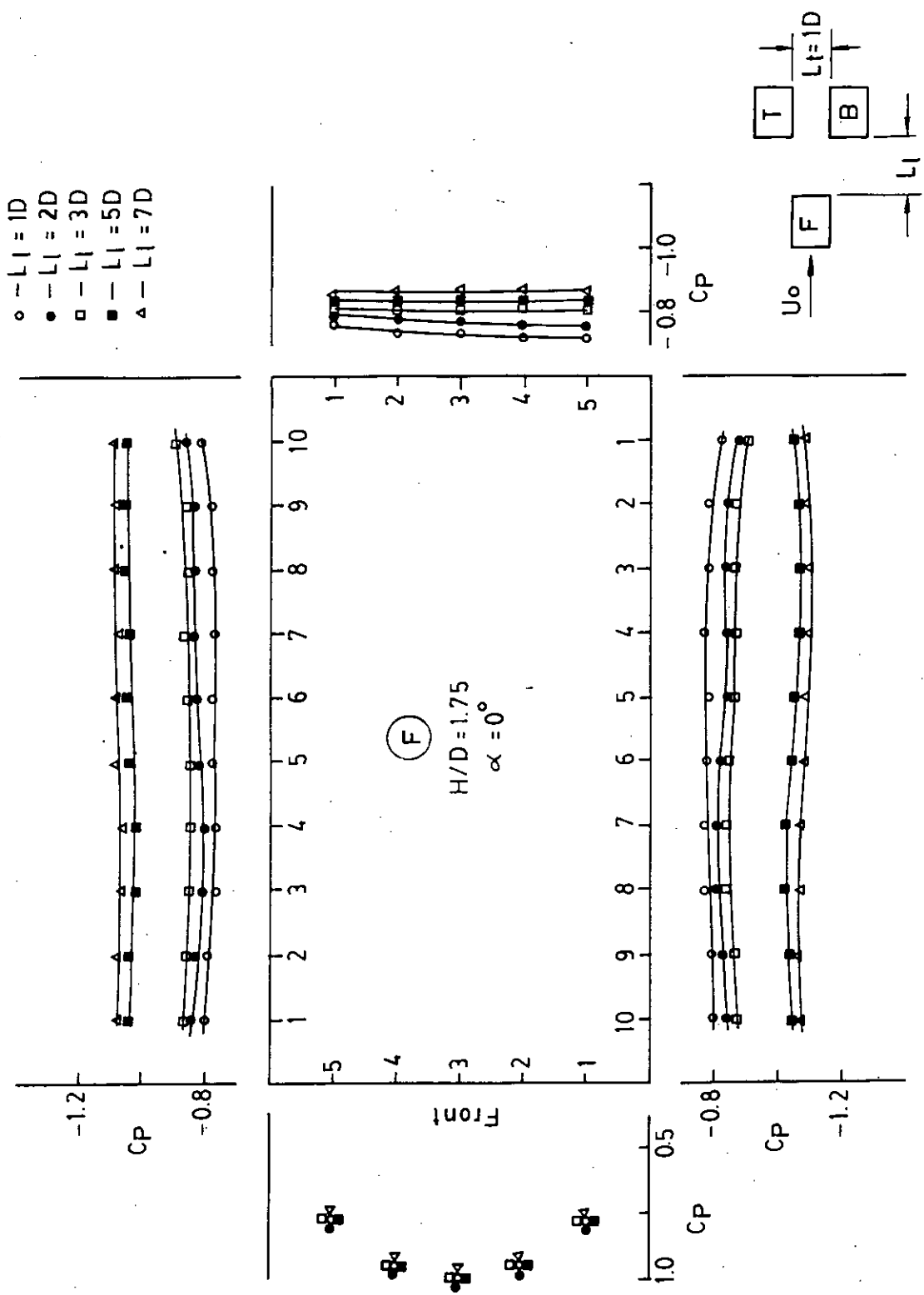


Figure 4-19: Effect of longitudinal spacing ($L1$) on C_p -values for upstream cylinder with side ratio (H/D) of 1.75, keeping transverse spacing constant at $1D$

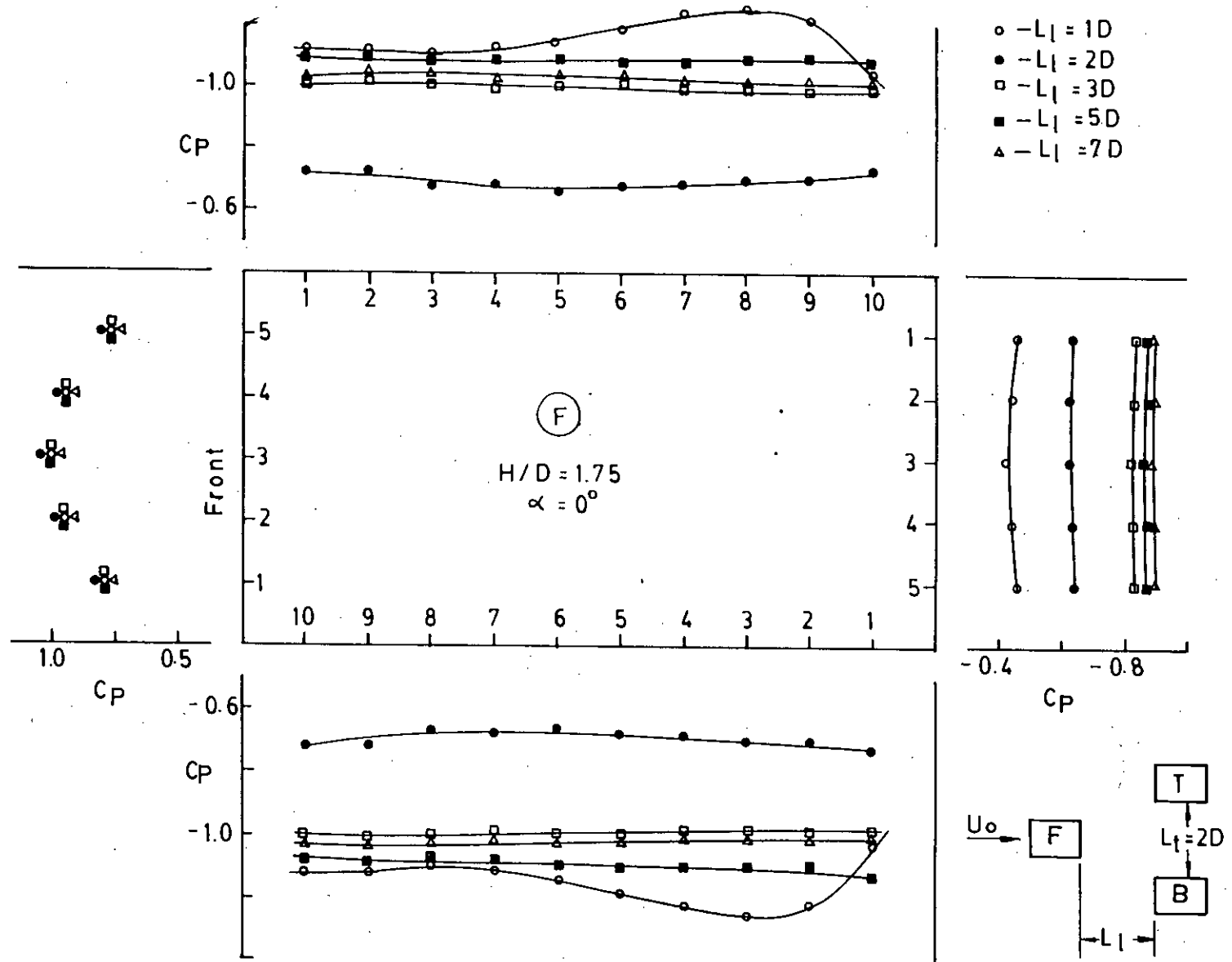


Figure 4-20: Effect of longitudinal spacing (L_l) on C_p -values for upstream cylinder with side ratio (H/D) of 1.75, keeping transverse spacing (L_t) constant at 2D

- - $L_t = 1D$
- - $L_t = 2D$
- - $L_t = 3D$
- - $L_t = 5D$
- △ - $L_t = 7D$

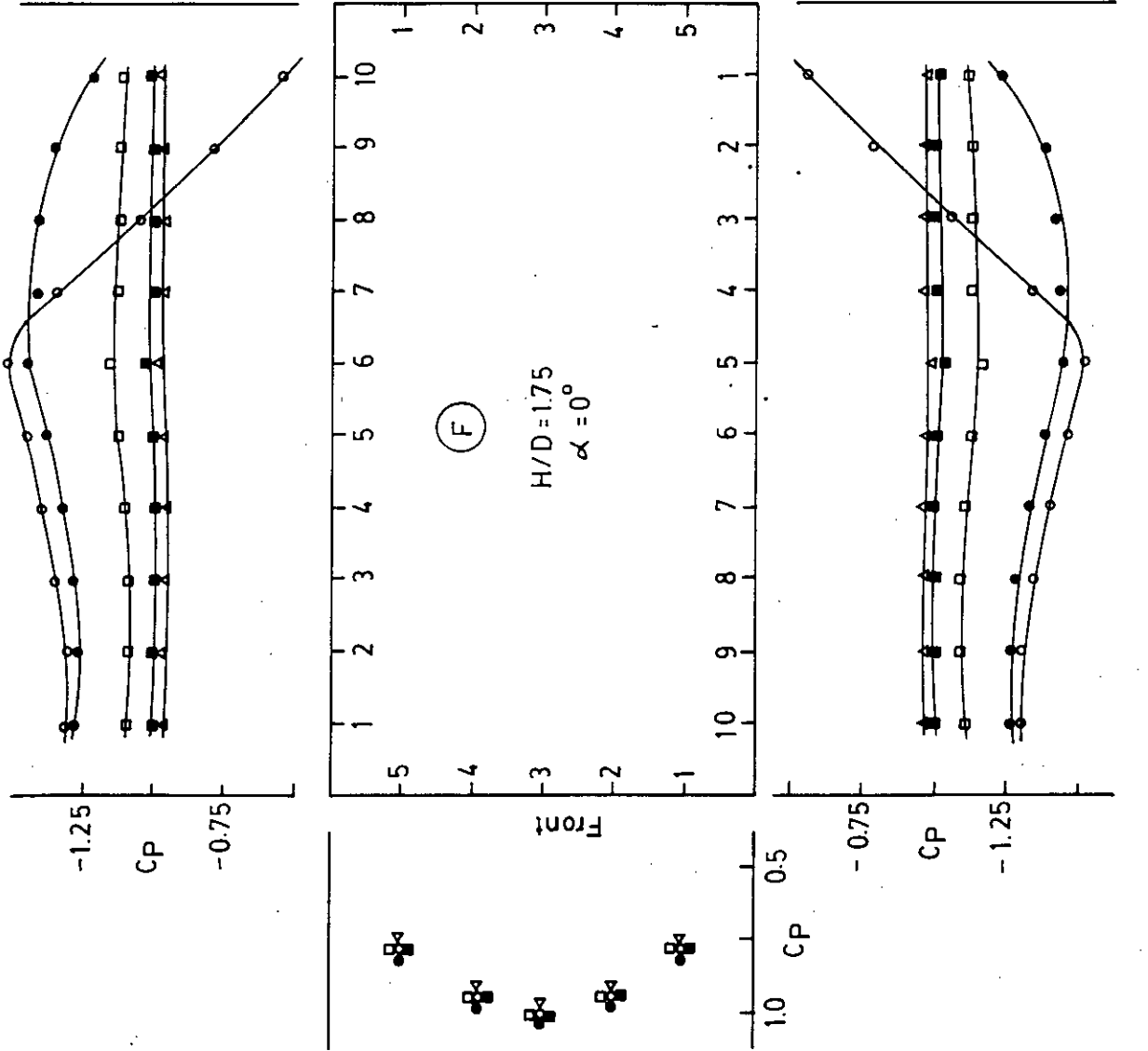


Figure 4.21: Effect of longitudinal spacing (L_t) on C_p -values for upstream cylinder with side ratio (H/D) of 1.75, keeping transverse spacing (L_t) constant at $4D$

- - $L_t = 1D$
- - $L_t = 2D$
- - $L_t = 3D$
- - $L_t = 5D$
- △ - $L_t = 7D$

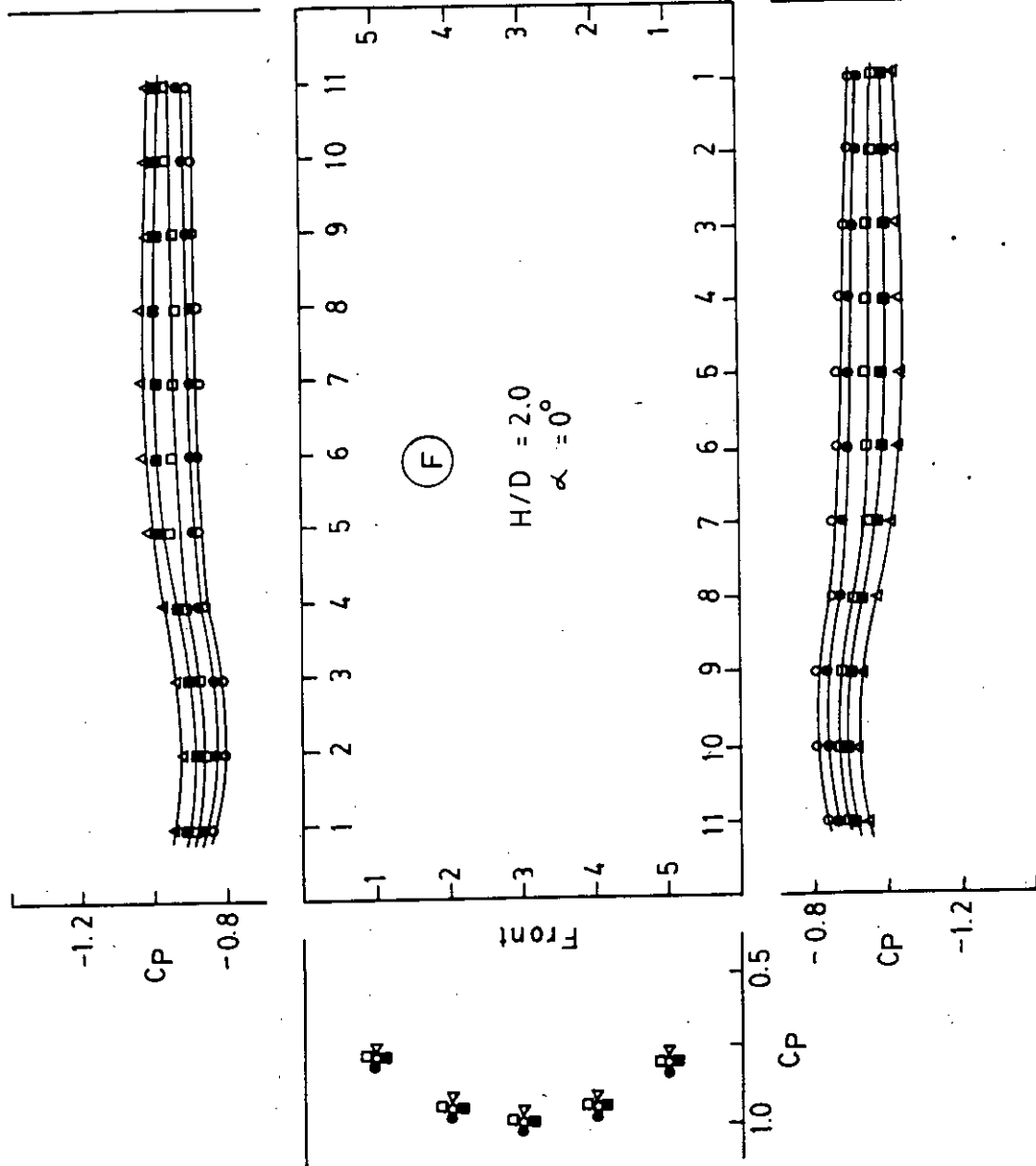


Figure 4-22: Effect of longitudinal spacing (L_t) on C_p -values for upstream cylinder with side ratio (H/D) of 2.0, keeping transverse spacing (L_t) constant at 1D

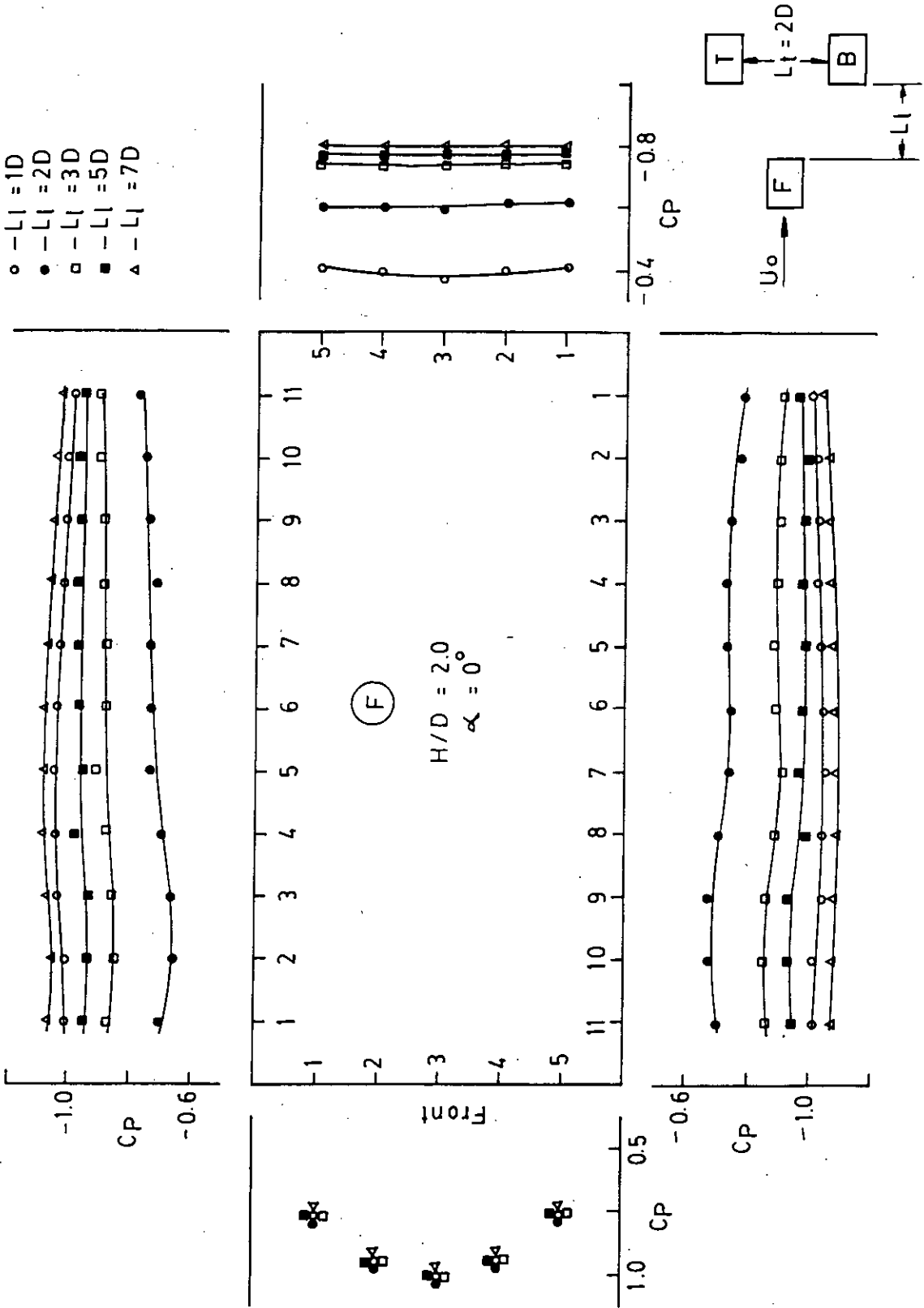


Figure 4-23: Effect of longitudinal spacing (L_j) on C_p -values for upstream cylinder with side ratio (H/D) of 2.0, keeping transverse spacing (L_j) constant at 2D.

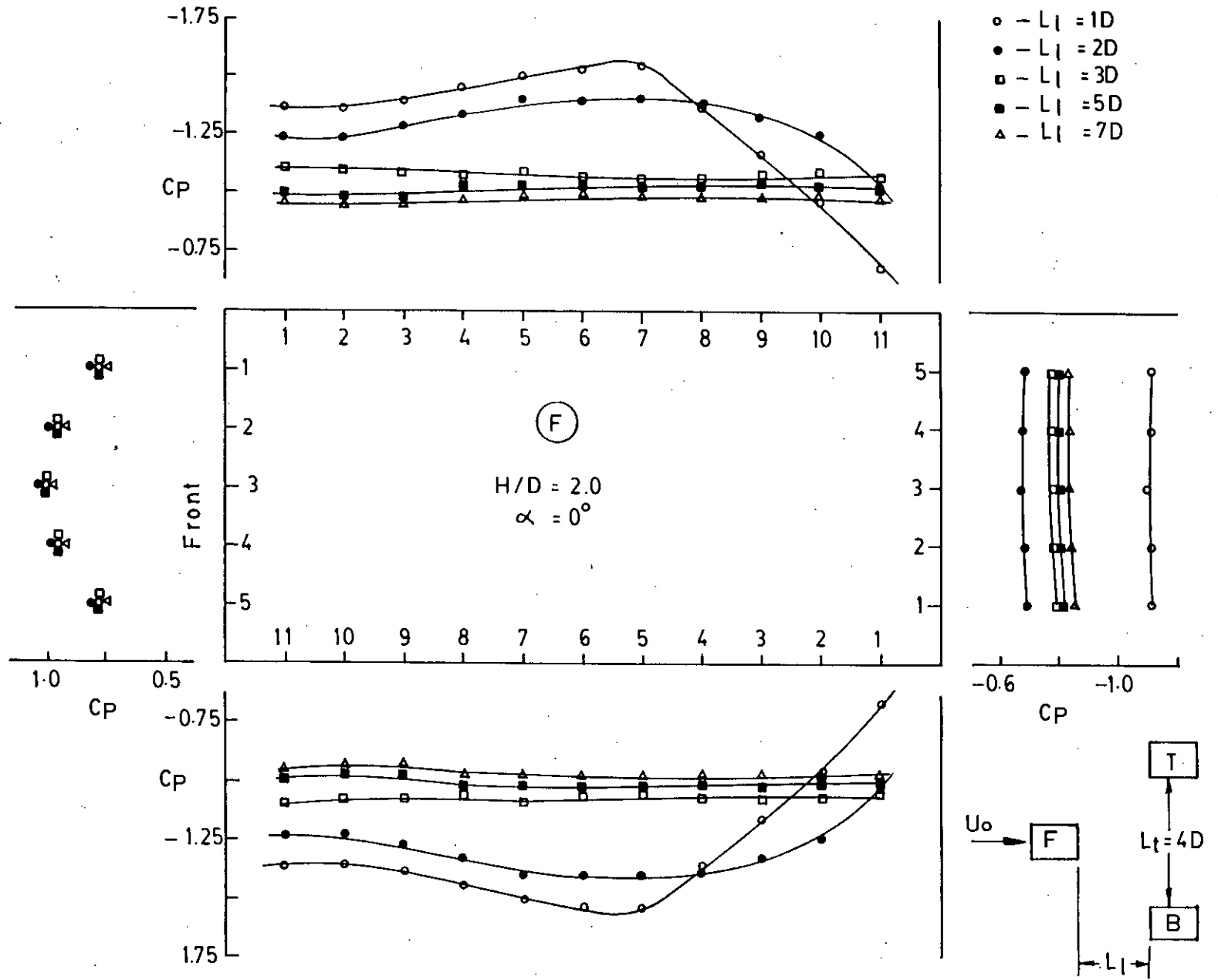


Figure 4-24: Effect of longitudinal spacing (L_l) on C_p -values for upstream cylinder with side ratio (H/D) of 2.0, keeping transverse spacing (L_t) constant at 4D

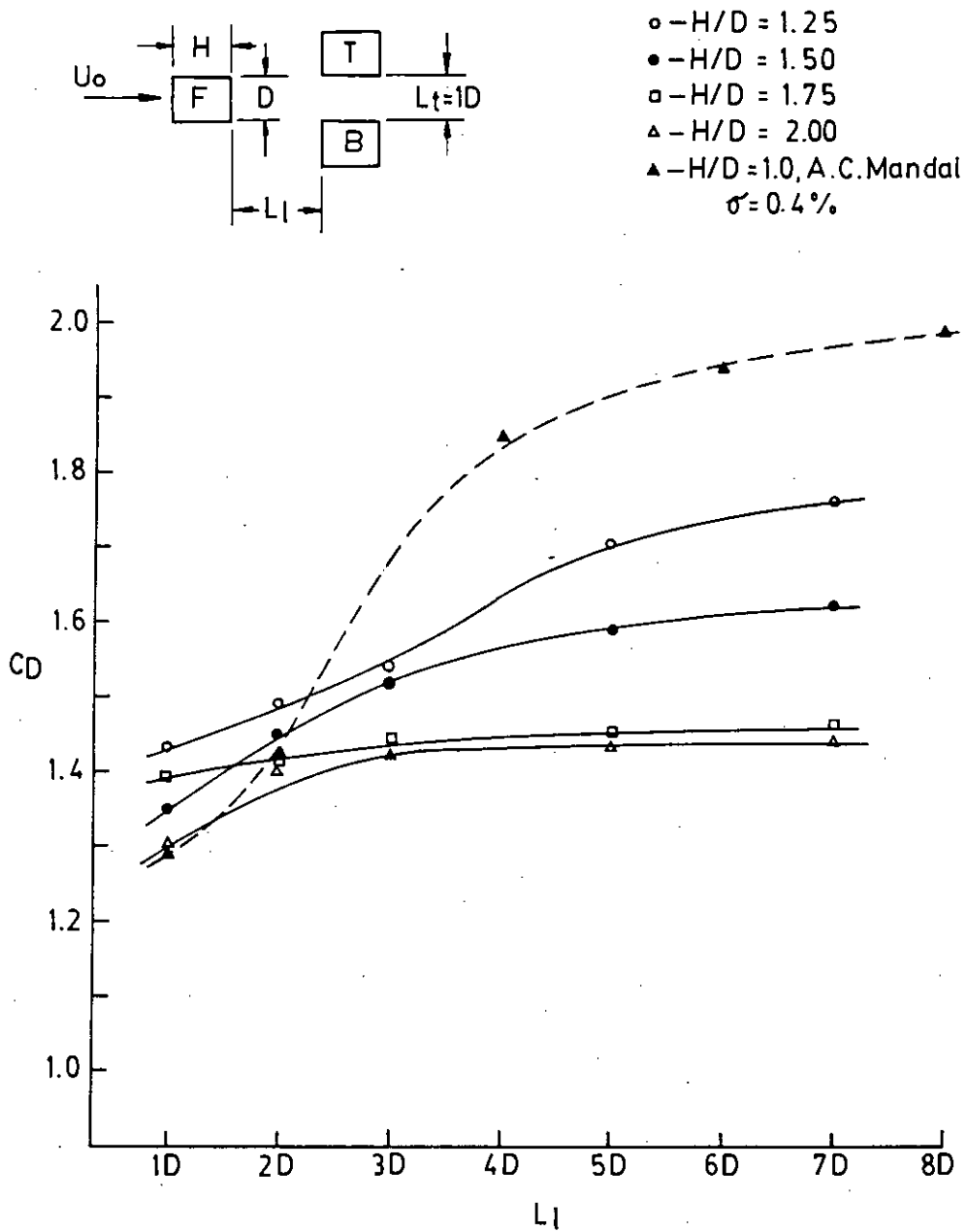


Figure 4-25: Variation of drag coefficient (C_D) with longitudinal spacing (L_1) on upstream cylinder for different side ratios (H/D) at constant transverse spacing (L_t) of $1D$

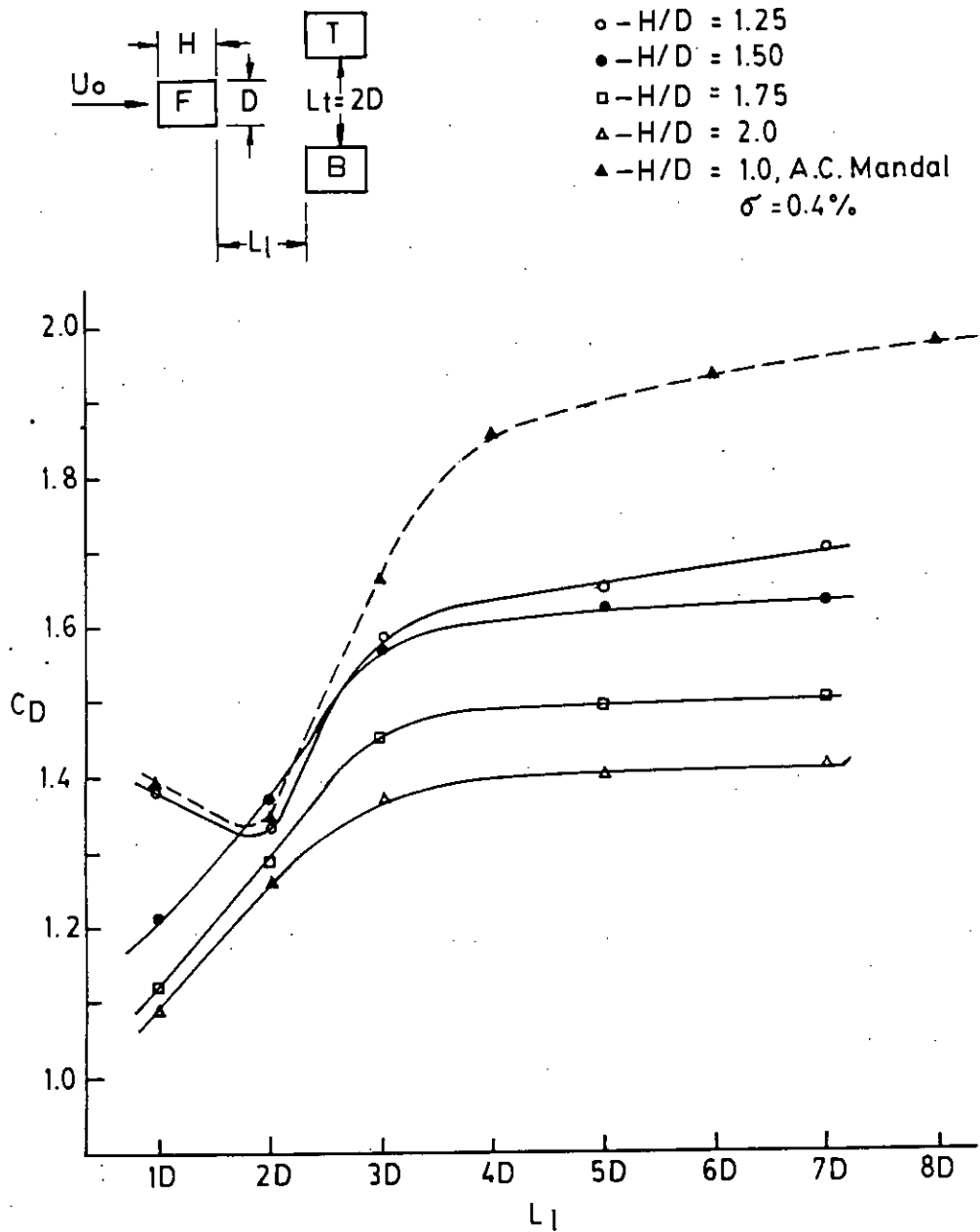
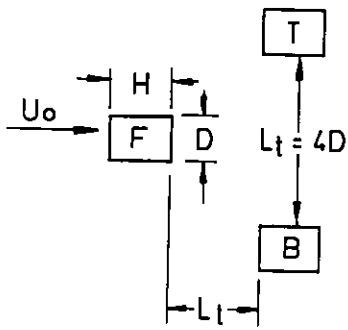


Figure 4-26: Variation of drag coefficient (C_D) with longitudinal spacing (L_1) on upstream cylinder for different side ratios (H/D) at constant transverse spacing (L_t) at $2D$



- - $H/D = 1.25$
- - $H/D = 1.50$
- - $H/D = 1.75$
- △ - $H/D = 2.0$
- ▲ - $H/D = 1.0$, A.C. Mandal
 $\sigma = 0.4\%$

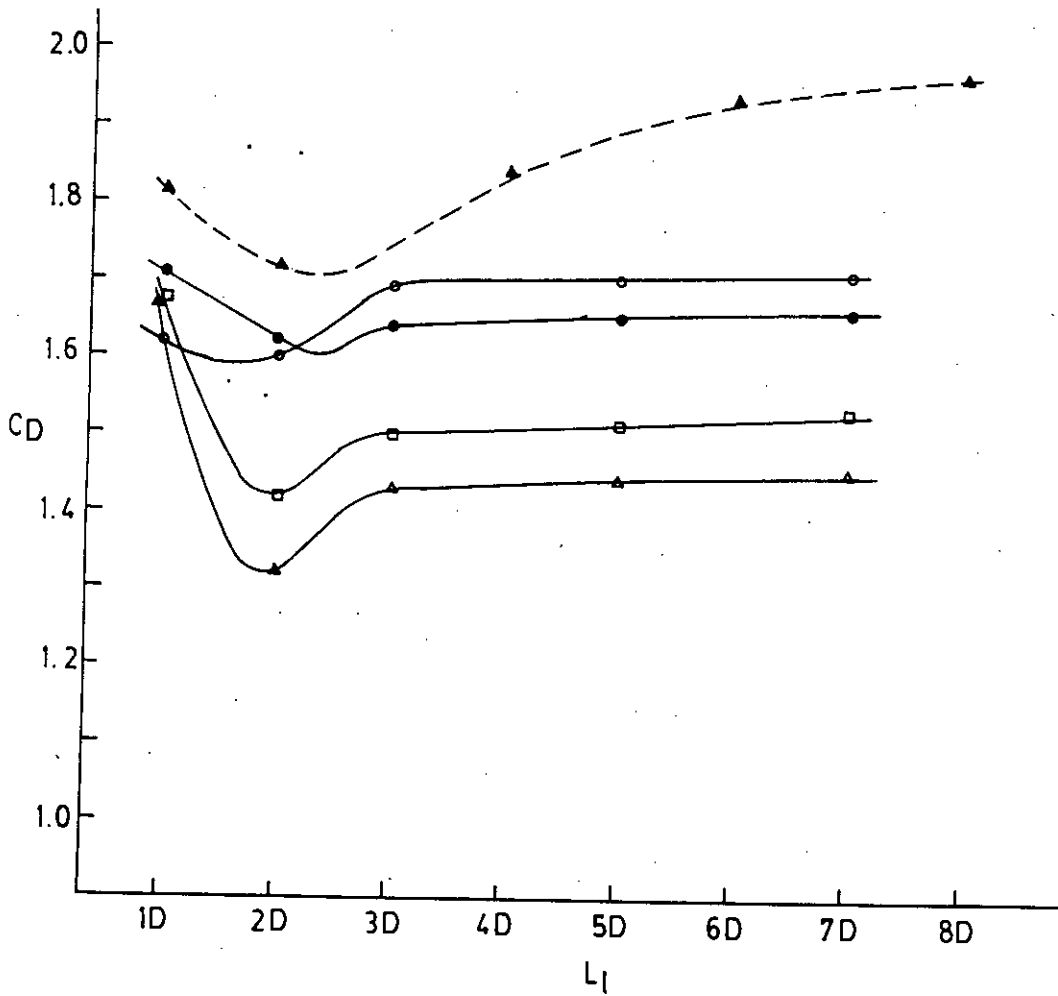


Figure 4-27: Variation of drag co-efficient (C_D) with longitudinal spacing (L_l) on upstream cylinder for different side ratios (H/D) at constant transverse spacing (L_t) at $4D$

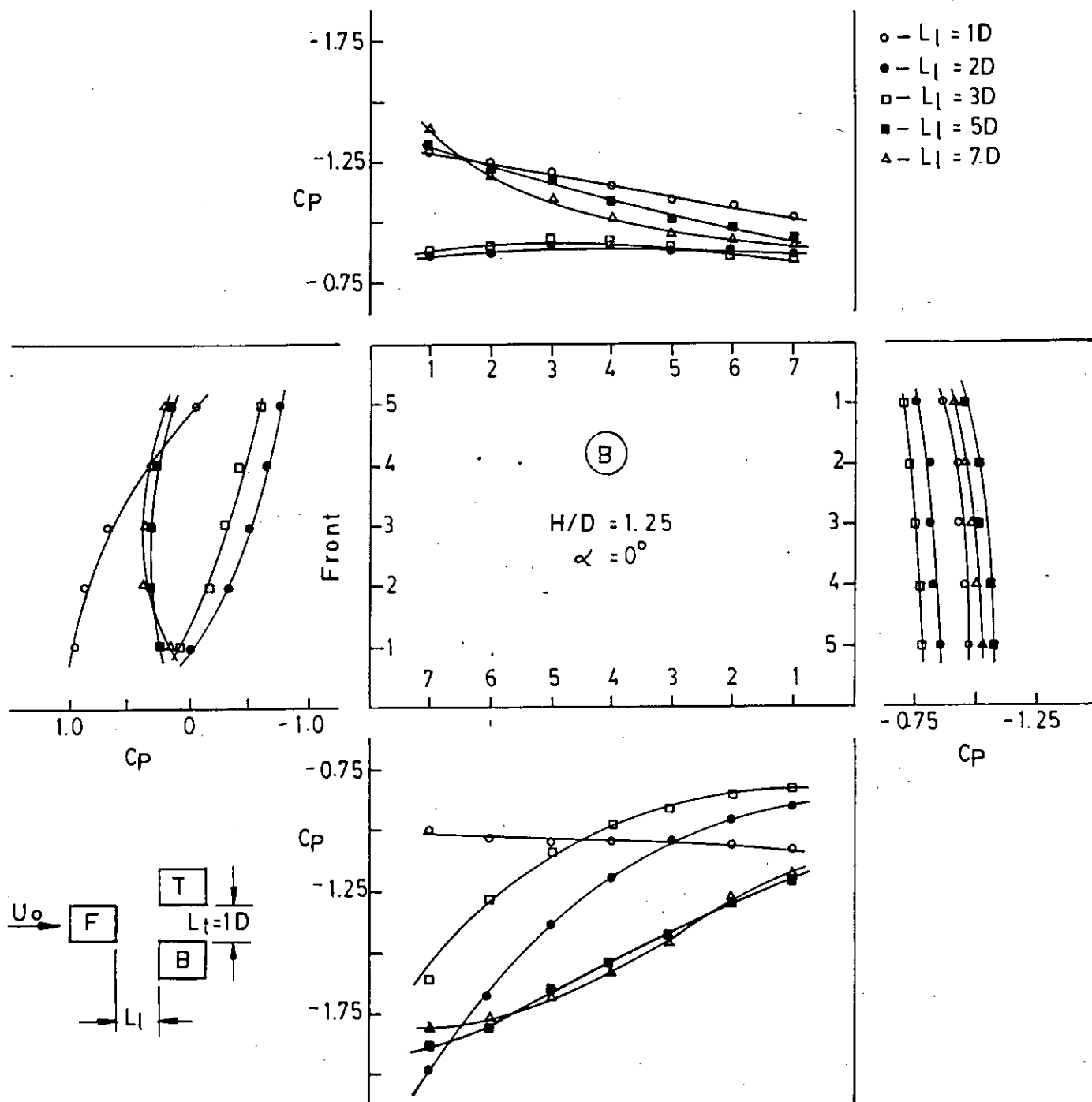


Figure 4-28: Effect of longitudinal spacing (L_l) on C_p -distributions for downstream cylinder with side ratio (H/D) of 1.25, keeping transverse spacing (L_t) constant at 1D

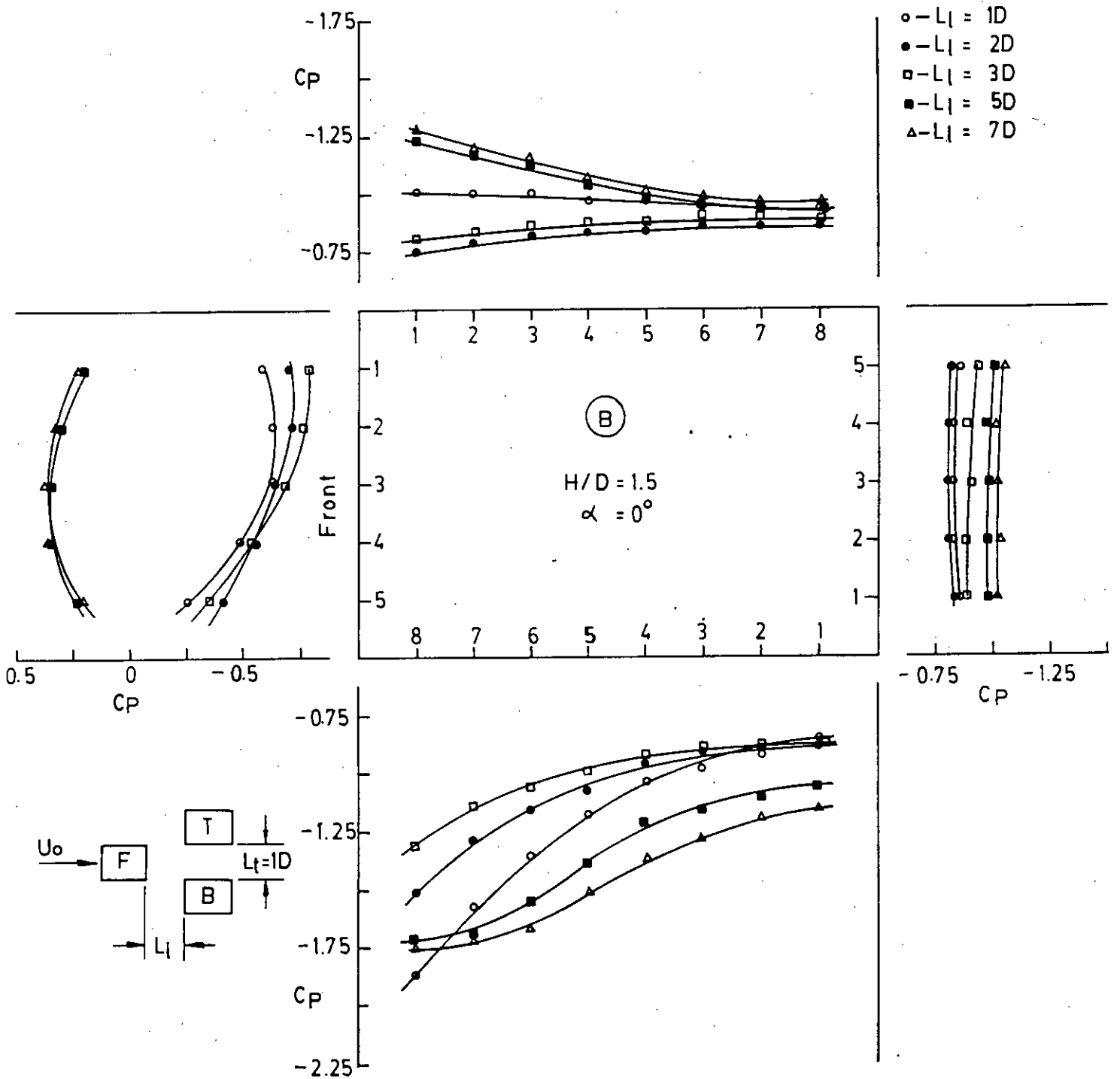


Figure 4-29: Effect of longitudinal spacing (L_l) on C_p -distributions for downstream cylinder with side ratio (H/D) of 1.5, keeping transverse spacing (L_t) constant at 1D

- - $L_t = 2D$
- - $L_t = 3D$
- - $L_t = 5D$
- △ - $L_t = 7D$

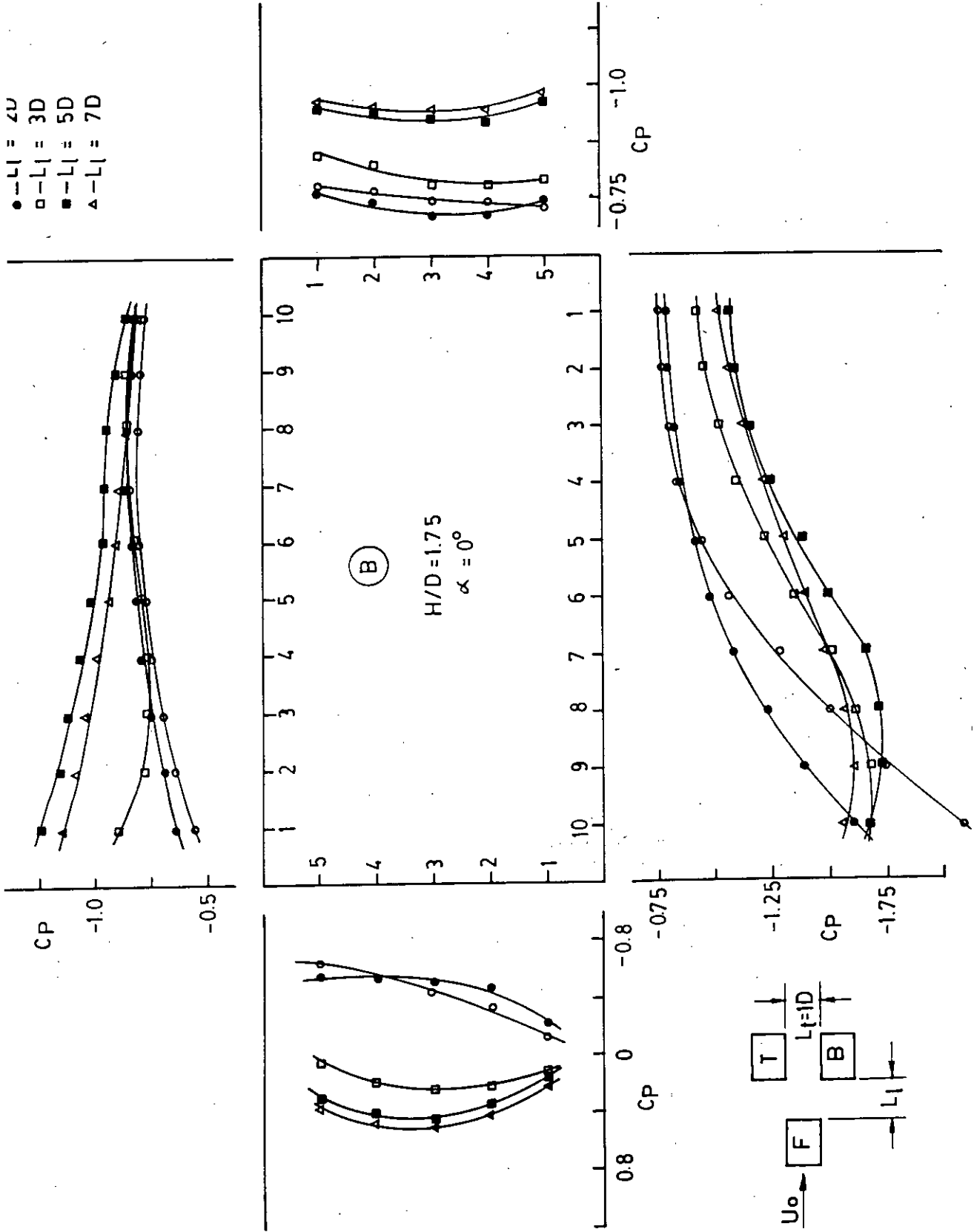


Figure 4-30 : Effect of longitudinal spacing (L_t) on C_p -distributions for downstream cylinder with side ratio (H/D) of 1.75, keeping transverse spacing (L_t) constant at 1D

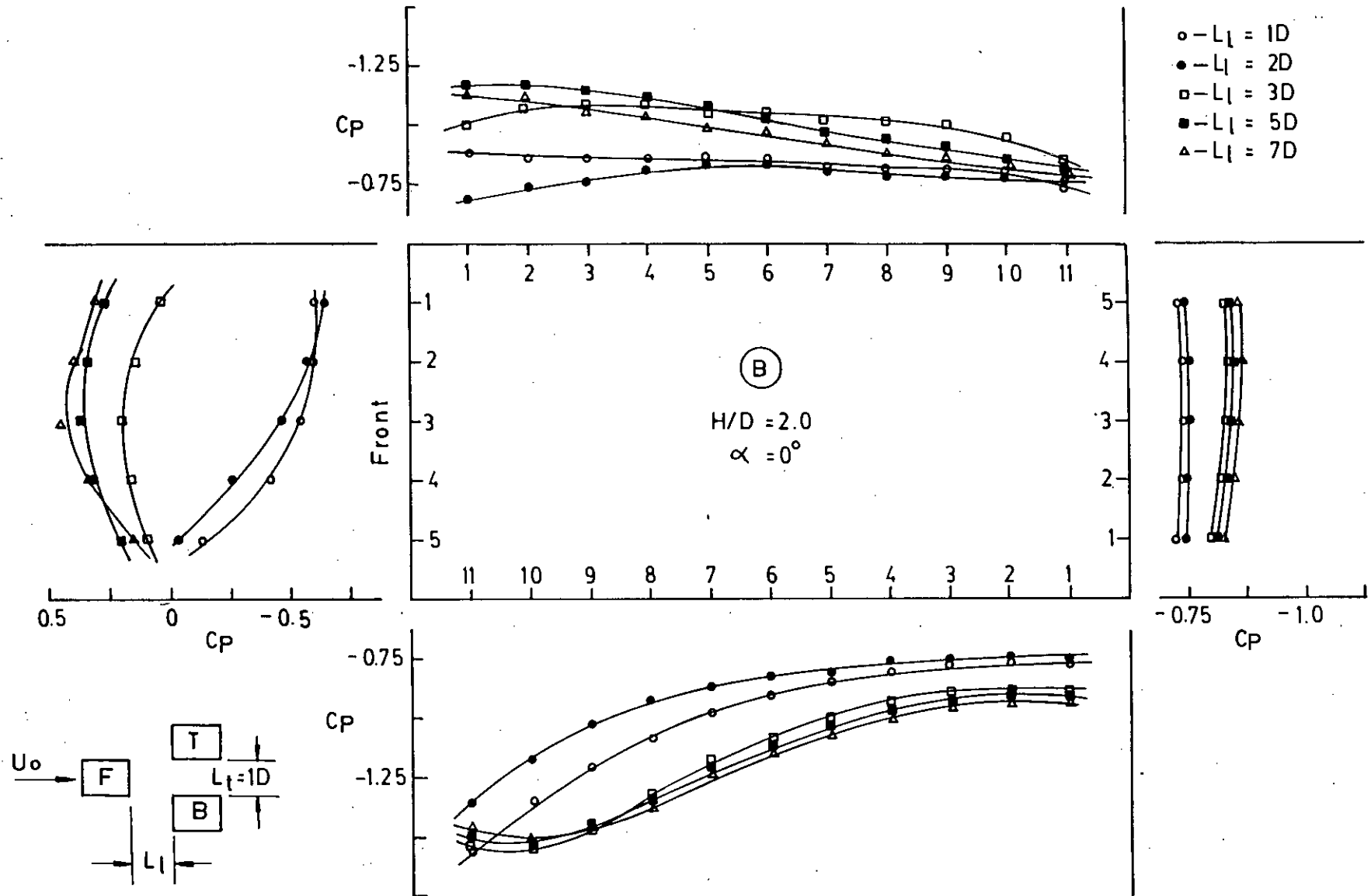


Figure 4.31 : Effect of longitudinal spacing (L_l) on C_p -distribution for downstream cylinder with side ratio (H/D) of 2.0, keeping transverse spacing (L_t) constant at 1D

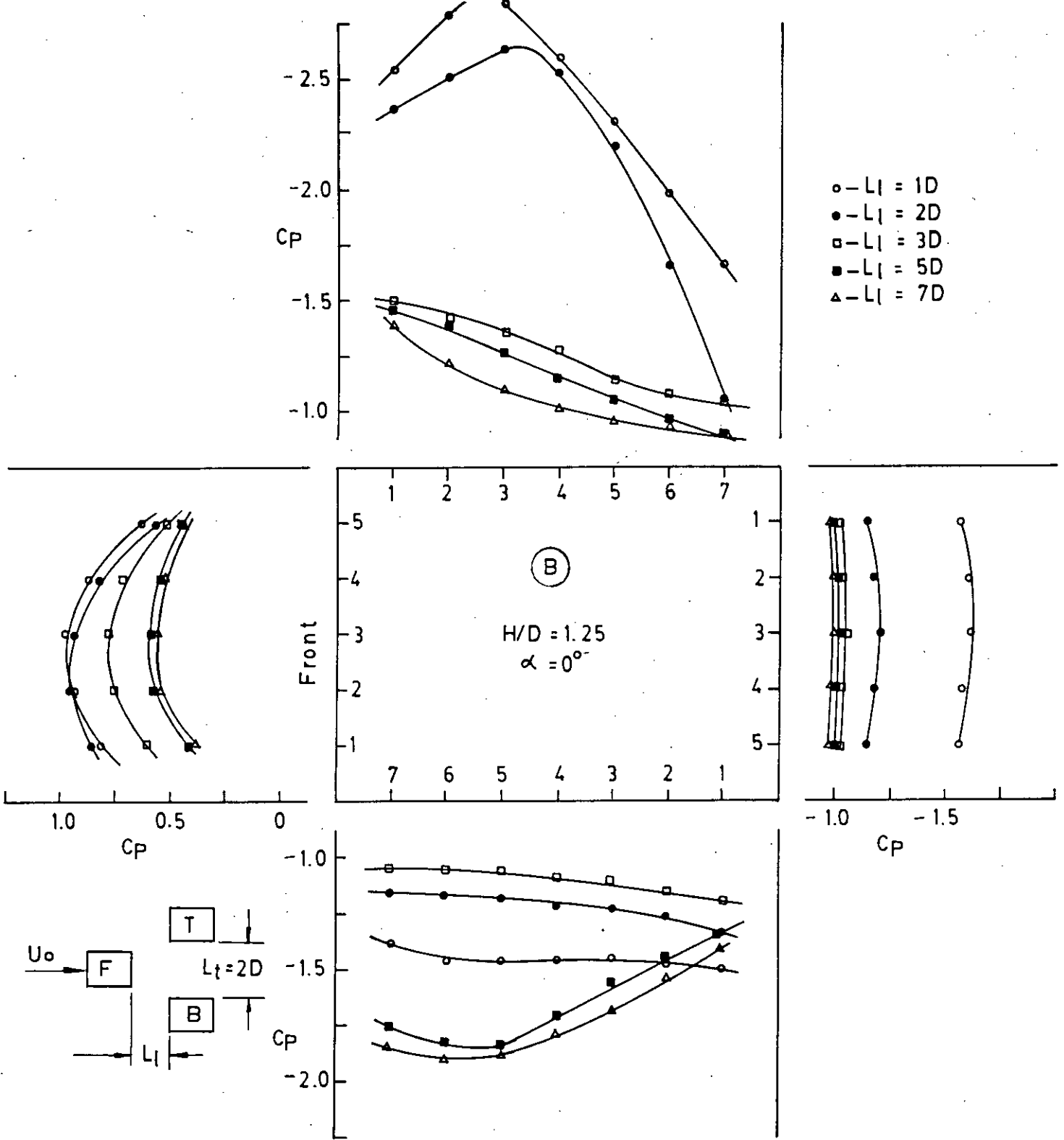


Figure 4-32: Effect of longitudinal spacing (L_1) on C_p -distribution for downstream cylinders with side ratio (H/D) of 1.25, keeping transverse spacing (L_t) constant at $2D$

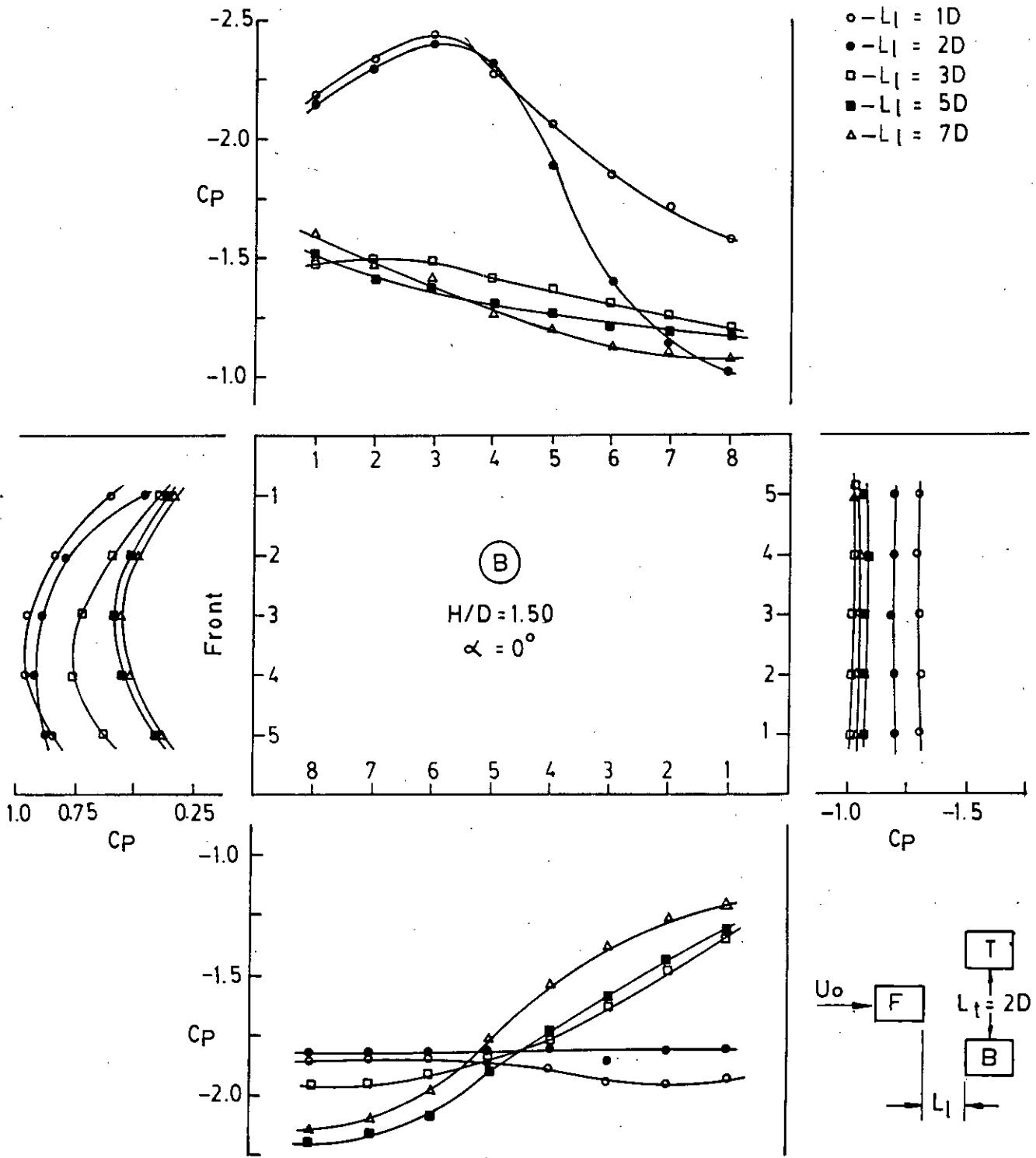


Figure 4-33: Effect of longitudinal spacing (L_l) on C_p -distribution for downstream cylinder with side ratio (H/D) of 1.50, keeping transverse spacing (L_t) constant at 2D

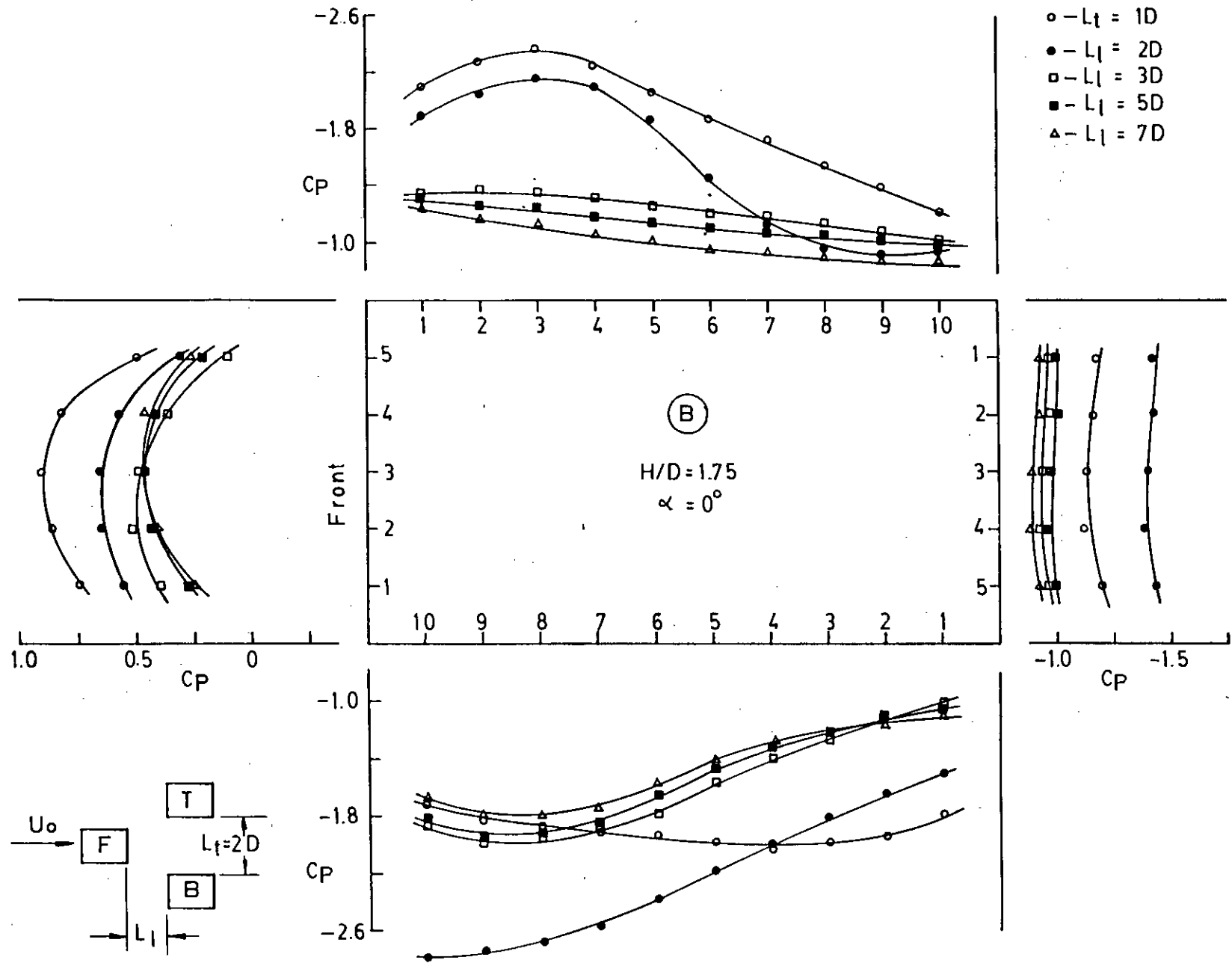


Figure 4-34 : Effect of longitudinal spacing (L_l) on C_p -distributions for downstream cylinder with side ratio (H/D) of 1.75, keeping transverse spacing (L_t) constant at 2D

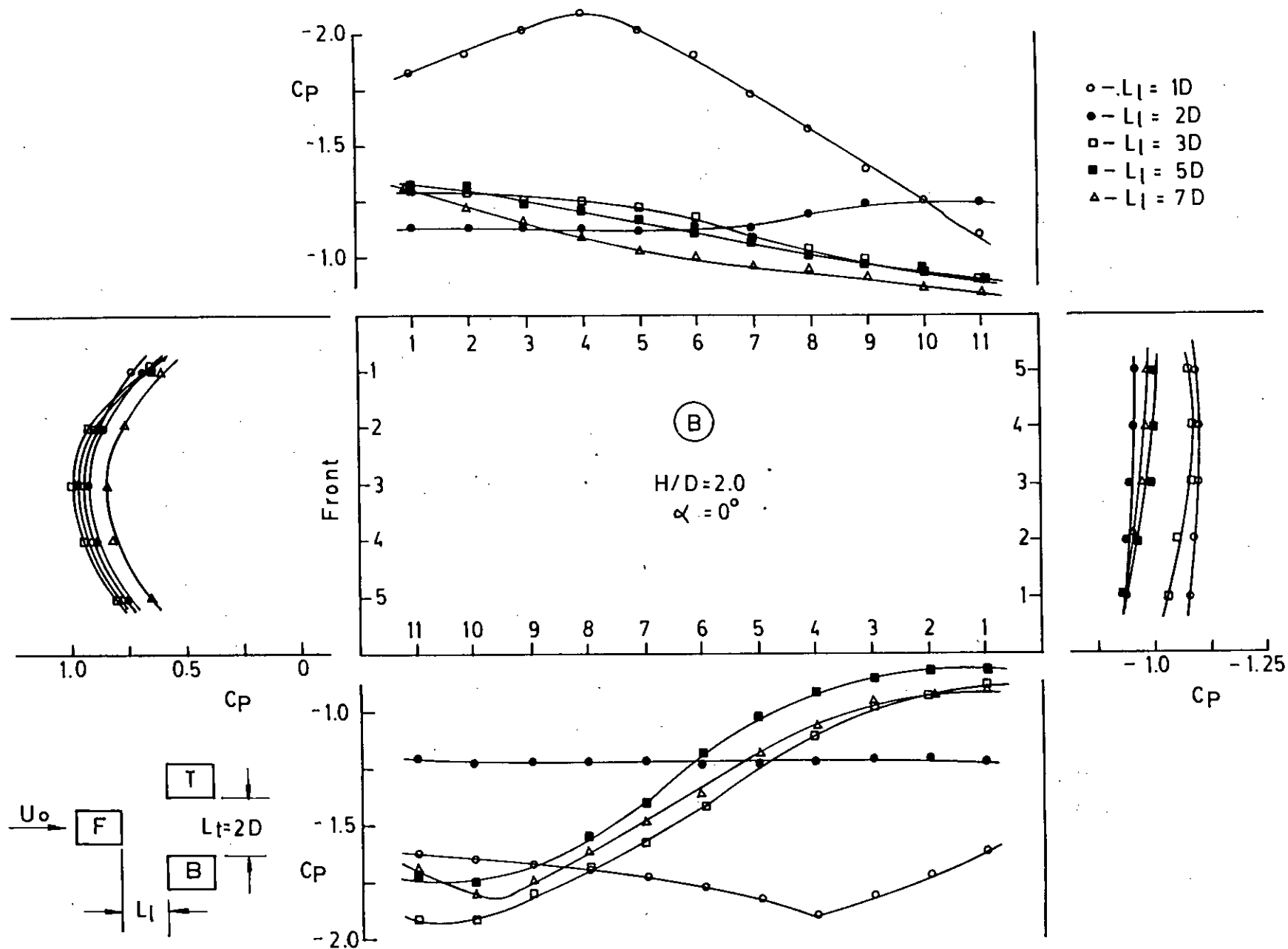


Figure 4-35 : Effect of longitudinal spacing (L_1) on C_p -distributions for downstream cylinder with side ratio (H/D) of 2.0, keeping transverse spacing (L_t) constant at 2D

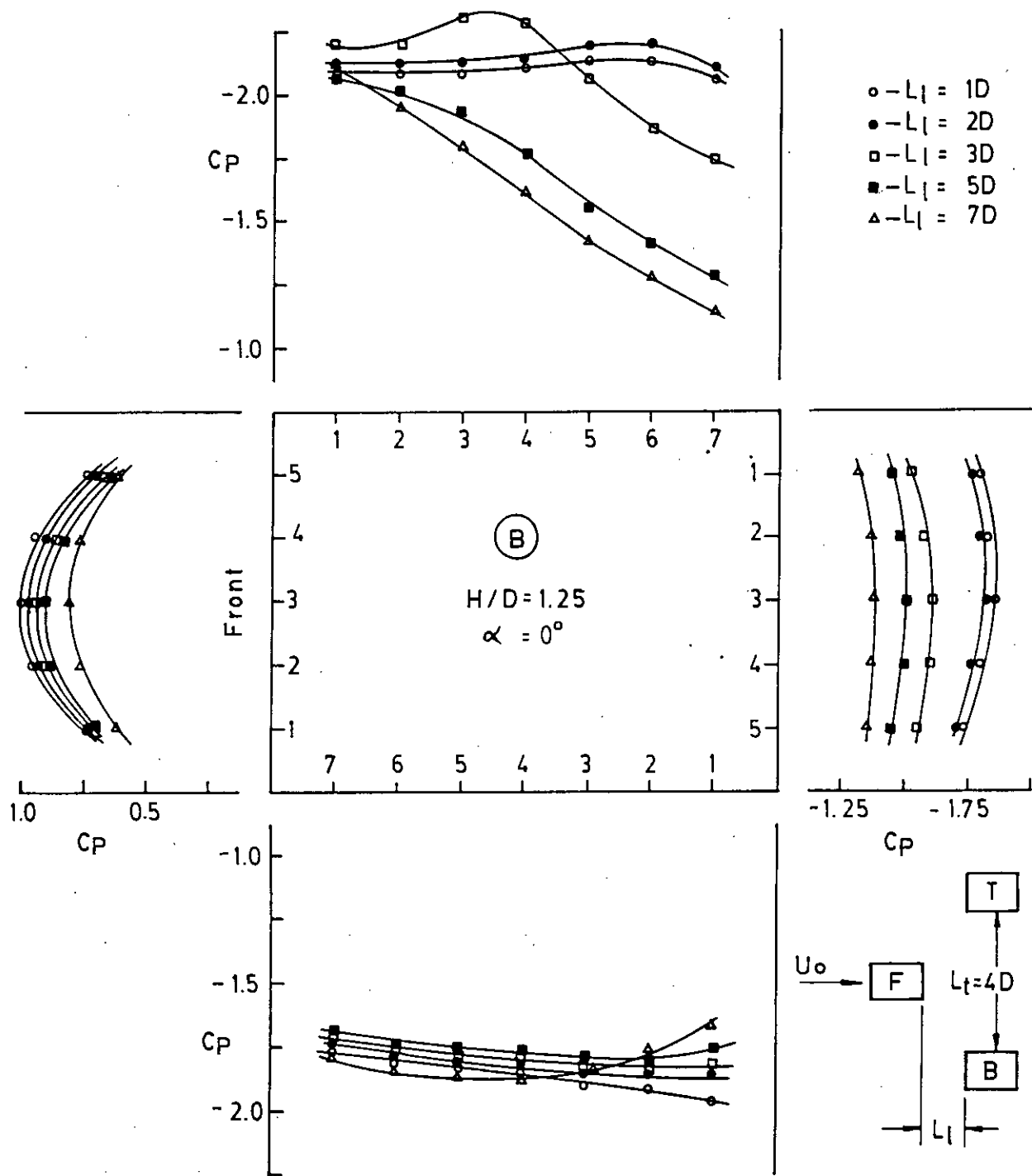


Figure 4-36: Effect of longitudinal spacing (L_l) on C_p -distribution for downstream cylinder with side ratio (H/D) of 1.25, keeping transverse spacing (L_t) constant at $4D$

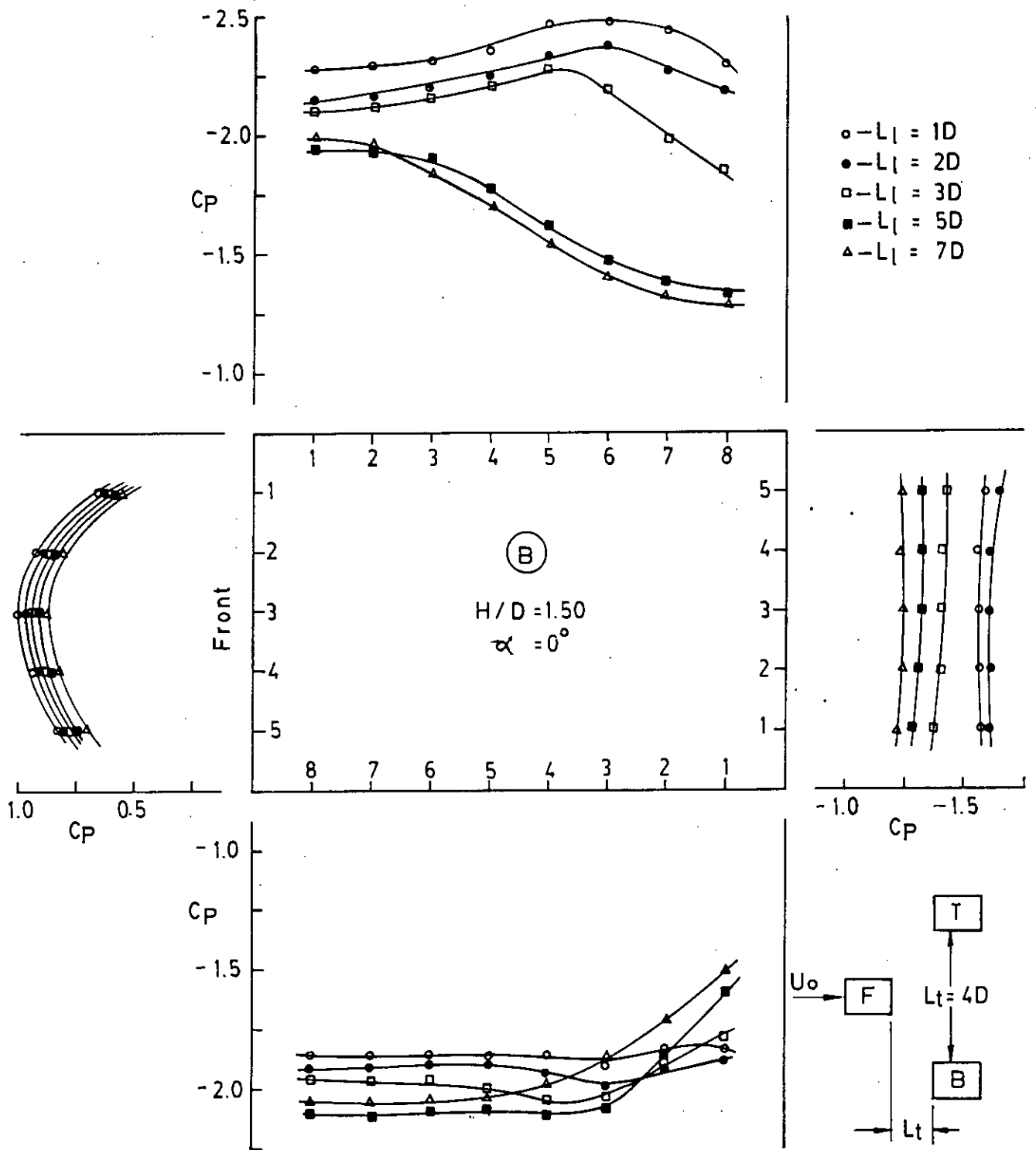


Figure 4-37: Effect of longitudinal spacing (L_t) on C_p -distribution for downstream cylinder with side ratio (H/D) of 1.25 keeping transverse spacing (L_t) constant at $4D$

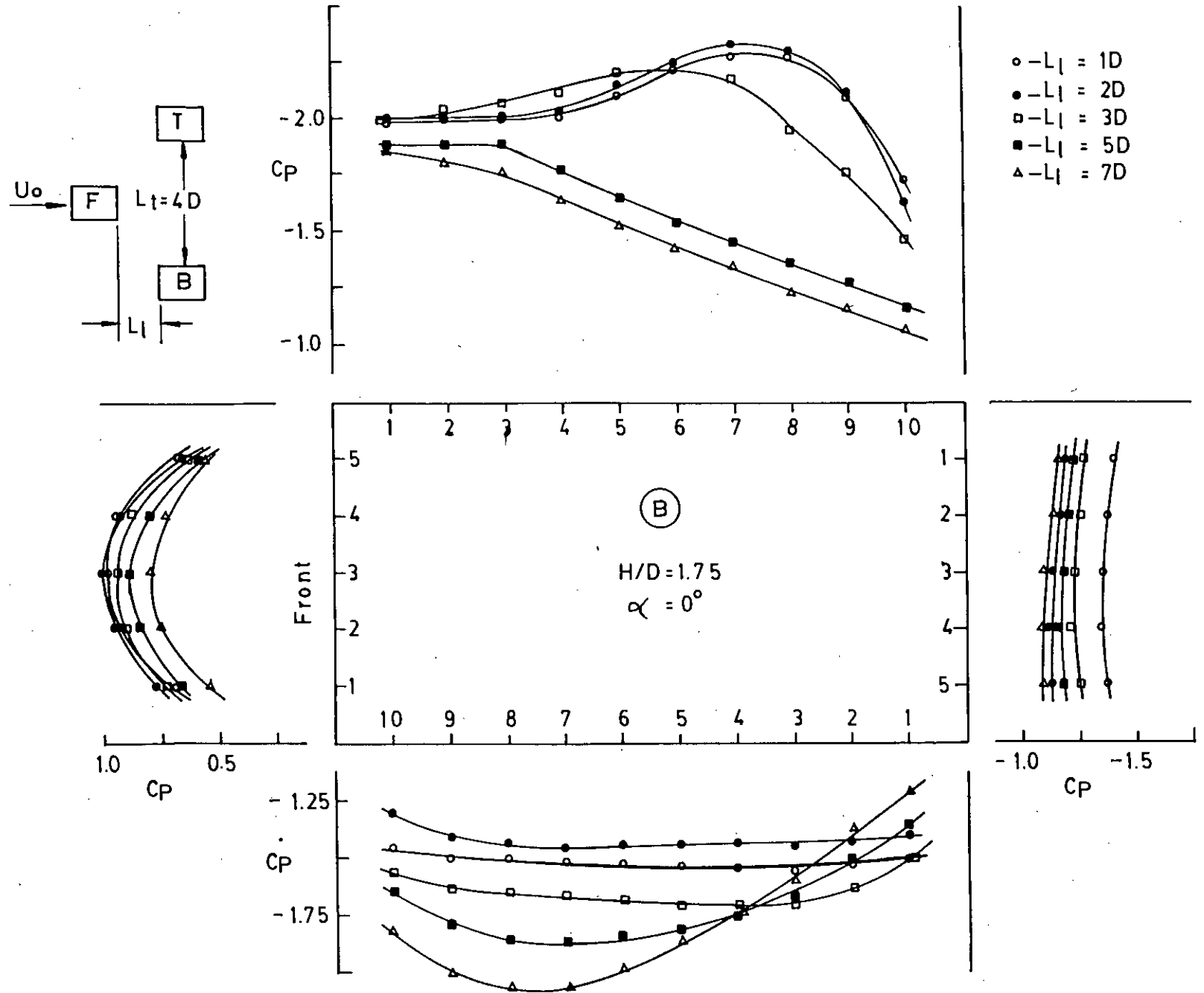


Figure 4-38: Effect of longitudinal spacing (L_l) on C_p -distribution for downstream cylinder with side ratio (H/D) of 1.75 keeping transverse spacing (L_t) constant at $4D$

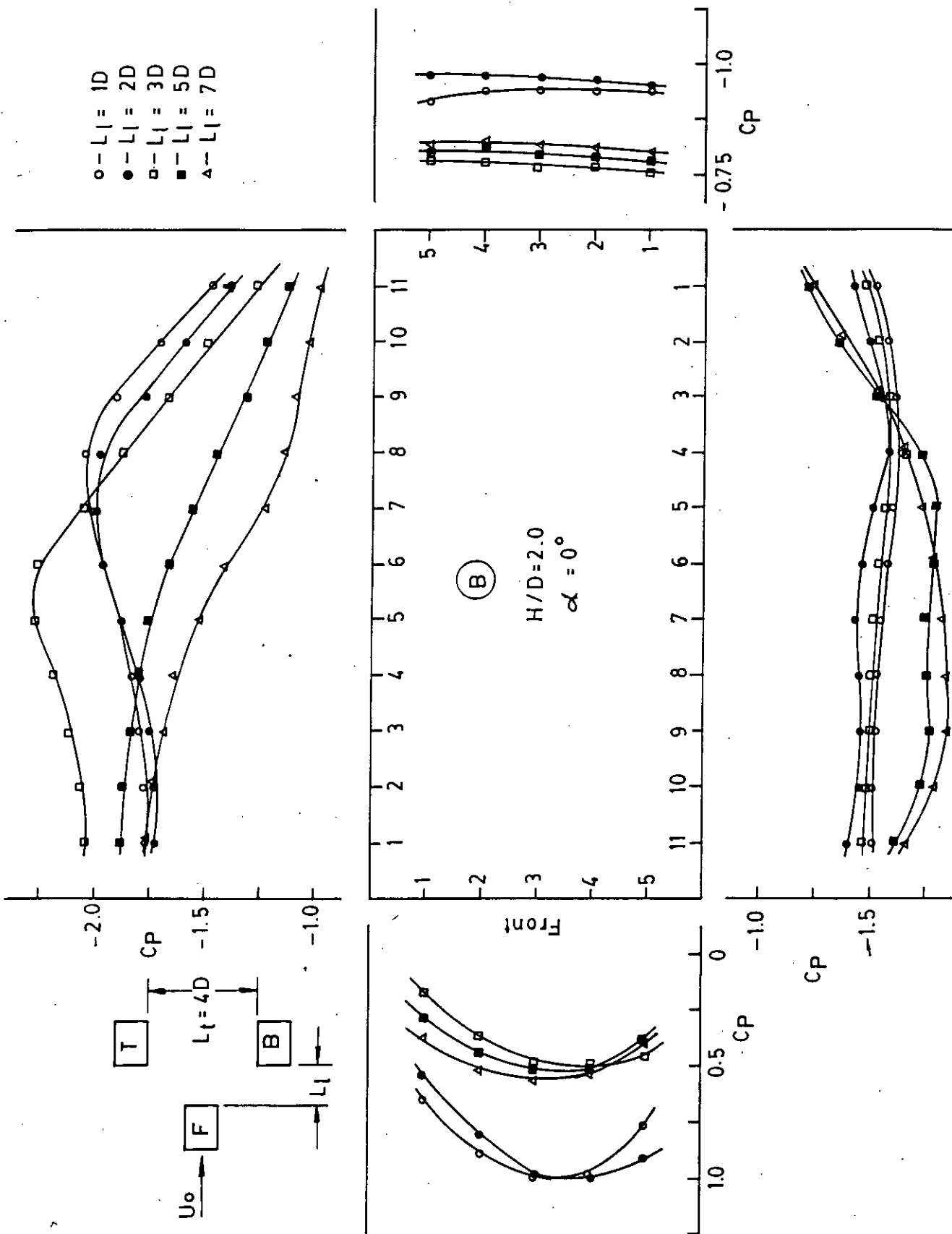
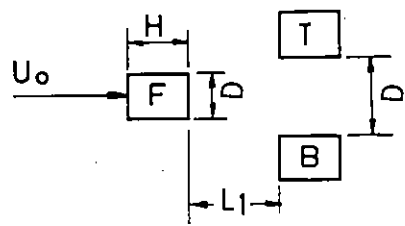


Figure 4.39 : Effect of longitudinal spacing (L_1) on C_p -distributions for downstream cylinder with side ratio (H/D) of 2.0, keeping transverse spacing (L_1) constant at 4D



- $H/D = 1.25$
- $H/D = 1.50$
- $H/D = 1.75$
- △ $H/D = 2.00$
- ▲ $H/D = 10, \text{A.C. Mandal}$

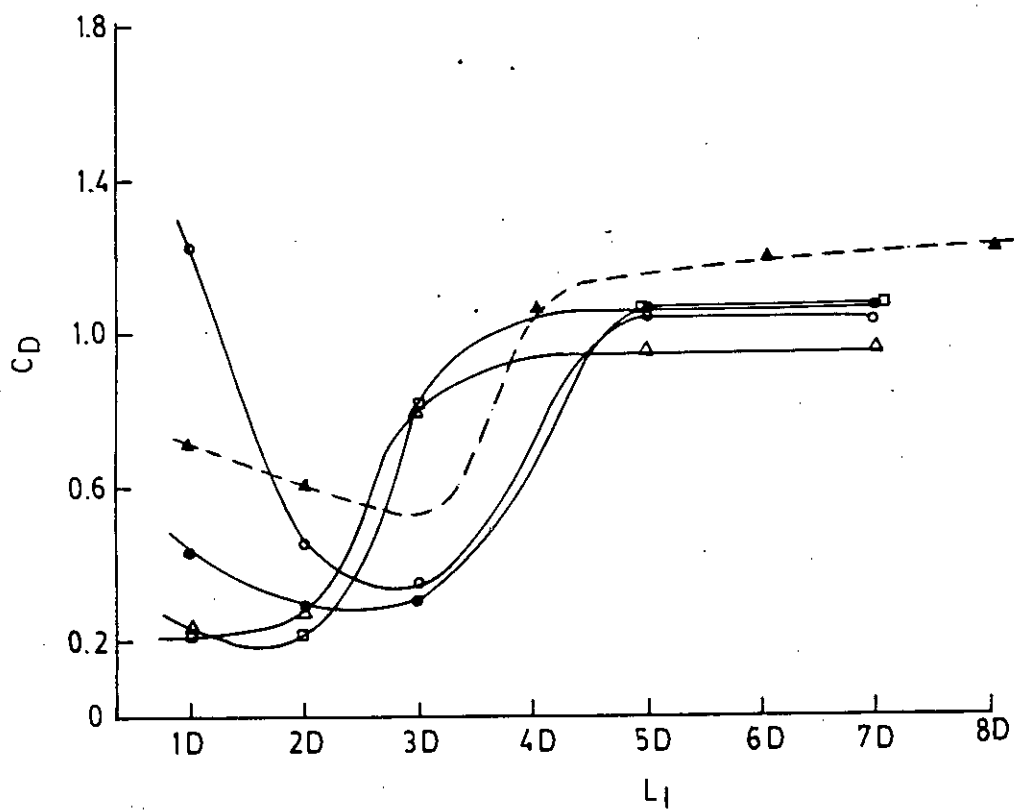


Figure 4.40: Variation of drag co-efficient (C_D) with longitudinal spacing (L_1) on downstream cylinder with different side ratios keeping transverse spacing (L_t) constant at $1D$

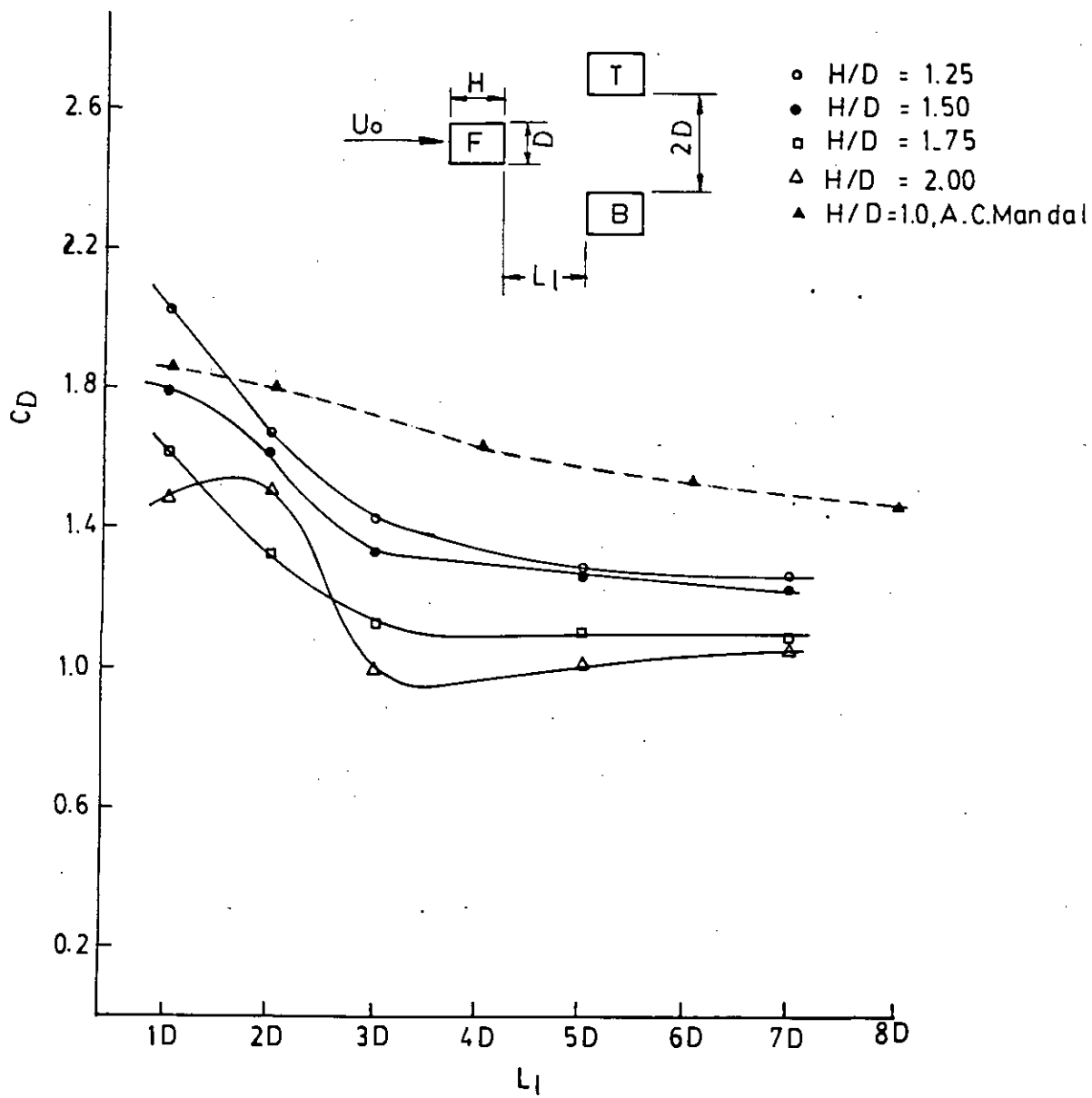


Figure 4-41: Variation of drag co-efficient (C_D) with longitudinal spacing (L_1) on down stream cylinder with different side ratios keeping transverse spacing (L_t) constant at $2D$

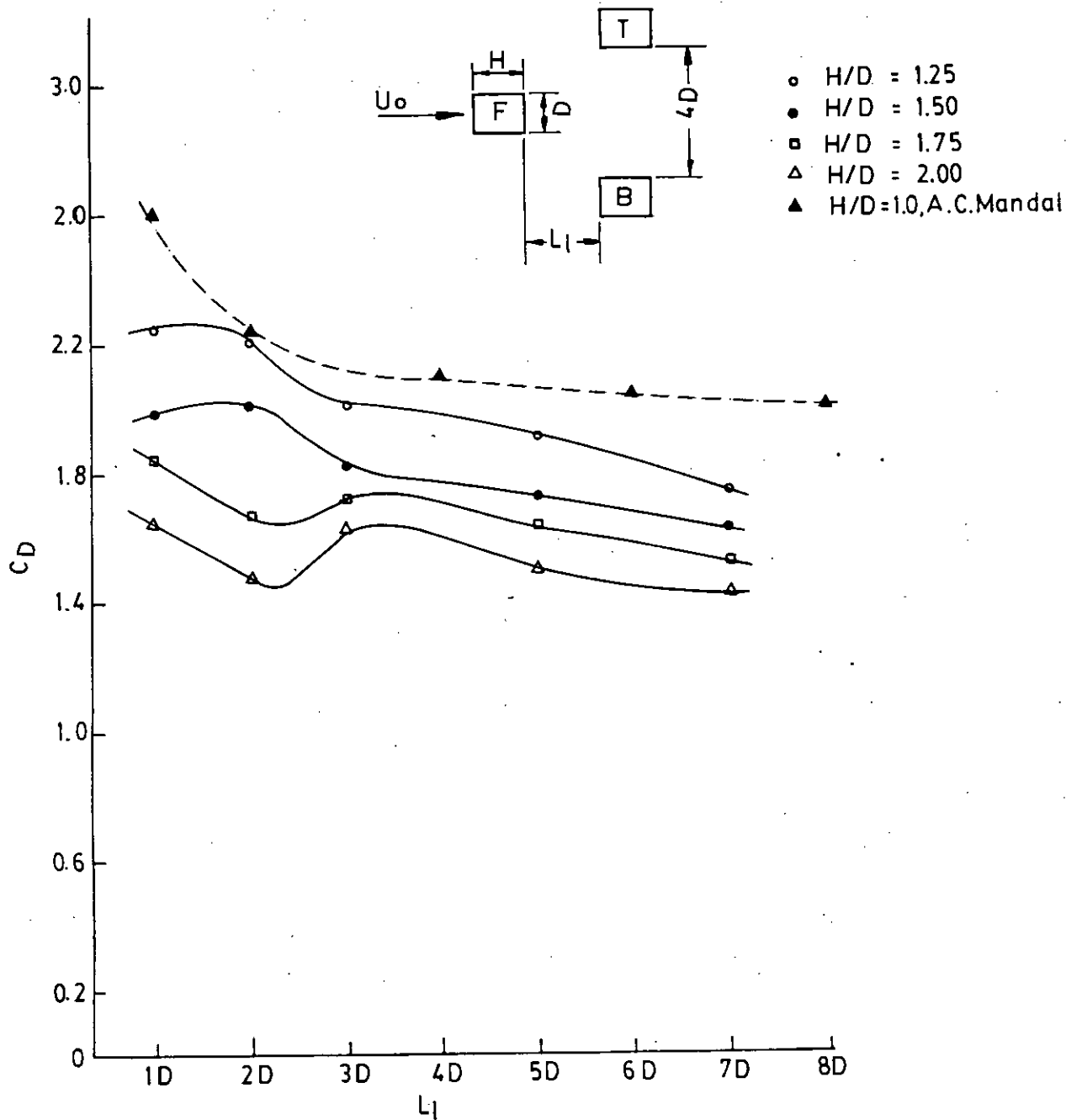


Figure 4.42: Variation of drag co-efficient (C_D) with longitudinal spacing (L_1) on downstream cylinder with different side ratios keeping transverse spacing (L_t) constant at $4D$

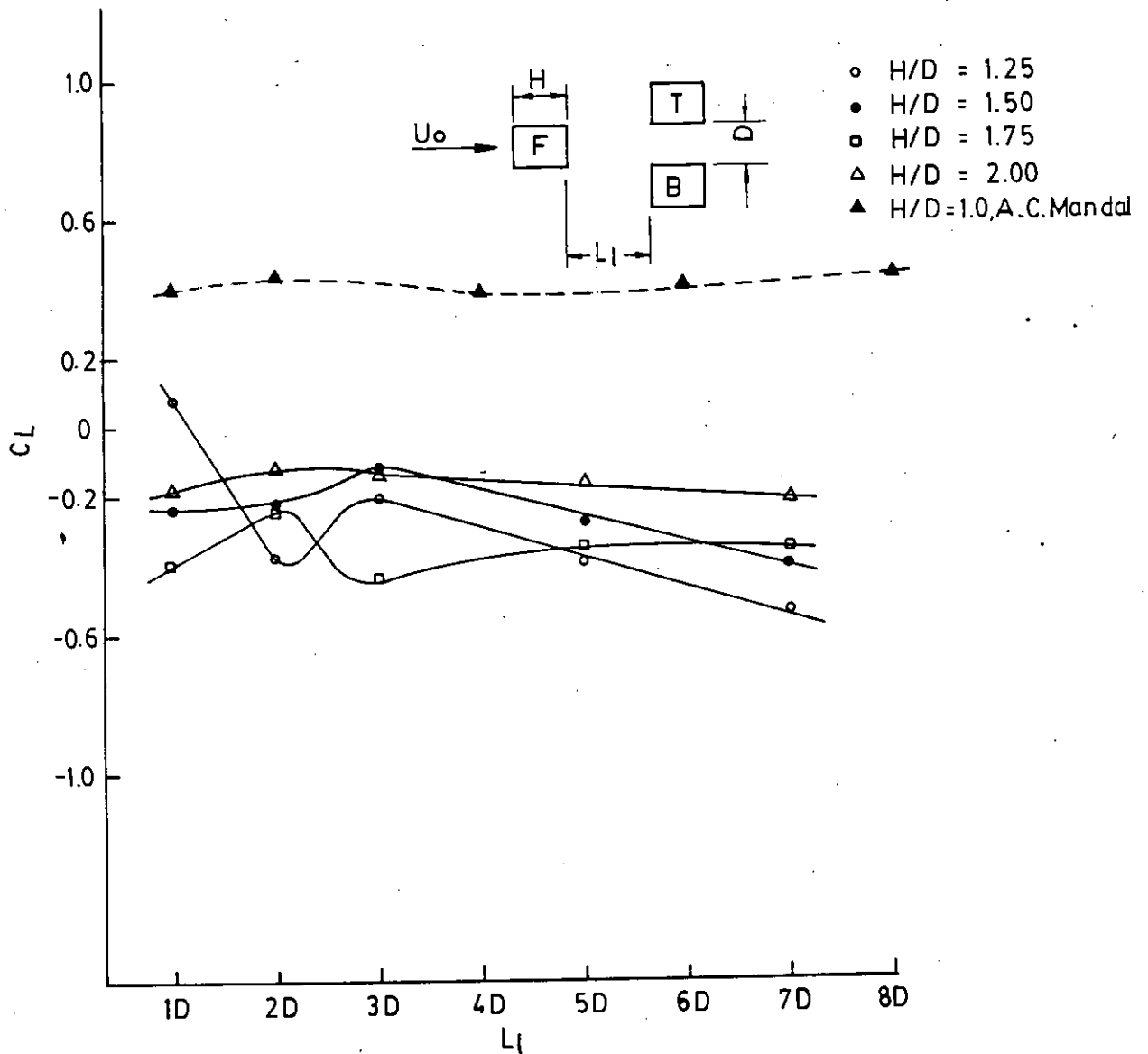


Figure 4.43: Variation of lift co-efficient (CL) with longitudinal spacing (L_l) on downstream cylinder with different side ratios keeping transverse spacing (L_t) constant at 1D

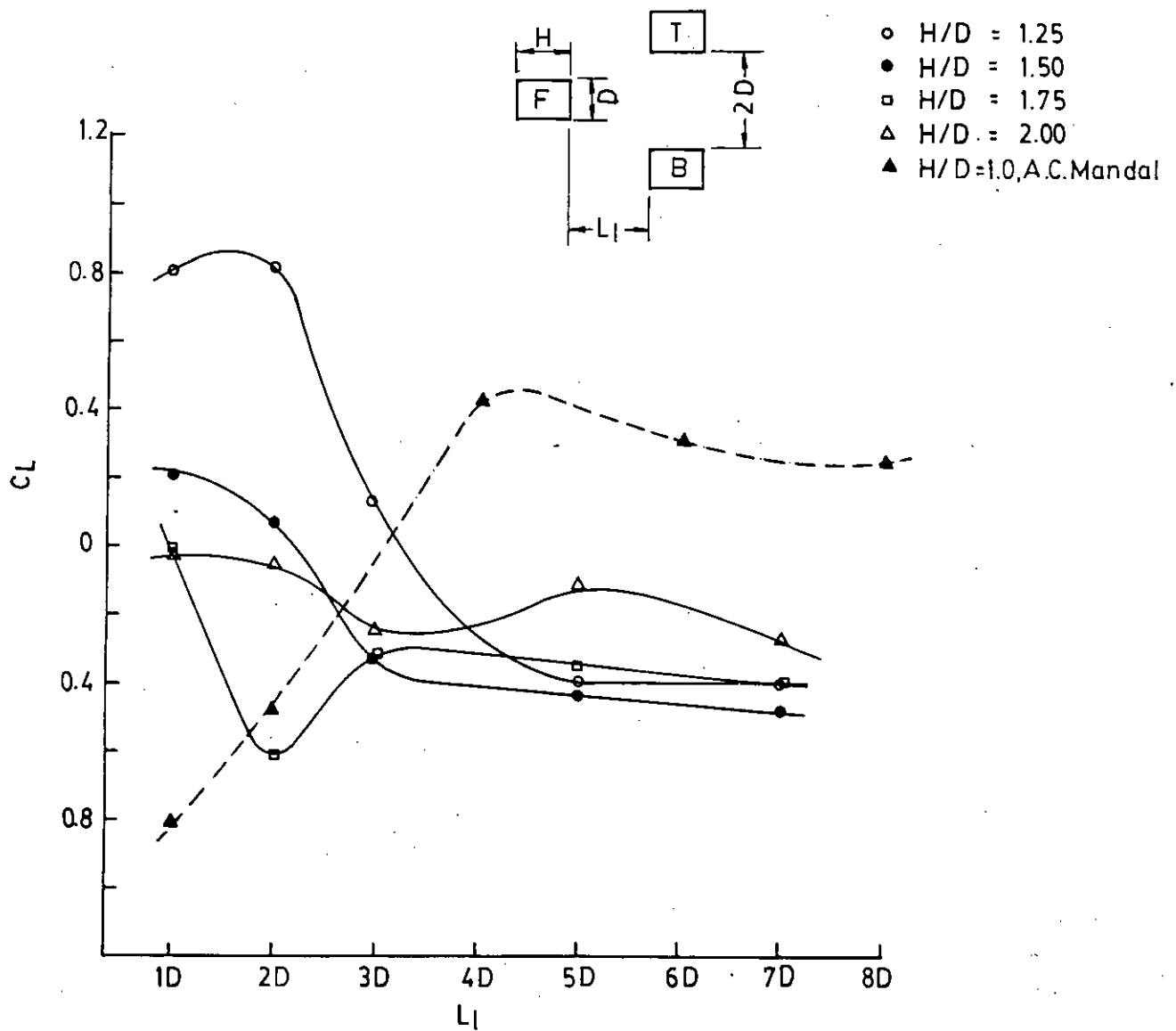


Figure 4.44: Variation of lift co-efficient (C_L) with longitudinal spacing (L_l) on downstream cylinder with different side ratios keeping transverse spacing (L_t) constant at $2D$

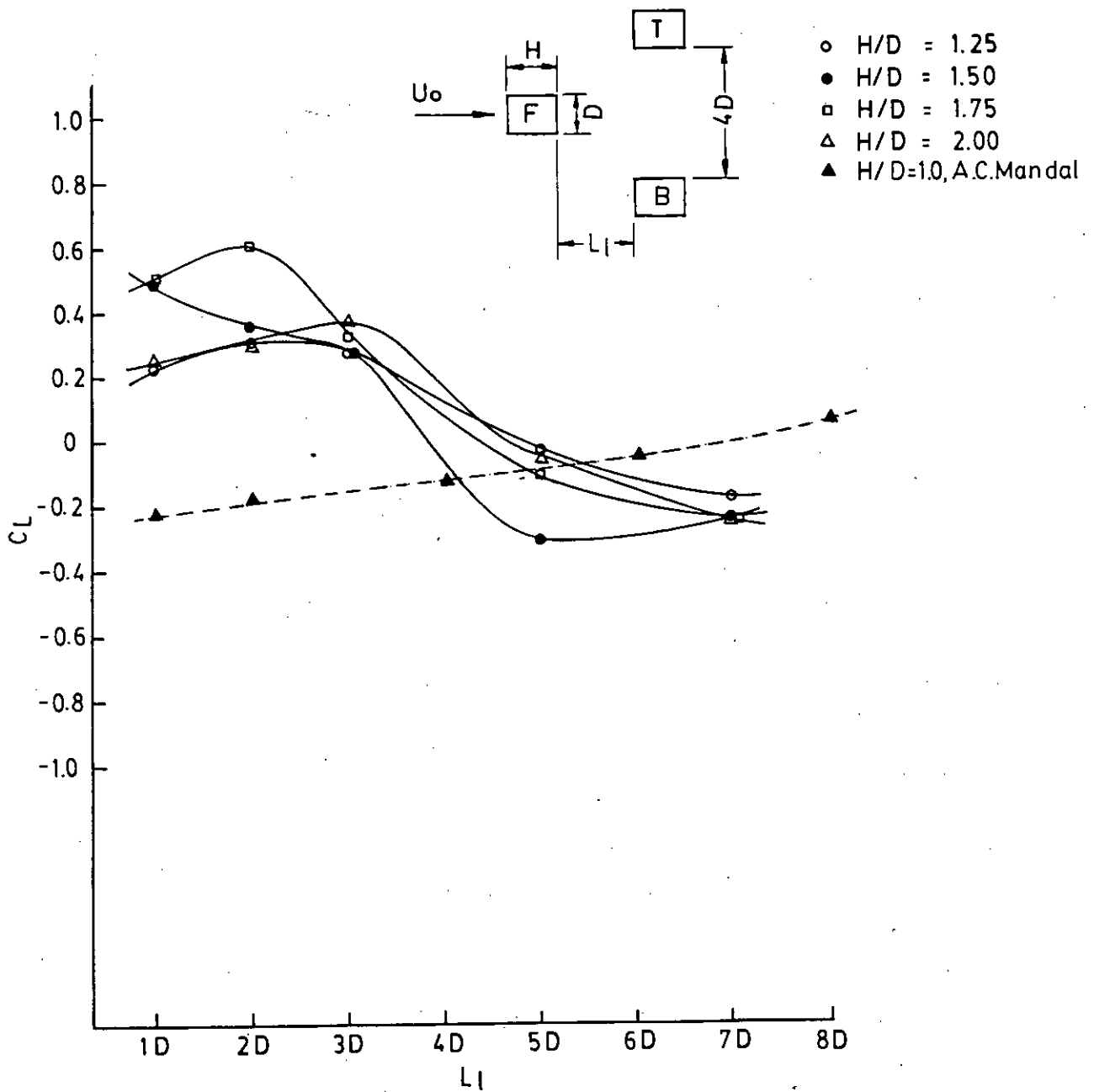


Figure 4.45: Variation of lift co-efficient (C_L) with longitudinal spacing (L_l) on downstream cylinder with different side ratios keeping transverse spacing (L_t) constant at $4D$

